

Limiting factors for planar solid oxide fuel cells under different trace compound concentrations

*Original*

Limiting factors for planar solid oxide fuel cells under different trace compound concentrations / Papurello, Davide; Lanzini, Andrea; Drago, Davide; Leone, Pierluigi; Santarelli, Massimo. - In: ENERGY. - ISSN 0360-5442. - 95:(2016), pp. 67-78. [10.1016/j.energy.2015.11.070]

*Availability:*

This version is available at: 11583/2648242 since: 2016-09-12T15:54:58Z

*Publisher:*

Elsevier Ltd

*Published*

DOI:10.1016/j.energy.2015.11.070

*Terms of use:*

This article is made available under terms and conditions as specified in the corresponding bibliographic description in the repository

*Publisher copyright*

Elsevier postprint/Author's Accepted Manuscript

© 2016. This manuscript version is made available under the CC-BY-NC-ND 4.0 license  
<http://creativecommons.org/licenses/by-nc-nd/4.0/>. The final authenticated version is available online at:  
<http://dx.doi.org/10.1016/j.energy.2015.11.070>

(Article begins on next page)

# **Limiting factors for planar solid oxide fuel cells under different trace compound concentrations**

1        *Davide Papurello<sup>\*</sup>, Andrea Lanzini, Davide Drago, Pierluigi Leone, Massimo Santarelli*

2        *Department of Energy (DENERG), Politecnico di Torino, Corso Duca degli Abruzzi, 24, 10129, Turin, Italy.*

3        *\*Corresponding author. Tel.: +393402351692. Email address: [davide.papurello@polito.it](mailto:davide.papurello@polito.it)*

## 4    **Abstract**

5    The present work investigates the performance of anode supported solid oxide fuel cells under the  
6    influence of different trace compounds. Electrochemical impedance spectroscopy (EIS) has been  
7    used to deconvolute the impedance spectra of an SOFC in order to identify the main losses. The  
8    impact of single and double contaminants on the SOFC performance has also been investigated.  
9    Typical biogas trace contaminants, obtained after a clean-up stage, such as sulfur, chlorine,  
10    aromatic compounds and siloxanes, have been taken into consideration. The results show how the  
11    ohmic contribution is almost independent of the H<sub>2</sub>S concentration. H<sub>2</sub>S acts mainly on the  
12    polarization losses and especially on the mass transport resistance. The impact of HCl on the SOFC  
13    performance is mainly connected to the charge transfer process. D4, as the model compound for  
14    siloxanes, already acts on SOFC performance at ppb(v) levels. The polarization losses have been  
15    influenced the most, and the largest increase has been recorded for the low frequency term, R<sub>low</sub>,  
16    related to the mass transport resistance for naphthalene and toluene. H<sub>2</sub>S, introduced with other  
17    contaminants, causes the instantaneous deterioration of the SOFC performance and the more the  
18    types of contaminants co-fed to the SOFC, the larger the initial anode degradation.

## 19   **Keywords**

20   Trace compounds, Biogas, SOFC, anode based fuel cell, Electrochemical Impedance Spectroscopy  
21   (EIS), Nyquist diagram.

## 22   **Nomenclature**

23   ASC, Anode Supported Cell;  
24   ASR, Area Specific Resistance;  
25   CPE, Constant Phase Element;  
26   DIR, Direct Internal Reforming;  
27   EIS, Electrochemical Impedance Spectroscopy;  
28   FU, Fuel Utilization;

- 29 OCV, Open Circuit Voltage;
- 30 OFMSW, Organic Fraction of Municipal Solid Waste;
- 31 POx, Partial Oxidation;
- 32 ppb(v), parts per billion by volume;
- 33 ppm(v), parts per million by volume;
- 34 Re, ohmic resistance;
- 35 Rp, polarization resistance;
- 36 S/C, Steam to Carbon ratio;
- 37 SOFC, Solid Oxide Fuel Cell;
- 38 TCE, Tetrachloroethylene;
- 39 TOFC, TOpsoe Fuel Cell;
- 40 TPB, Three Phase Boundary;
- 41 VOCs, Volatile Organic Compounds;
- 42 WGS, Water Gas Shift;
- 43 WWTPs, Waste Water Treatment Plants.

44

## 45 **Introduction**

46 Among all the different fuel cells that are available, Solid Oxide Fuel Cells (SOFCs) can be  
47 considered as the most flexible energy generators in relation to fuel selections [1][2][3]. SOFC  
48 systems offer electrical efficiencies of more than 50%, even for small-case units with low calorific  
49 fuels [1][4]. Various types of fuels can be adopted, from fossil fuels to biogenous fuels  
50 [5][3][1][6][7]. The possible fossil fuels for SOFCs include kerosene, gasoline, natural gas, coal gas  
51 and liquid petroleum gas. Fuels from renewable matrices, mostly biogas, are appropriate for high  
52 temperature fuel cell energy production. Biogenous fuels, with respect to fossil fuels, allow the  
53 global warming potential impact to be reduced in order to meet EU 20-20-20 requirements. The

European climate and energy change protocol, EU 20-20-20, incorporates these points in order to reduce the energy demand from fossil fuels that are not renewable, and to increase the exploitation of resources that are already distributed locally [5][8]. However, these practical fuels contain minor constituents as impurities. These impurities are mainly volatile organic compounds (VOCs), which are contained in a biogas mixture that originates from the dry anaerobic digestion of the organic fraction of municipal solid waste (OFMSW) [9]. As reported by Papurello et al., (2014, 2015, 2015(1)), a gas cleaning section is mandatory to feed a SOFC generator due to the stringent VOC requirements currently in force, which are especially rigorous as far as sulfur, chlorine and siloxane compounds are concerned [1,10,11]. Sigot et al., (2015) have provided another example of sulfur and siloxane removal for biogas conversion in a solid oxide fuel cell [12] in which the SOFC tolerance limits for trace contaminants have been matched with already available gas cleaning technologies. Sasaki et al., (2011) investigated the chemical degradation of SOFCs with trace compounds through long-term poisoning tests of up to 3000 h, in which microstructural observations were considered [5]. H<sub>2</sub>S, PH<sub>3</sub>, Cl<sub>2</sub> and D<sub>5</sub> were among the trace compounds that Sasaki et al., (2011) investigated, together with their effect on an NiScSz anode based fuel cell. The compounds with the most detrimental effects on SOFC performance are H<sub>2</sub>S, HCl and siloxanes [5,13–18]. As reported by Haga et al. (2008), D<sub>5</sub> was selected as the model compound for siloxanes, and 10 ppm(v) was demonstrated to be fatal for SOFCs [19]. No studies have been conducted on siloxanes at ultra-low concentrations, even though they seem to have an important influence on cell performances at the ppm(v) level [20]. In order to conduct a detailed investigation into the effect of VOCs on the performance of SOFCs, proper testing and modeling tools have to be identified, especially considering the remarkable growth in SOFC pilot plant applications [1].

These following methods have been used to detect the performance limiting factors of an in-operating fuel cell. A powerful method adopted to analyze fuel cell operation and diagnostics is electrochemical impedance spectroscopy (EIS) [21–27]. The use of EIS analysis as a diagnosis tool

79 is well known at a laboratory level. EIS analysis could be adopted for the on-line diagnostics of  
80 operating fuel cell stacks in order to follow and to investigate the SOFC performance of real  
81 machines. The other possible methods that could be used as alternatives to investigate cell  
82 performance losses could be detrimental for cell operation. For instance, if I-V curve analysis is  
83 adopted for the evaluation of the area specific resistance (ASR) for each test condition, detrimental  
84 problems could arise related to the current density variation and these could compromise the  
85 integrity of the entire test. Leone et al., (2013) conducted an interesting study on the limiting factors  
86 for a planar SOFC under different flow and temperature conditions with EIS analysis [27]. The EIS  
87 analysis of a fuel cell is carried out under transient and almost equilibrium conditions in order to  
88 avoid causing rapid changes in the current [23,26–31] . Two possible conditions can be selected: an  
89 open circuit voltage (OCV) or a current density value. In the latter case, polarization of the cell  
90 becomes an independent variable. The potential difference between the thermodynamic open circuit  
91 potential and the operational potential is the polarization or the overpotential of a fuel cell [32]. This  
92 voltage loss is a function of the current density, and it mainly depends on the processes that occur  
93 during fuel cell operation. It is generally difficult to interpret the obtained impedance diagrams. For  
94 this reason, a specific method is adopted for the EIS spectra deconvolution to separate the ASR  
95 value into the different contributions that describe the cell losses related to the cell functional layers  
96 [23,28–31]. Three main potential losses [33] can be recognized and connected to: (i) the ohmic  
97 resistances of the materials and interfaces due to the transport of ions and electrons through the  
98 materials; (ii) concentration polarizations that are caused by the resistance to fuel and oxidant mass  
99 transport through the electrodes; (iii) activation polarizations related to the electrochemical  
100 reactions of the electrolyte/electrodes. With these techniques, impedance diagrams can at least  
101 provide a breakdown of the total loss (ASR). The ASR value can be divided into ohmic resistance,  
102  $R_e$ , measured at high frequency, and polarization resistance,  $R_p$ , measured at medium and low  
103 frequencies, reflecting losses due to chemical, electrochemical, and transport processes.

104 The goal of this work was to investigate cell performance losses related to the different trace  
105 compound concentrations contained in a biogenous fuel adopting an EIS analysis.

## 106 **Materials and methods**

107 A simulated gas mixture representing different fuel conditions has been considered with different  
108 trace compounds. Experiments were performed with nickel-based anode supported solid oxide fuel  
109 cells (ASC). Three circular planar type seal-less anode supported cells were used. The tested cells  
110 have a diameter of 80 mm and a screen printed cathode of 78 mm:

- 111 1. the ASC700 cell ([SOFCpower, Italy](#)) consists of a 240-260  $\mu\text{m}$  porous Ni/8YSZ anode support,  
112 a 8-10  $\mu\text{m}$  dense electrolyte YSZ and a 50-60  $\mu\text{m}$  porous GDC/LSCF cathode bilayer;
- 113 2. the ASC4 cell ([H.C. Starck, Germany](#)) consists of a 465-555  $\mu\text{m}$  porous NiO/YSZ anode  
114 support with a 5-10  $\mu\text{m}$  NiO/YSZ porous active layer, a 4-6  $\mu\text{m}$  dense electrolyte YSZ and a  
115 2.4  $\mu\text{m}$  YDC blocking layer plus a 30-60  $\mu\text{m}$  porous LSCF cathode layer;
- 116 3. the TOFC cell ([Topsoe fuel cell, Denmark](#)) consists of a porous Ni/8YSZ anode support, a  
117 dense electrolyte YSZ and a porous CGO/LSCF cathode bilayer.

118 The design of SOFC supported anodes has been extensively investigated over the last few years  
119 because of their relatively easy of manufacturing and potentially high power density. Moreover, the  
120 cathode material of LSCFs has been investigated for intermediate temperature SOFC applications  
121 [23,28–33] and a polarization resistance of 0.018  $\Omega\text{cm}^2$  has been shown at 750 °C as well as  
122 relative stability (400% of increased polarization resistance in 700 h) [34].

123 Planar SOFCs have been used for the experimental test session. They were fed with synthetic  
124 biogas and syngas obtained by mixing pure gas feeds from CH<sub>4</sub>, CO<sub>2</sub>, CO, N<sub>2</sub> and H<sub>2</sub> cylinders  
125 (Siad, Italy). A variable concentration of trace compounds was added to the fuel stream. If it is not  
126 explicitly reported the trace compound was added to the fuel mixture and the EIS analysis was  
127 conducted after a stabilization time within 2 h. An extensive experimental campaign was scheduled

128 and the details are reported in Table 1. The experiments were performed by varying the fuel  
129 composition and the trace compound concentrations in order to investigate SOFC losses.

Pollutant test	Conc. Range (ppm(v))	Cell adopted	H <sub>2</sub> (ml min <sup>-1</sup> )	CO (ml min <sup>-1</sup> )	CO <sub>2</sub> (ml min <sup>-1</sup> )	CH <sub>4</sub> (ml min <sup>-1</sup> )	N <sub>2</sub> (ml min <sup>-1</sup> )	H <sub>2</sub> O (ml min <sup>-1</sup> )	H <sub>2</sub> O (g h <sup>-1</sup> )	T (°C)	FU	Fuel condition
H <sub>2</sub> S high conc.	0.84-6.4	ASC700	151.5	136.4	68.2	15.2	386.4	60.2	2.9	750	30.0	Syngas
H <sub>2</sub> S high conc.	0.8-6.7	ASC4	250	0	41.7	62.5	0	124.5	6	750	20.9	DIR 50% biogas
H <sub>2</sub> S low conc.	0.078-0.174	ASC4	250	0	41.7	62.5	0	124.5	6	750	20.9	DIR 50% biogas
HCl	1-1000	ASC700	348	133.7	62.1	5		136.5	6.58	750	29.9	biogas reformat
D4	0.11-1.92	TOFC	348	133.7	62.1	5		136.5	6.58	750	20.8	biogas reformat
C <sub>7</sub> H <sub>8</sub>	3.8-24.2	ASC700	151.5	136.4	68.2	15.2	386.4	269.8	13	750	30.0	Syngas
C <sub>10</sub> H <sub>8</sub>	0-9.3	ASC700	151.5	136.4	68.2	15.2	386.4	269.8	13	750	30.0	Syngas
C <sub>2</sub> H <sub>2</sub>	371.2	ASC700	250	0	42	63	0	0.0	0	750	20.8	POx 50% biogas
H <sub>2</sub> S	1.34	ASC700	250	0	42	63	0	0.0	0	750	20.8	POx 50% biogas
H <sub>2</sub> S + C <sub>2</sub> Cl <sub>4</sub>	0-4/1.7-0	ASC700	151.5	136.4	68.2	15.2	386.4	269.8	13	750	30.0	Syngas
H <sub>2</sub> S + C <sub>2</sub> H <sub>2</sub>	1.34/371.2	ASC700	250	0	42	63	0	0.0	0	750	20.8	POx 50% biogas
H <sub>2</sub> S + C <sub>7</sub> H <sub>8</sub>	4/3.7	ASC700	151.5	136.4	68.2	15.2	386.4	269.8	13	750	30.0	Syngas

130 **Table 1 – Test conditions.**

131 The oxidant flow (air) at the cathode side was 0.5 Nl min<sup>-1</sup> during the start-up and shut-down  
132 procedures, otherwise it was fixed at 1.2 Nl min<sup>-1</sup> for all the performed experiments. The fuel gas  
133 mixtures, contained in certified gas bottles ([Siad spa, Italy](#)), were fed to the anode and regulated by  
134 means of mass flow controllers ([Bronkhorst, The Netherlands](#)). All the cells were first activated  
135 with hydrogen. The fuel mixture was restored to clean conditions after each poisoning phase with  
136 the trace compound of interest. Four gas mixtures were adopted for the experimental tests:

- 137 1. A syngas mixture, used to represent a wood gasification plant.
- 138 2. A direct internal reforming case (DIR 50%), used to represent a mixture of biogas reformed  
139 internally with steam (50% vol.-electrochemical), while the remaining part was reformed  
140 externally.
- 141 3. A partial oxidation case (POx 50%), used to represent a biogas mixture reformed internally with  
142 air (50% vol.-electrochemical), while the remaining part was reformed externally.



143 4. A biogas reformat case, used to represent a biogas mixture completely reformed externally in a  
144 steam reformer with a steam-to-carbon (S/C) ratio equal to 2.

145 The electrochemical characterization of the fuel cell was carried out with an electronic load  
146 ([Kikusui Electronics Corp., Japan](#)) in conjunction with an additional power supply in current-  
147 following mode ([Delta Elektronica, The Netherlands](#)). Electrochemical impedance spectroscopy  
148 analyses were performed using a GAMRY FC350 in the 10 Hz to 300 kHz range. The oven  
149 temperature was kept constant at 750 °C. Temperature control was provided by a thermocouple  
150 placed in the center of the anodic ceramic housing, 1 mm from the anode surface. The seal-less cell  
151 arrangement was adopted to allow the excess fuel and oxidant in the outer border of the cell to  
152 combust. Nickel and platinum double meshes were used for current collection at the anode and  
153 cathode electrodes, respectively.

## 154 **Results**

155 The electrochemical impedance analysis results are reported in this section. The analysis focused on  
156 a more detailed investigation of cell performance, which was affected by the trace compounds  
157 through the deconvolution of the impedance spectrum. The Nyquist diagrams that were obtained for  
158 the different measurement conditions are also reported. The behavior of the cell was simulated by  
159 means of the equivalent electrical circuit shown in figure 1, and the impedance data were analyzed  
160 at different trace compound concentrations. The equivalent circuit is constituted by the ohmic  
161 resistance,  $R_e$  and two parallel combinations of a resistance and a constant phase element, CPE  
162 [25]. The polarization resistance,  $R_p$ , is obtained by summing the  $R_{high}$  and  $R_{low}$  resistances. The  
163 first term is related to the electrochemical processes that take place at the electrodes, whereas the  
164 second contribution accounts for the mass transport phenomena [35].

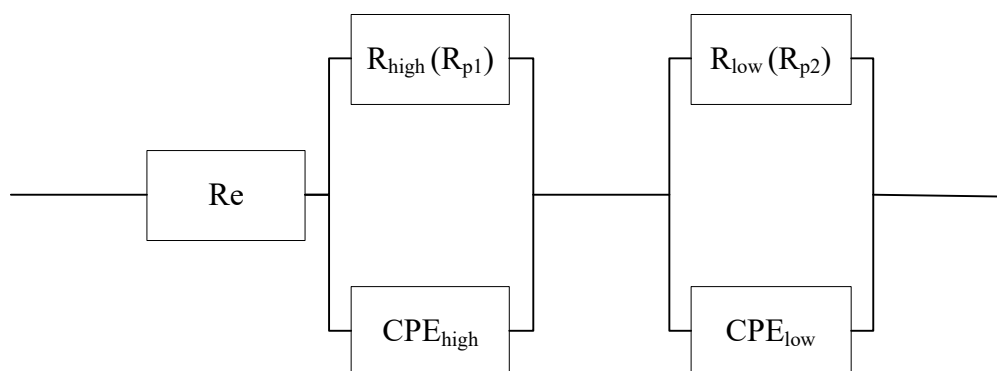


**Figure 1 – Equivalent fuel cell circuit:  $R_e$ ,  $R_{high}$  and  $CPE_{high}$  are associated with the high frequency semi-circle,  $R_{low}$  and  $CPE_{low}$  with the low frequency semi-circle.**

### The influence of Hydrogen sulfide on SOFC performance

The main pollutant compound for SOFC operation is widely recognized to be  $H_2S$  [3,13–15,36–38]. As reported elsewhere, the  $H_2S$  concentration is one of the main trace compounds contained in a biogas mixture [9]. Four separate tests were carried out with three different commercial cells: ASC4, ASC700 and TOFC. The operating temperature was fixed at 750 °C, while the current density was fixed at 0.32 A cm<sup>-2</sup>. The first test was carried out in order to investigate the impact of  $H_2S$  on cell performance, considering a concentration ranging from 0.8 to 6.4 ppm(v), with a mixture that simulates a syngas produced from a wood gasifier. This concentration range has here been named “high concentration”, as it is high compared to the limit  $H_2S$  concentration value currently fixed for SOFCs, which is around 1 ppm(v) [5,6,39–41]. The second test considered the same  $H_2S$  concentration range in order to simulate the partial direct internal reforming (DIR 50%) of a biogas mixture derived from, for example, an anaerobic digestion process. In the next step, the  $H_2S$  test was conducted with the goal of testing the  $H_2S$  concentration limit and studying its impact on SOFCs in a POx biogas mixture. Finally, a low  $H_2S$  range, from 78 to 174 ppb(v), was tested to identify any changes in SOFC performance.

### High $H_2S$ concentration test

184 Figure 2 depicts the Nyquist diagram for the ASC700 cell with a variable H<sub>2</sub>S concentration, while  
 185 figure 3 shows the Nyquist diagram for the ASC4 cell.

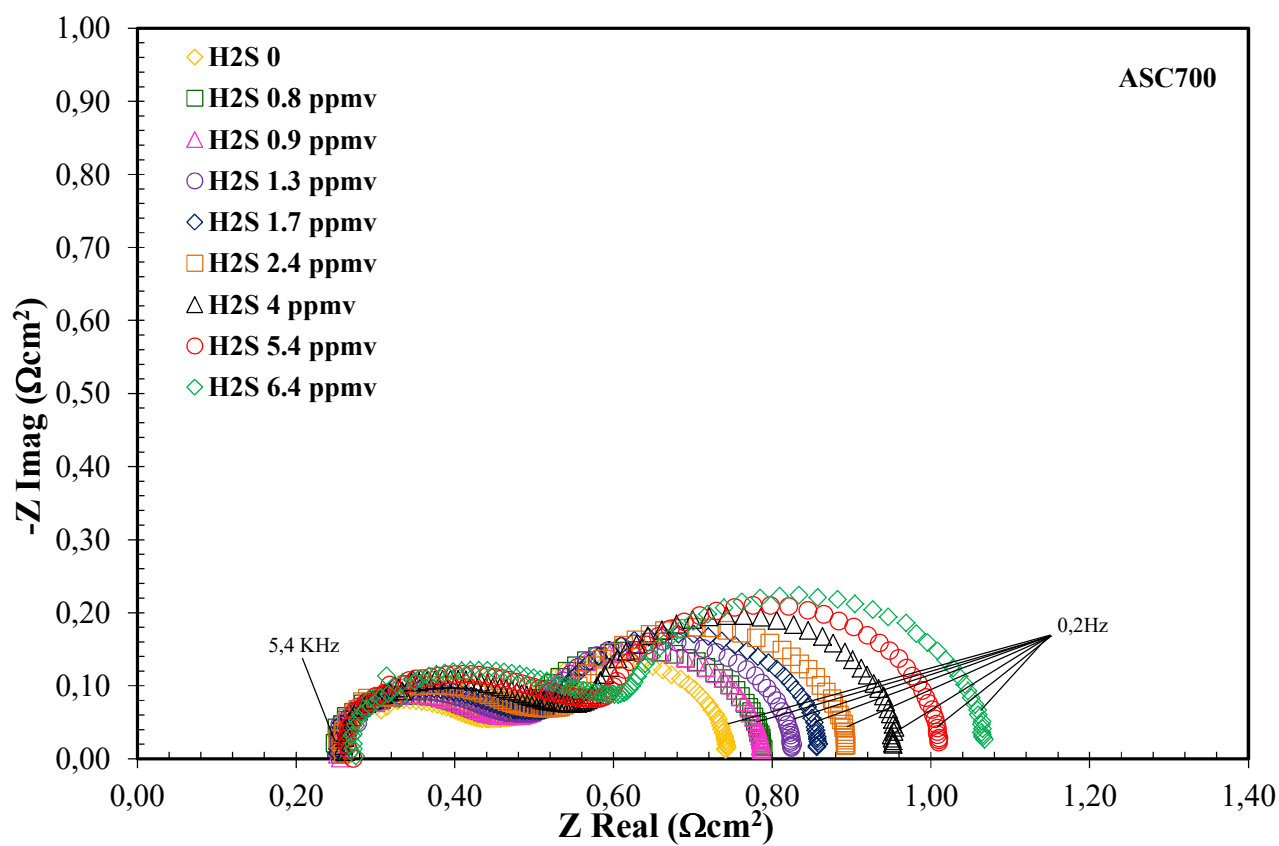


Figure 2 – Nyquist diagram for variations of the H<sub>2</sub>S concentration – ASC700.

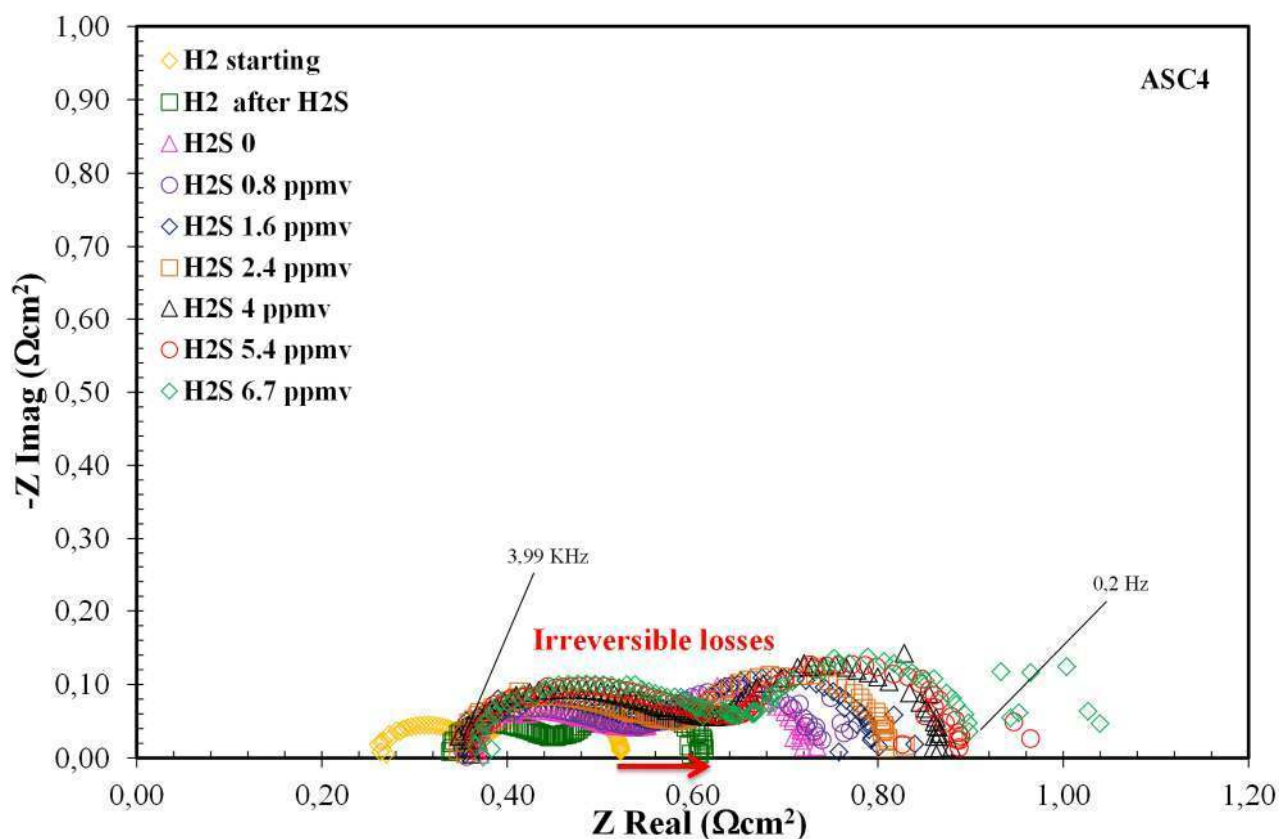
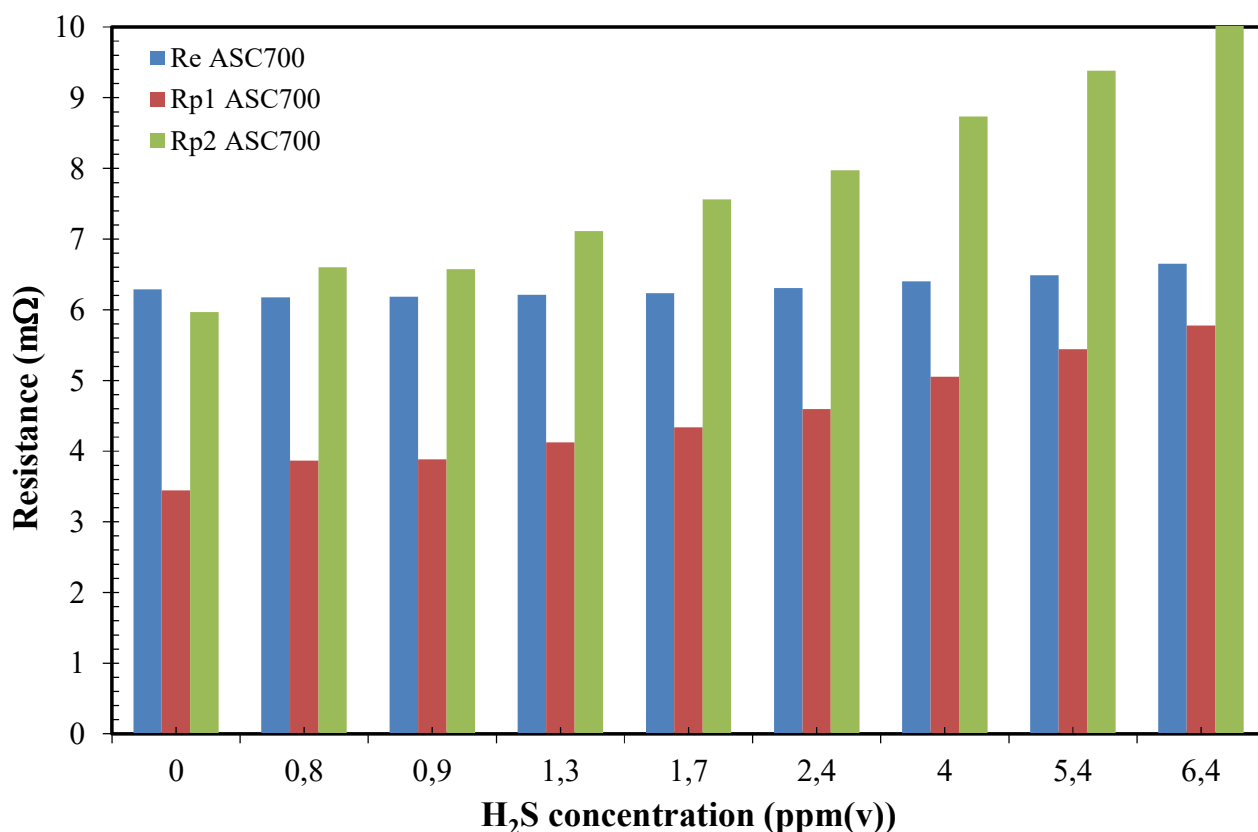


Figure 3 – Nyquist diagram for variations of the H<sub>2</sub>S concentration – ASC4.

The ohmic contribution to the ASR value represents the materials and interface resistances due to the transport of ions and electrons through the materials. This value is almost independent of the fuel composition and it is only minimally affected by the H<sub>2</sub>S concentration value, as shown in figures 2-3 and 4-5. Comparing the ohmic value of ASC700 and ASC4, it is evident that the latter shows a higher value. This is due to the lower fuel flow compared to the ASC700 case (N<sub>2</sub> content), which causes air backflow. The reason for this air backflow is that the seal-less design could lead to nickel oxidation. The nitrogen content, which on one hand allows nickel oxidation to be avoided, on the other hand, causes a dilution effect of the gas mixture, thereby increasing the total ASR value (see the ASC700 cell results). The H<sub>2</sub>S concentration, as reported in figures 2-3 and 4-5, does not cause an important variation of the ohmic resistance value, but instead acts on the  $R_{\text{high}}$  and  $R_{\text{low}}$  values. By increasing the H<sub>2</sub>S concentration, an increase in the low frequency circle amplitude is obtained, compared to the high frequency circle (see figures 2-3). This result can also be confirmed

202 by observing figures 4-5, where the  $R_{p2}$  ( $R_{low}$ ) trend rises when the  $H_2S$  concentration increases.  
 203 This is due to the mass transport resistance through the electrodes caused by the sulfur blocking  
 204 sites. An increase in the  $R_{high}$  value is also registered when the  $H_2S$  concentration rises. This is due  
 205 to the three phase boundary (TPB) reduction from the nickel active sites which is blocked by the  
 206 sulfur compound.



207  
 208 **Figure 4 – Re and Rp values for variations of the  $H_2S$  concentration – ASC700.**

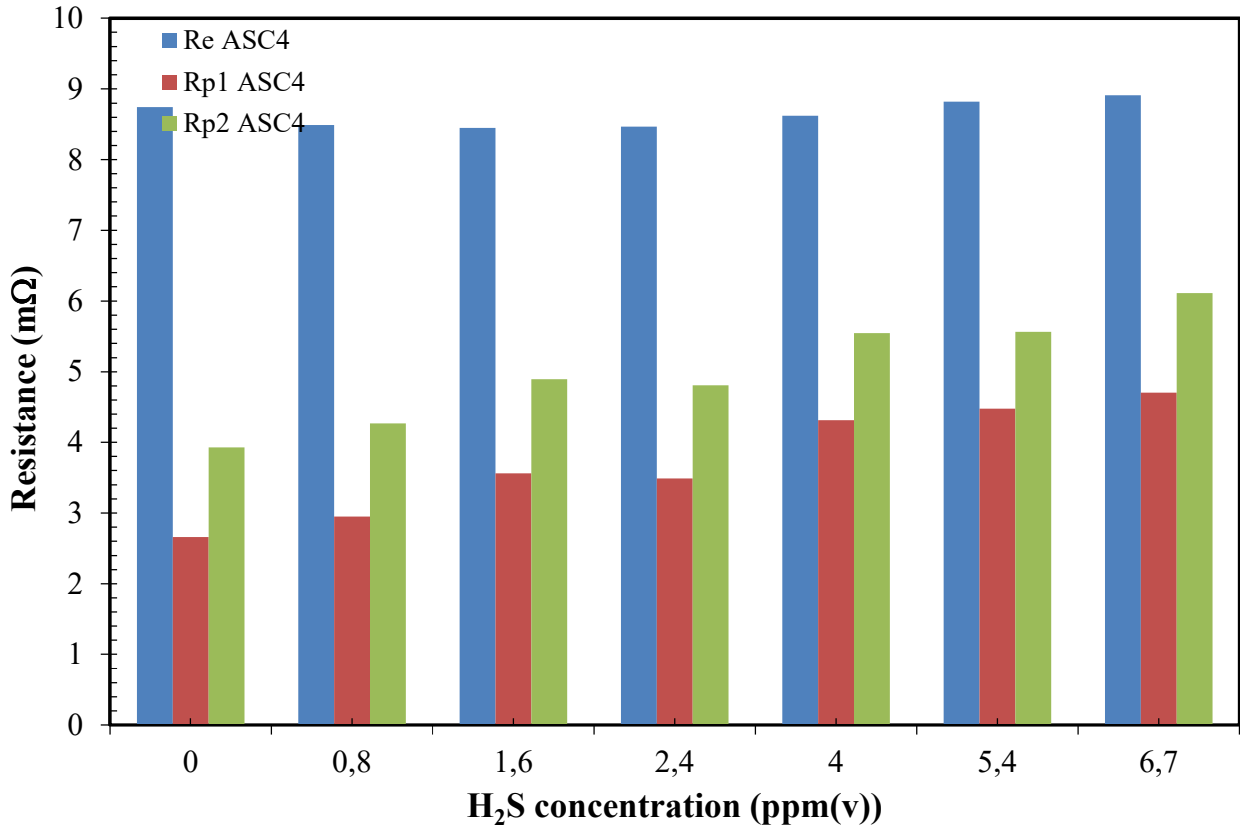


**Figure 5 – Re and Rp values for variations of the H<sub>2</sub>S concentration – ASC4.**

Figure 3 shows that, after the H<sub>2</sub>S “high concentration” test, the cell performance is irreversibly affected, as shown by the Nyquist profile for H<sub>2</sub> before and after the H<sub>2</sub>S. As reported above, pollutants affect the performance of a SOFC and the voltage potential of a single cell, in terms of electrical power, which is reduced according to the following equation:

$$\Delta P = \Delta R \cdot I^2 \text{ (eq.1)}$$

Where  $\Delta P$  is the power loss due to the variation of the overall resistance of the cell ( $\Delta R$ ), which is obtained from the sum of the ohmic and polarization contributions.

Considering an H<sub>2</sub>S concentration in the 0.8 to 6.4 ppm(v) range, the power loss increases by up to 10.7%, compared to the nominal power value. This means that if the exposure time to the pollutants is increased, the electrical power loss will also increase, due to an overall higher ASR value.

#### H<sub>2</sub>S threshold value test

Figure 6 depicts the Nyquist diagram for the POx test, with the threshold concentration value of  $\text{H}_2\text{S}$  fixed at 1 ppm(v) on the basis of results from literature studies. The gas mixture has an important effect on the ohmic value, and a high increase is recorded, compared to the ASC4 case with “high sulfur concentration values”. This is due to the amount of air that is added to the reactive fuel sent to the anode side, which may cause combustion and Ni oxidation phenomena. Even at this concentration value, the  $\text{H}_2\text{S}$  concentration influences the polarization losses and, more precisely, the mass transport ( $R_{\text{low}}$ ), and, to a lesser extent, the electrochemical contribution ( $R_{\text{high}}$ ).

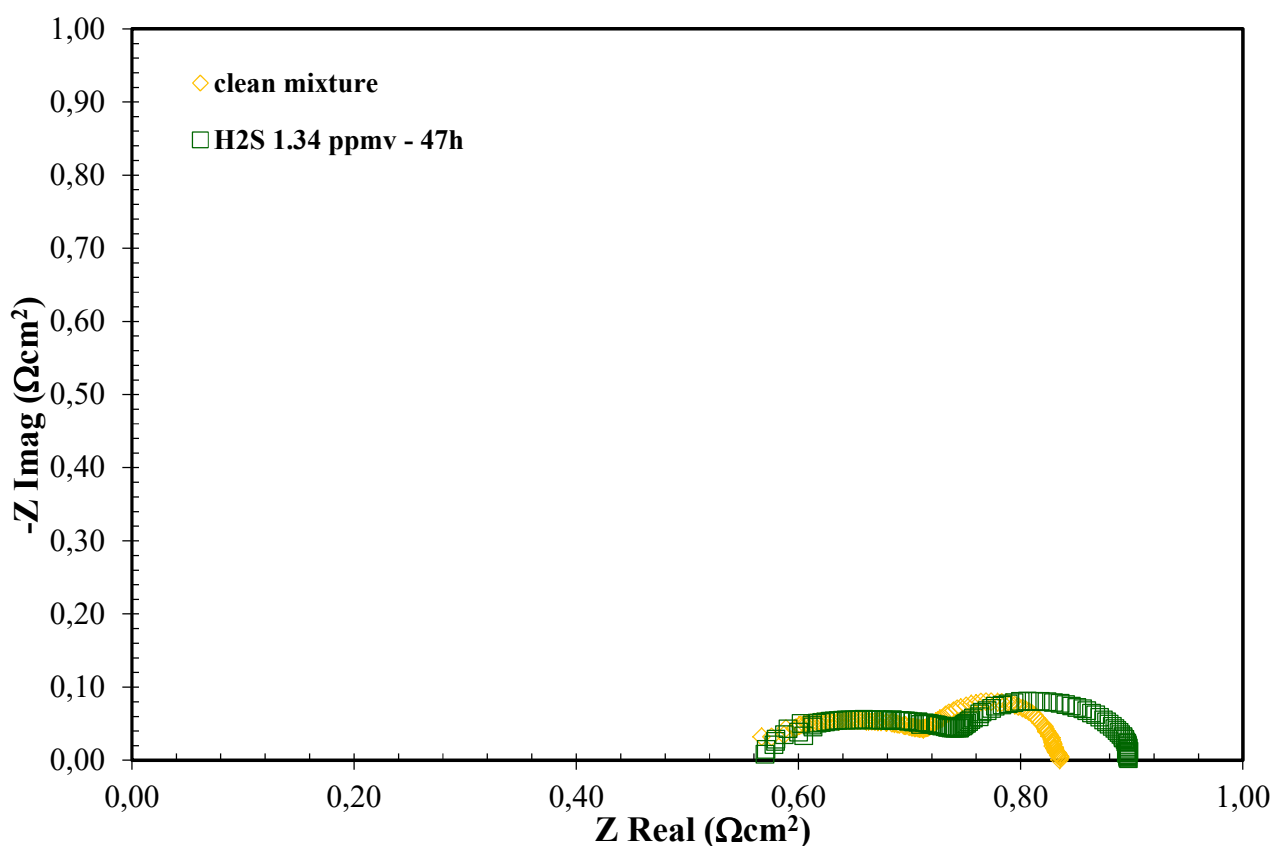


**Figure 6 – Nyquist diagram for the  $\text{H}_2\text{S}$  threshold concentration value – ASC700.**

It has been found that increasing the exposure time to the  $\text{H}_2\text{S}$  concentration raises the total ASR value. This is mainly due to the mass transport limitation, caused by Sulfur adsorption on active sites, as can be seen by observing the amplitude of the low frequency circle, which increases more than the high frequency circle (see figure 7).

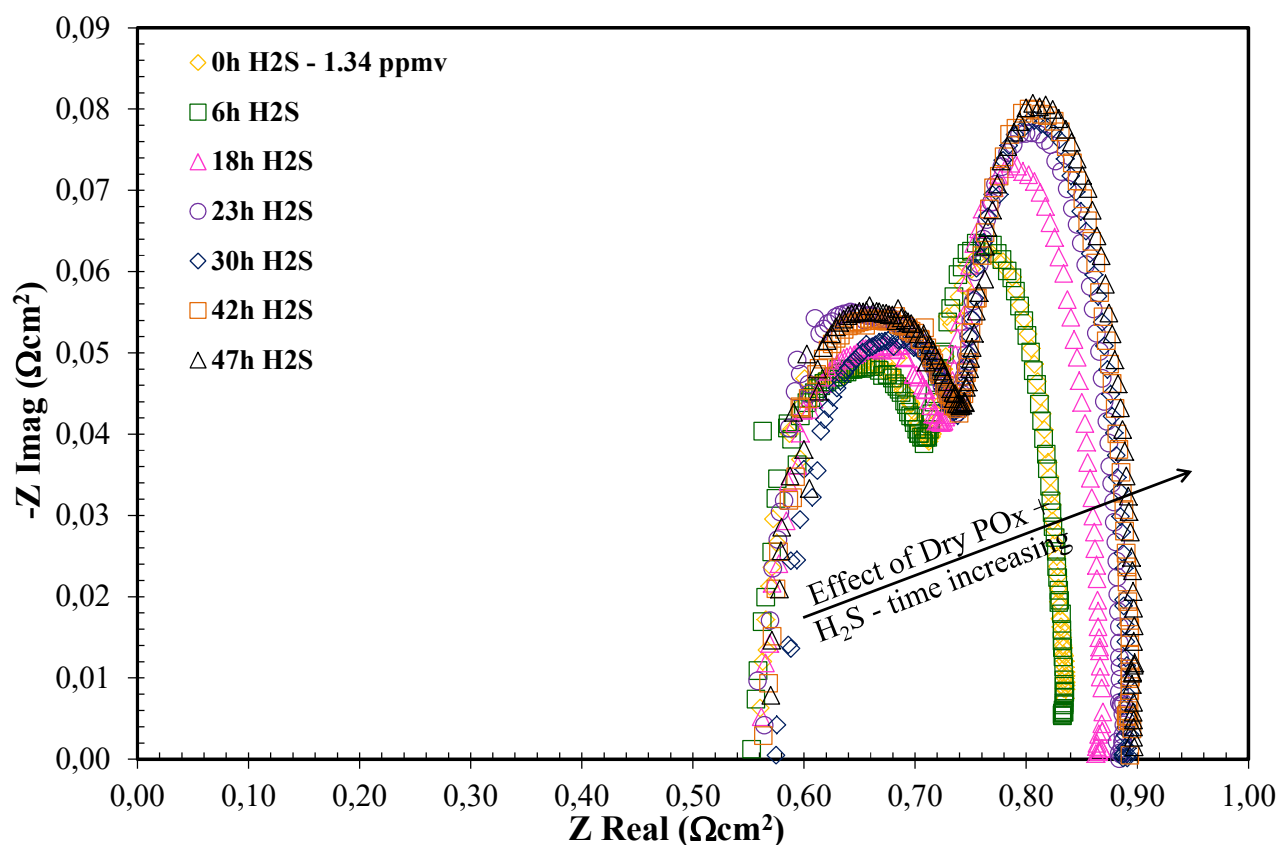


Figure 7 – Nyquist diagram for the H<sub>2</sub>S threshold concentration value – time variation – ASC700.

#### Low H<sub>2</sub>S concentration test

Figure 8 shows the Nyquist diagram for an SOFC cell fed with a gas mixture in which increasing concentrations of H<sub>2</sub>S, that is, from 78 ppb(v) to 174 ppb(v), have been added. These H<sub>2</sub>S concentration values are below the tolerable threshold value of 1 ppm(v). In fact, Figure 9 shows an almost constant trend for the three different contributions to the ASR value. It appears evident that these H<sub>2</sub>S concentrations are well tolerated by the SOFC cell. The ohmic resistance is the main contribution. The ohmic losses account for more than 50% of the total cell resistance, and an enhancement of the performance could be achieved by developing thin layer electrolytes and improved interfaces.



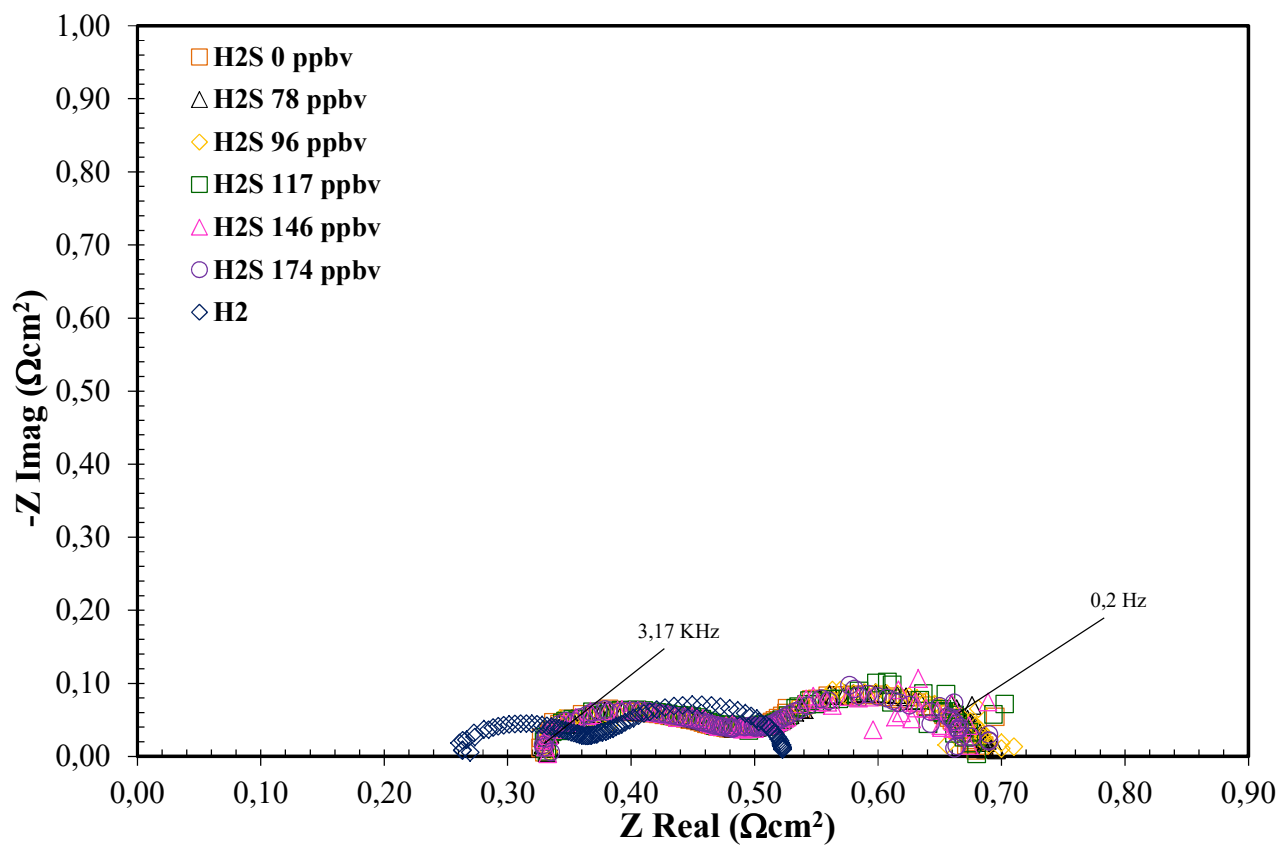
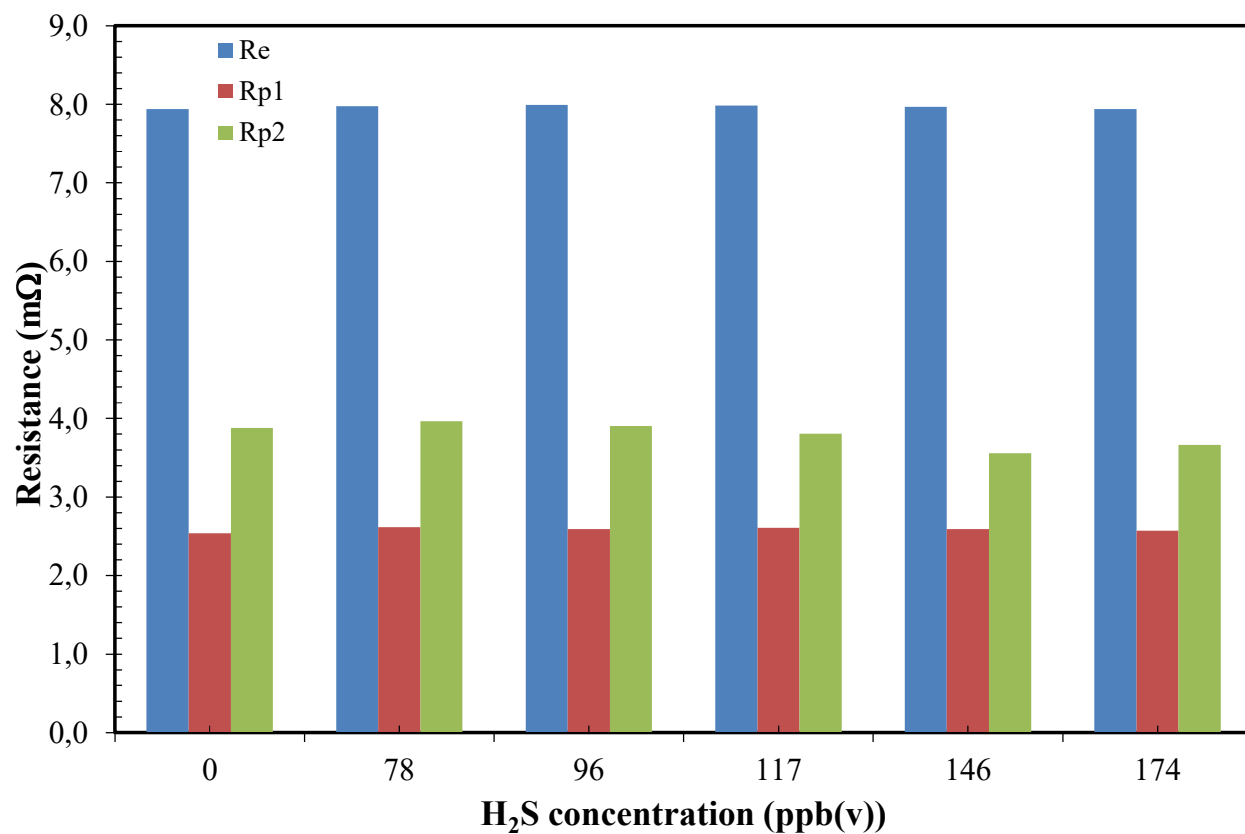


Figure 8 – Nyquist diagram for variations of the H<sub>2</sub>S “low concentration level” – ASC4.



**Figure 9 – Re and Rp values for variations of the H<sub>2</sub>S “low concentration level” – ASC4.**

Figure 8 shows how the ohmic contribution is low in the H<sub>2</sub> case, compared to the mixture adopted with the pollutants. This is due to the different electrochemical molar flows that are available.

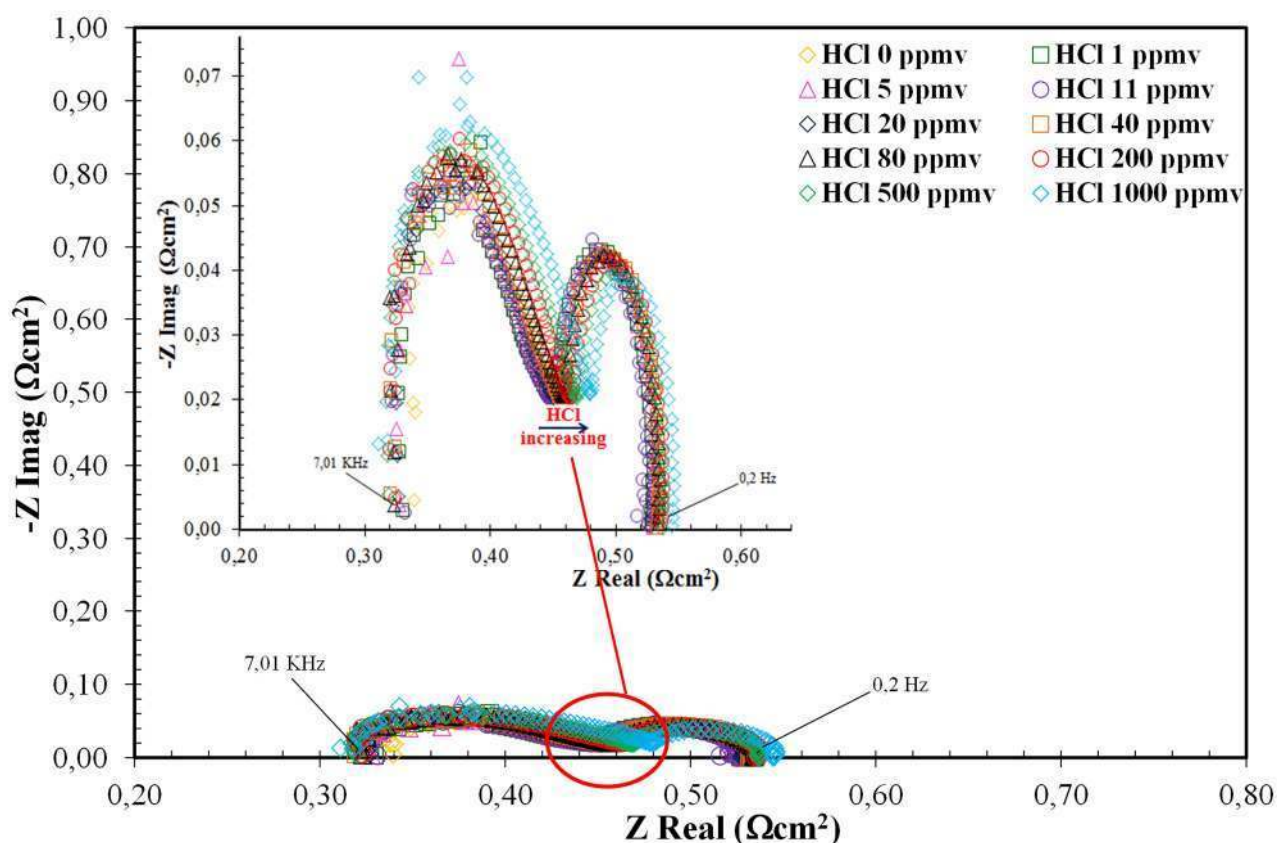
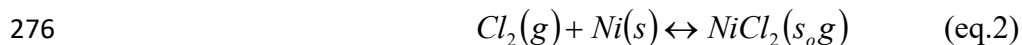
If H<sub>2</sub>S concentrations ranging from 78 to 174 ppb(v) are considered, the power loss remains quite stable and ranges from 0.13 – 0.4% of the nominal power value at zero time. This means that if the exposure time to the pollutants is increased, the electrical power loss will remain unchanged.

#### The influence of Hydrogen chloride on SOFC performance

The dependence of hydrogen chloride on the limiting factors of an anode supported fuel cell has been investigated, considering the addition of a variable concentration of HCl, ranging from 1 ppm(v) to 1000 ppm(v), to the gas reformat mixture. Figure 10 shows the Nyquist diagram with variations in the HCl concentration content in the gas mixture. Increasing the HCl content to 100, 500 or even 1000 ppm(v), does not result in a notable increase in ASR. Figure 11 clearly highlights how, below 20 ppm(v), the HCl concentration does not affect the SOFC performance. The three contributions to the EIS analysis are almost constant. If the HCl concentration is increased from 40 to 1000 ppm(v), the most influential contribution is from  $R_{high}$ . The first circle, related to the high frequency, rises and the trace compound concentration therefore increases. This circle is related to the electrochemical processes that occur at the electrodes. In accordance with these results, it has been shown how the Ni catalyst mainly acts by adsorbing HCl. HCl behaves in a similar way to H<sub>2</sub>S, but less aggressively; in fact, the tolerable limit appears to be around 20 ppm(v) or more.

These results are in agreement with those of Cayan et al., (2008), where HCl was added to an anode supported fuel cell (NiYSZ/YSZ/LSM) and unstable performance occurred at 40 and 160 ppm(v) [42]. Another study by Aravind et al., (2008) has shown how the impact of 9 ppm(v) of HCl on an NiGDC anode supported fuel cell produced no significant losses [43]. Another study on an NiYSZ cell with HCl + NH<sub>3</sub> (1 ppm(v) + 5000 ppm(v)) has shown no significant performance degradation

273 [44]. Ammonia, which is often present in coal syngas, does not represent a pollutant for SOFCs, as  
 274 reported by Cayan et al., (2008) [42]. According to Haga et al., (2008), chlorine compounds react  
 275 with Ni particles [19]. The formation of  $\text{NiCl}_2$  may be described by reaction (1):



277

278 **Figure 10 – Nyquist diagram for variations of the HCl concentration – ASC700.**

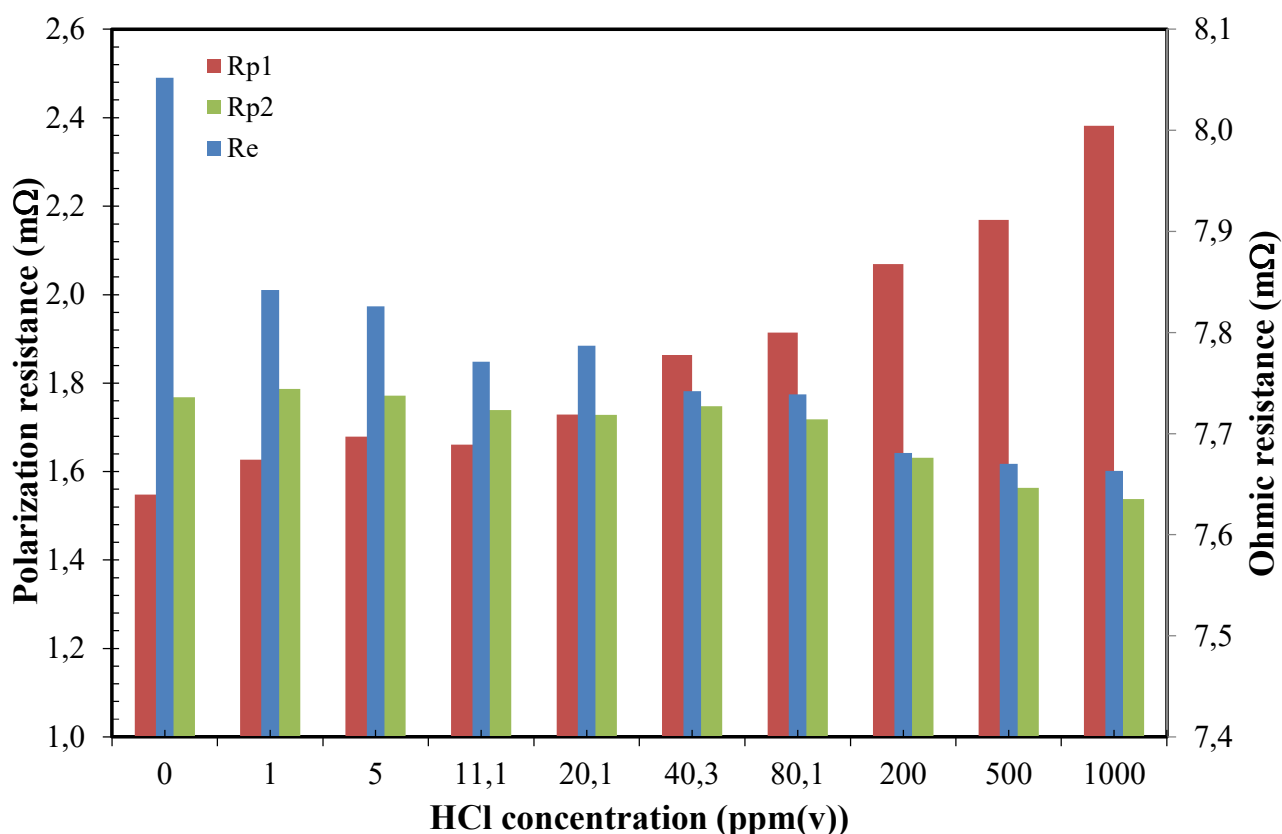


Figure 11 – Re and Rp values for variations of the HCl concentration – ASC700.

If HCl concentrations ranging from 1 to 1000 ppm(v) are considered, the related power losses remain quite stable, and range from 0.17 – 0.3% of the nominal power. This means that if the exposure time to the pollutants is increased, the electrical power loss will remain unchanged. This is due to compensation among the resistance terms, as can be seen in figure 11. The ohmic contribution increases for lower values of the polarization terms at lower HCl concentrations, while the ohmic value decreases and the polarization term increases for higher HCl concentrations.

#### The influence of Octamethylcyclotetrasiloxane on SOFC performance

Siloxanes, which are organosilicon compounds, are often contained in the biogas obtained from the anaerobic digestion of sewage sludge and, to a lesser extent, in the biogas of OFMSW. Siloxanes originate from many different industrial processes and consumer products, such as hygiene products, cosmetics and biopharmaceuticals, fuel additives, car waxes, detergents and antifoams [45,46]. The influence of siloxanes on SOFC performance has been studied by a few researchers.

293 Haga et al., (2008) showed that changes in cell voltage occurred when adding 10 ppm(v) of D5 in  
294 3%-humidified H<sub>2</sub> at 800 °C, 900 °C, and 1000 °C. The cell voltage decreased gradually in time  
295 and, after 30–50 h, resulted in a fatal degradation of the cell performance. This degradation was  
296 confirmed from an observation of the formation of SiO<sub>2</sub> (s) in the porous cermet anodes. Madi et al.,  
297 (2015) studied the effect of D4 in a single anode based SOFC [20]. The results highlighted an  
298 important influence of siloxanes on SOFC performance. In the present study,  
299 octamethylcyclotetrasiloxane (D4) was tested with a biogas reformat mixture in a commercial  
300 TOFC cell. The concentration ranged from 111 ppb(v) to 1.92 ppm(v). This concentration range  
301 was selected to reproduce a possible biogas mixture from a real plant. In fact, data recorded from a  
302 real WWTP (SMAT site) showed a D4 concentration that ranged from 0.1 to 0.25 ppm(v) and an  
303 L4 concentration that ranged from 0.2 to 0.92 ppm(v). Figure 12 depicts the Nyquist diagram for  
304 the TOFC cell fed with a variable D4 concentration. Figure 13 shows the three contributions to the  
305 cell losses. As can be seen from the results, if the D4 concentration is increased, the R<sub>high</sub> value  
306 rises, while the other two terms remain constant. The upper right part of Figure 12 shows how the  
307 cell performance is irreversibly affected by the D4 test. This is due to silica precipitation, which  
308 may cause a decrease in the active triple phase boundary (TPB) areas.

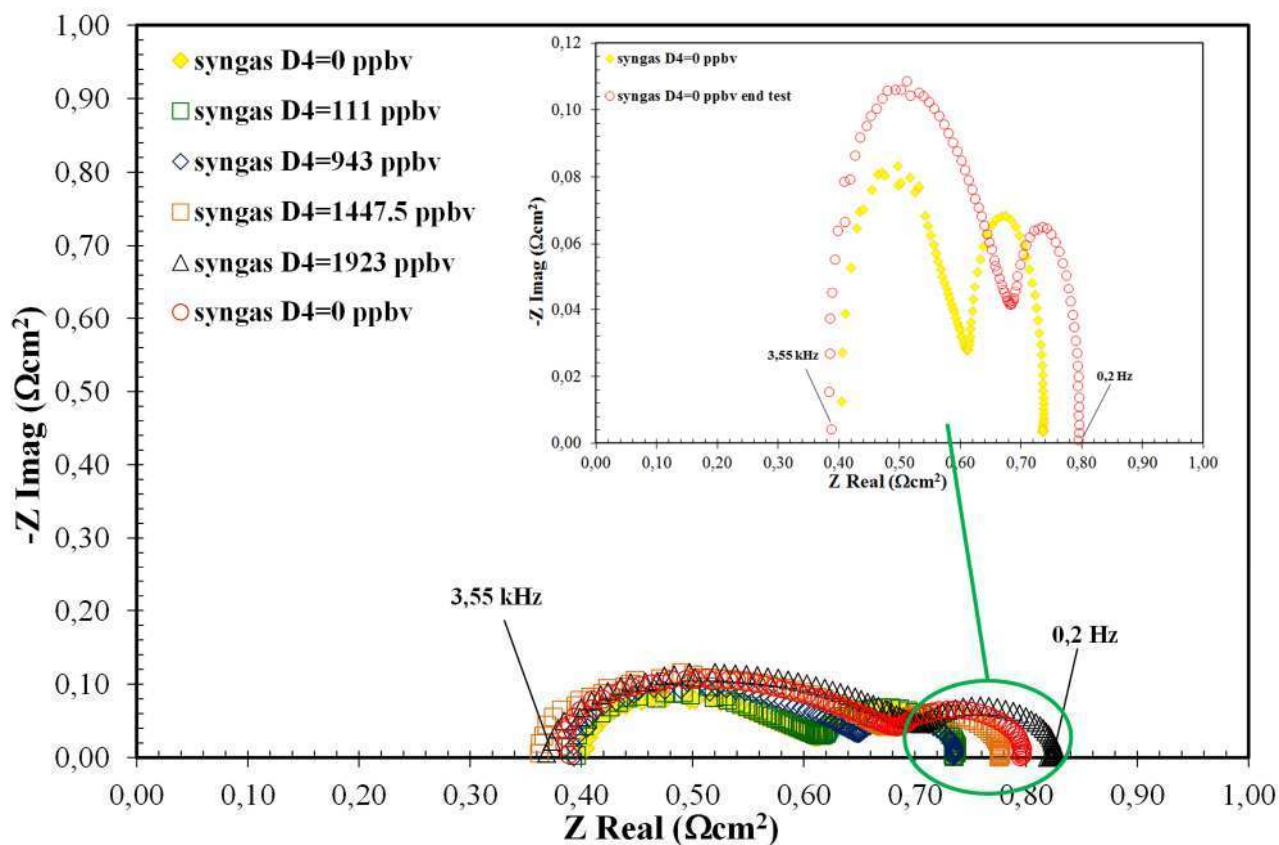
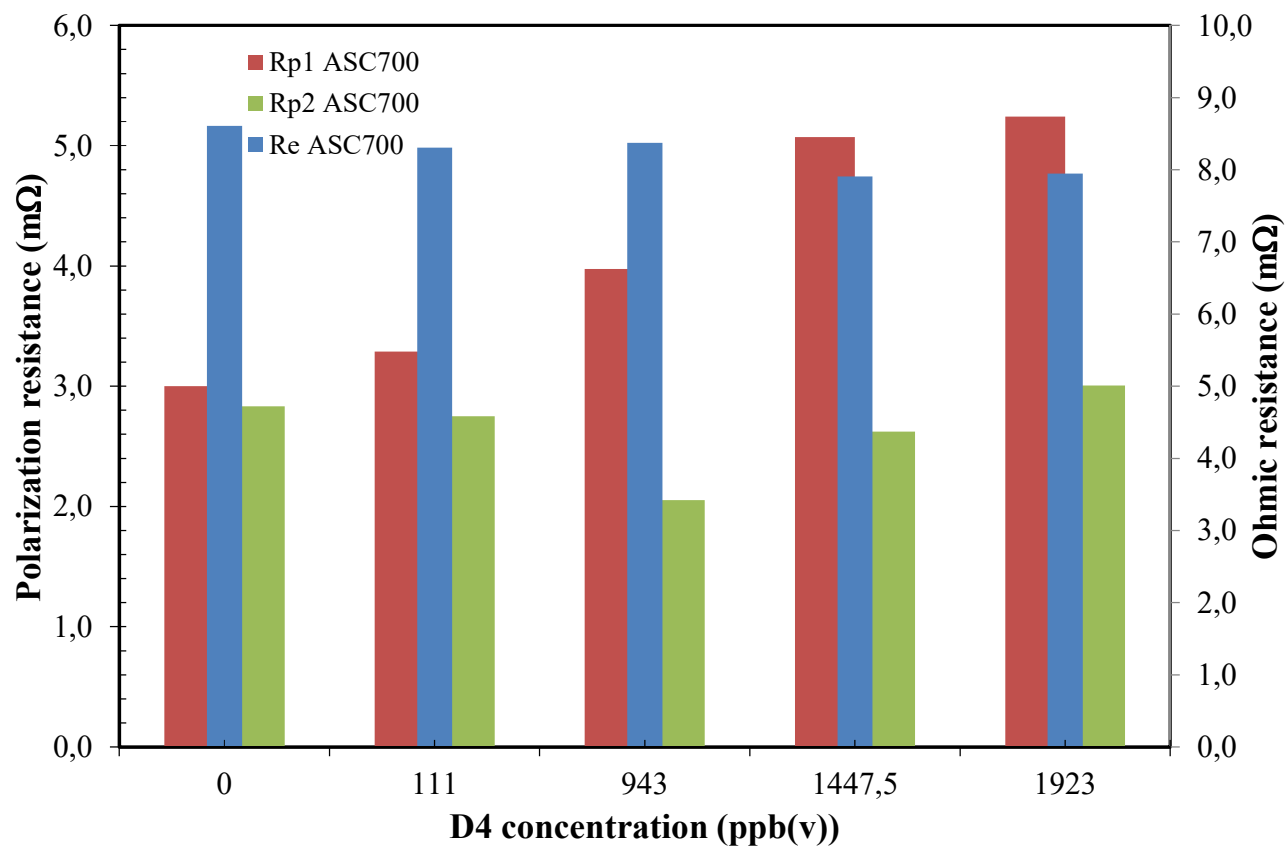


Figure 12 – Nyquist diagram for variations of the D4 concentration – TOFC.



**Figure 13 – Re and Rp values for variations of the D4 concentration – TOFC.**

If D4 concentrations ranging from 111 to 1923 ppb(v) are considered, the power losses increase for D4 values above 1 ppm(v). The power loss ranges from 0.17 – 2.32 % of the nominal power value. This means that if the exposure time to the pollutants is increased, the electrical power loss will also rise, thereby increasing the resistance value, especially as far as the  $R_{p1}$  term is concerned.

#### The influence of tars, toluene and naphthalene on SOFC performance

##### Naphthalene

The direct use of biosyngas may degrade the performance of SOFCs as it contains a number of minor species. Among these trace species, tars have been identified as one of the main concerns in the development of gasifier + SOFC power systems, as they can potentially deactivate the anode catalysts and degrade the performance of the fuel cells through carbon deposition. Aravind et al., (2008) studied the performance of an Ni-GDC anode operation with a naphthalene content of about 110 ppm(v) in an  $H_2+N_2$  matrix. No performance loss was observed and no carbon or other product gas trace constituent contamination of the anodes was found when the SOFC membranes were examined by means of SEM/EDS after the tests [43].

The results reported in this section are in agreement with those of Aravind et al., (2008). An  $H_2+N_2$  mixture with a naphthalene content of 25 ppm(v) does not in fact show any remarkable cell performance decrease (see figure 14). If a syngas mixture is instead considered, the cell performance is influenced to a great extent by the  $C_{10}H_8$  content. Figure 14 depicts the Nyquist curves with and without the pollutant concentration. A syngas mixture with 9.3 ppm(v) of  $C_{10}H_8$  shows a notable resistance increase.

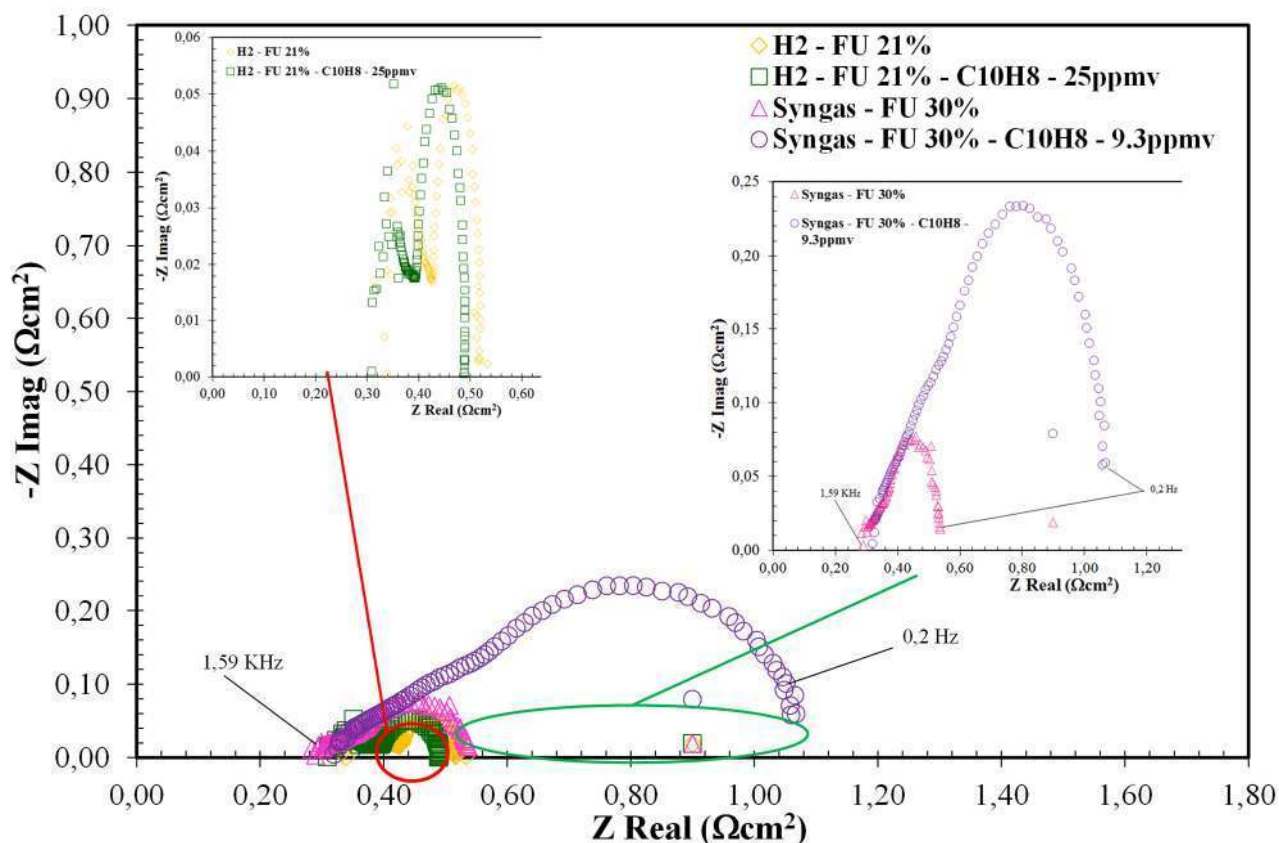
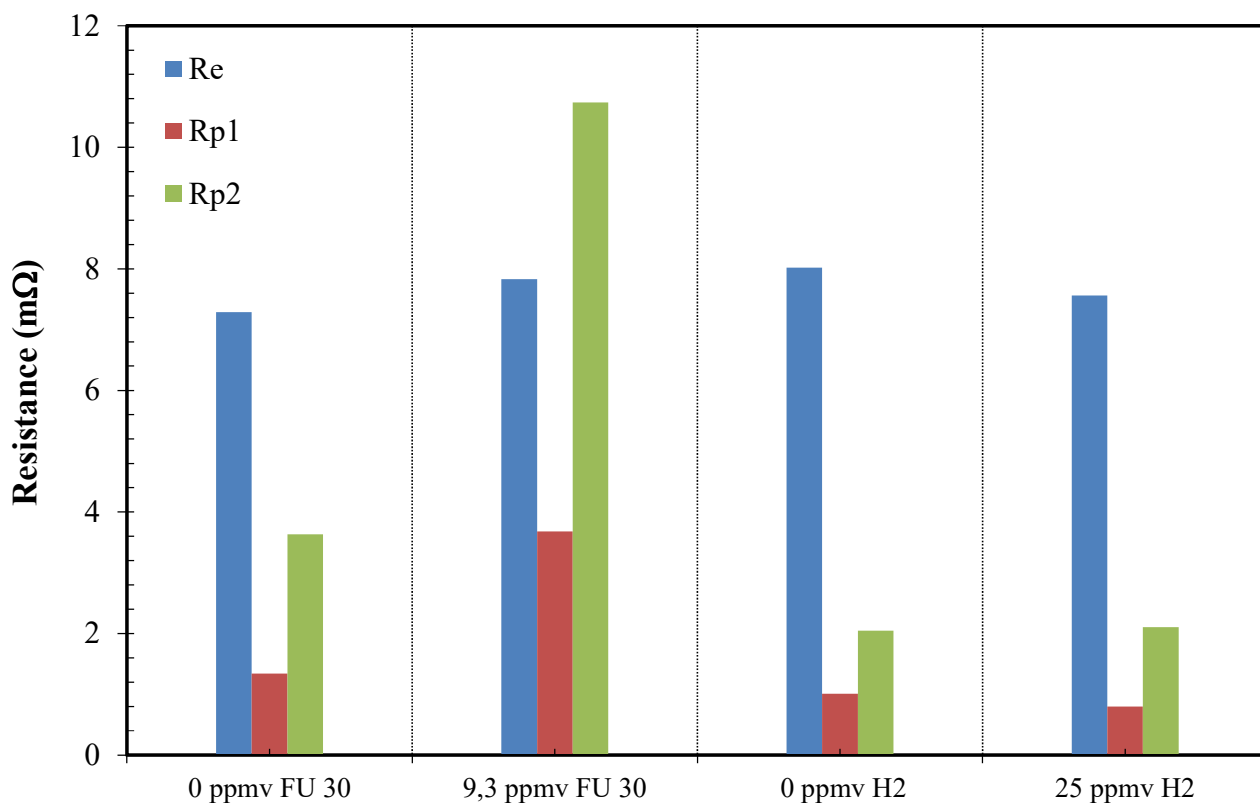


Figure 14 – Nyquist diagram for variations of the  $C_{10}H_8$  concentration FU 30% – ASC700.

In figure 15 the three contributions of loss, are showed: at high, medium and low frequency value. For the  $H_2$  case, the ohmic term ( $R_e$ ) and the polarization terms ( $R_{p1}$  and  $R_{p2}$ ) remain constant throughout the test. This demonstrates that the  $C_{10}H_8$  concentration is not a problem in this condition, as also reported in literature studies [43]. On the contrary, if a syngas mixture and a  $C_{10}H_8$  concentration of 9.3 ppm(v) are considered, the polarization losses show a significant increase. The low frequency term ( $R_{p2}$ ), related to the resistance of the mass transport phenomena, shows the largest increase. The high frequency term ( $R_{p1}$ ), related to the electrochemical processes, also increases, but to a lesser extent.





**Figure 15 – Re and Rp values for variations of the  $C_{10}H_8$  concentration – ASC700.**

These results show how a low  $C_{10}H_8$  concentration could be dangerous, depending on which gas mixture is used to feed the fuel cell. The adsorption and desorption of naphthalene obviously interfere with the reforming of methane and WGS (i.e., CO conversion to  $H_2$ ) by decreasing the reactive surface of the anodes.

If  $C_{10}H_8$  concentrations ranging from 0 to 9.3 ppm(v) are considered, the power losses increase to achieve 15.5% of the nominal power value at zero time. This means that, if the exposure time to the pollutants is increased, the electrical power loss will also rise, thereby increasing the resistance value, especially as far as the Rp2 term is concerned.

### Toluene

Toluene is one of the lightest tar compounds and it can be easily detected in biogenous fuels, such as biogas from organic waste [9]. Several studies have investigated the impact of tars on the

356 performance of SOFCs [18,43,47–49]. Most of these studies have focused on the influence of the  
357 tar compound without considering the carbon content in the gas mixture [18,47,48]. Lorente et al.,  
358 (2012) studied Ni/CGO and Ni/YSZ cells under a tar load of 15 g/Nm<sup>3</sup> (with toluene as the model  
359 compound) [18]. In this study, it was found that Ni/CGO shows a better performance (less carbon  
360 formation) than Ni/YSZ in the presence of toluene. This result is in agreement with the expected  
361 behavior of ceria-based anodes, which have been recognized to be effective in suppressing carbon  
362 deposition due to the redox nature of ceria [50]. The amount of carbon deposited on the catalyst was  
363 seen to decrease for an increasing steam content in the gas [18]. Toluene, due to the high reactivity  
364 of lower weight hydrocarbons, represents the worst case scenario for tar compounds and for this  
365 reason it has been selected in the present study. No attempts have been made to study the effects of  
366 low toluene concentrations on SOFC performance. The results of tests on low concentrations of  
367 toluene, considering a slip over from a gas cleaning section, are presented in this section. The  
368 experimental works have demonstrated that if the most dangerous compounds for SOFCs: sulfurs,  
369 aromatic, terpenes and carbonyl compounds, are lowered to just a few ppm(v), the performances of  
370 SOFCs remain stable [1].

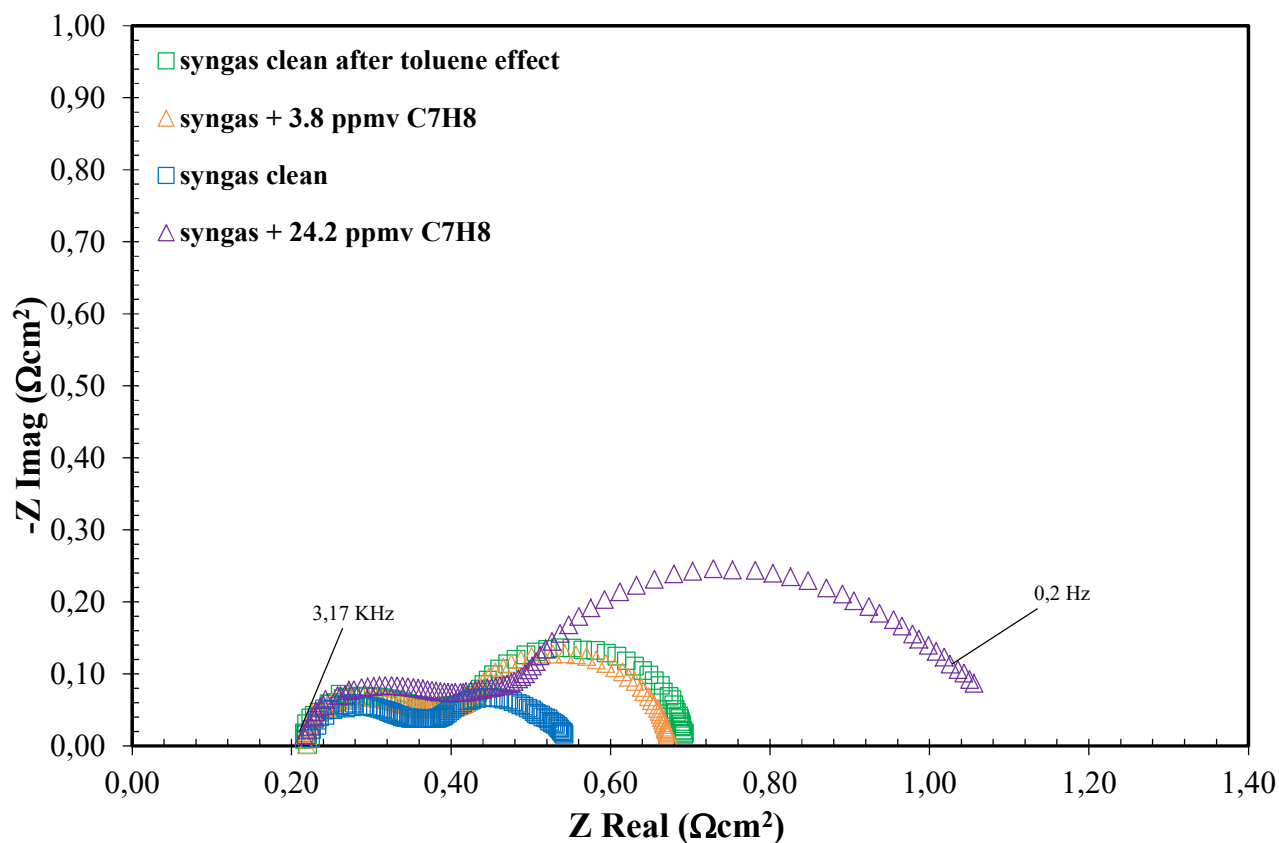
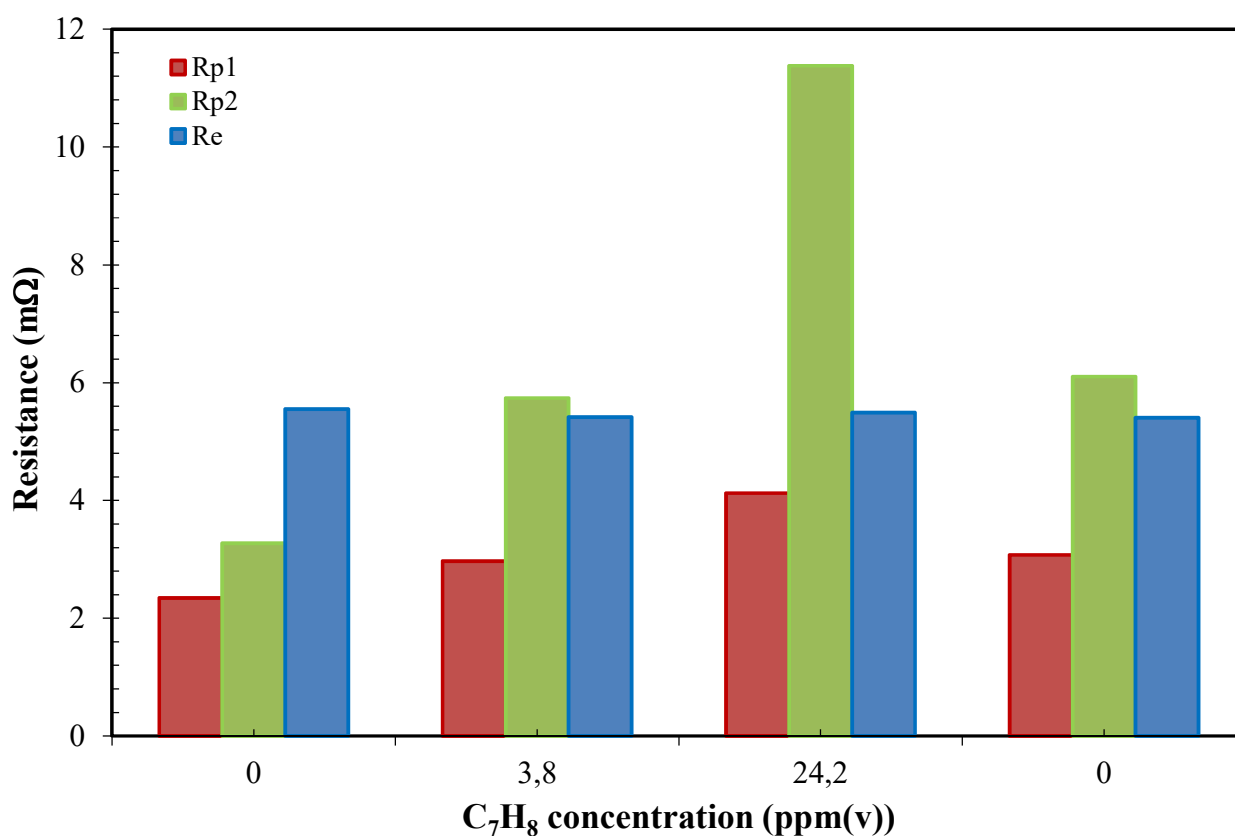


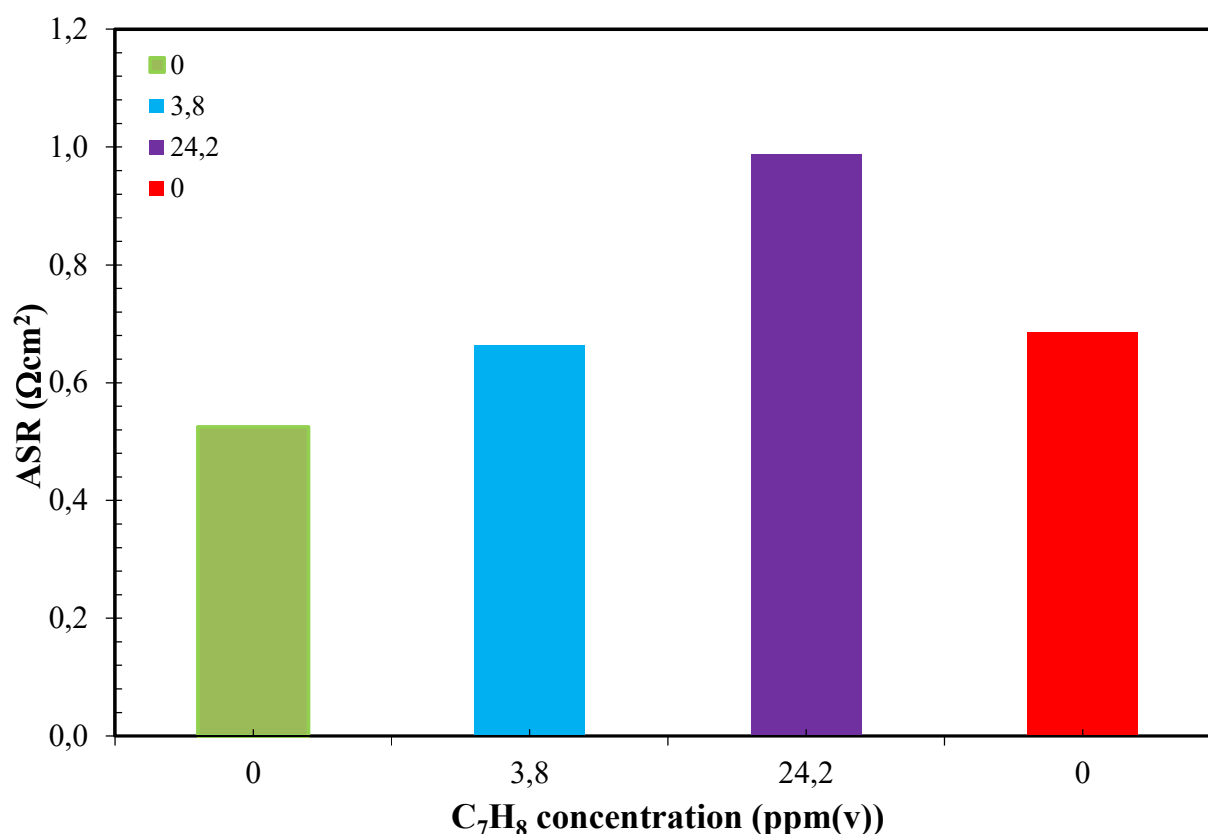
Figure 16 – Nyquist diagram for variations of the C<sub>7</sub>H<sub>8</sub> concentration – ASC700.

Figure 16 shows the Nyquist diagram of a SOFC cell being fed with a syngas mixture with variations in the C<sub>7</sub>H<sub>8</sub> concentration. As can be seen, already after 3.8 and 24.2 ppm(v) of toluene, the SOFC performances are irreversibly influenced. In fact, if the toluene content is removed, the impedance curve does not recover the starting value. The ohmic contribution remains unchanged, but the polarization losses increase, see figure 17. If the toluene concentration is increased, the polarization losses increase significantly, especially at the low frequency value. This circle is related to the mass transport phenomenon.



**Figure 17 – Re and Rp values for variations of the C<sub>7</sub>H<sub>8</sub> concentration – TOFC.**

As reported for the naphthalene test, toluene adsorption and desorption obviously interferes with the reforming of methane and WGS (i.e., CO conversion to H<sub>2</sub>) by decreasing the reactive surface and SOFC performance.



**Figure 18 – Area specific resistance diagram for variations of the C<sub>7</sub>H<sub>8</sub> concentration – ASC700.**

Figure 18 shows the ASR values. A slight increase in the ASR can be observed at 3.8 ppm(v) – which is an almost tolerable limit for SOFC performance – but if the toluene concentration increases to 24.2 ppm(v), the performance decreases to a great extent (+40% losses).

If C<sub>7</sub>H<sub>8</sub> concentrations ranging from 0 to 24.2 ppm(v) are considered, the power losses increase to achieve 14.58% of the nominal power value at zero time. This means that if the exposure time to the pollutants is increased, the electrical power loss will also rise, thereby increasing the resistance value, especially as far as the Rp2 term is concerned.

#### The influence of ethylene Hydrocarbons on SOFC performance

Ethylene is a common hydrocarbon that can be detected in almost all biogenous fuels. Ethylene is a fuel like methane, and like the latter it has to be reformed into hydrogen and carbon monoxide. Ethylene concentrations above a certain level, which mainly depends on the operating temperature,

are difficult to reform. The steam reforming of ethylene is dealt with in this section, considering a concentration value that is representative of a biogas obtained from organic waste digestion. Figure 19 shows the impedance spectra of two gas mixtures containing 0 ppm(v) of ethylene and 371.2 ppm(v) of  $C_2H_2$ . By observing the zoom window, it can be seen that ethylene does not influence SOFC performance negatively.

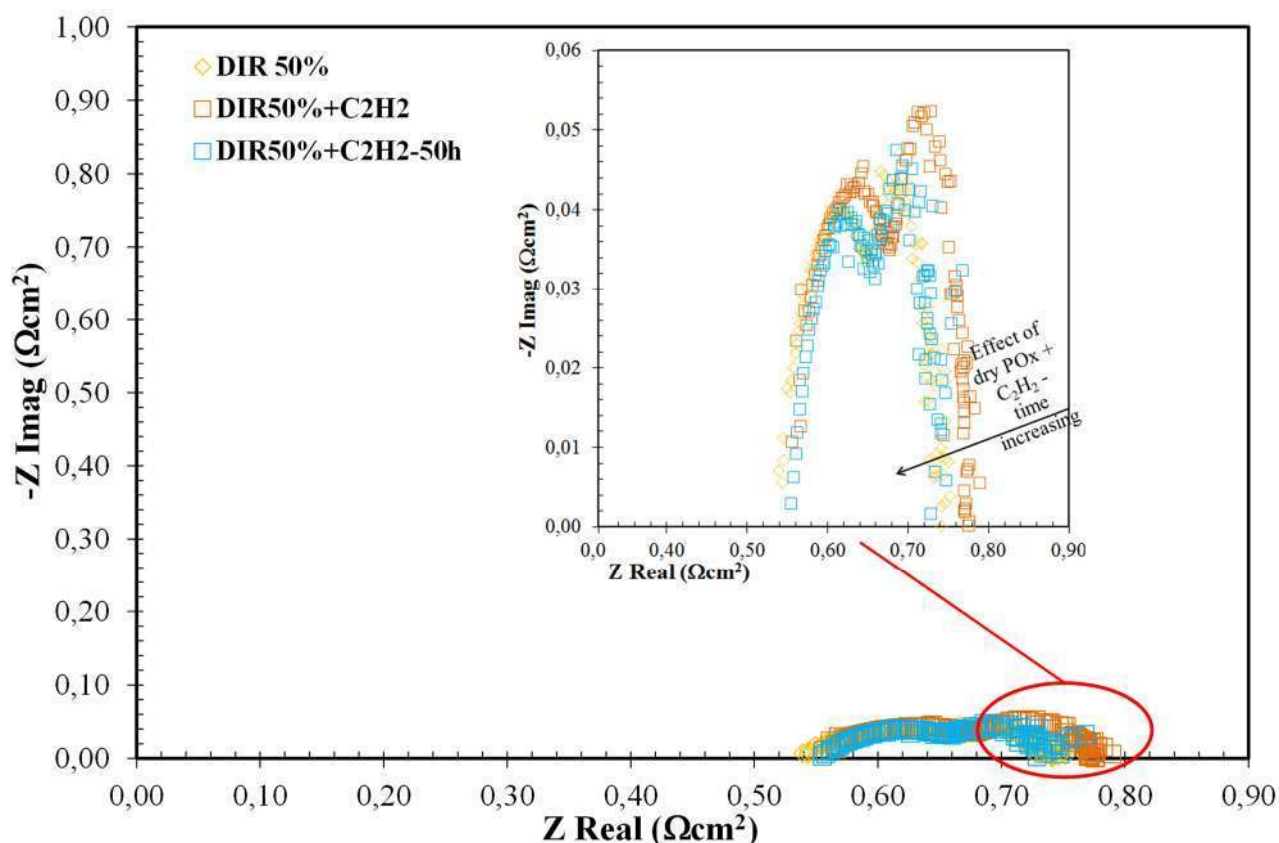


Figure 19 – Nyquist diagram for variations of the  $C_2H_2$  concentration – ASC700.

Figure 20 depicts the contribution of the performance losses. Instead of increasing the polarization losses, ethylene improves SOFC performance. This is due to the increase in the available electrochemical fuel, which is caused by an improvement in the reforming reactions.

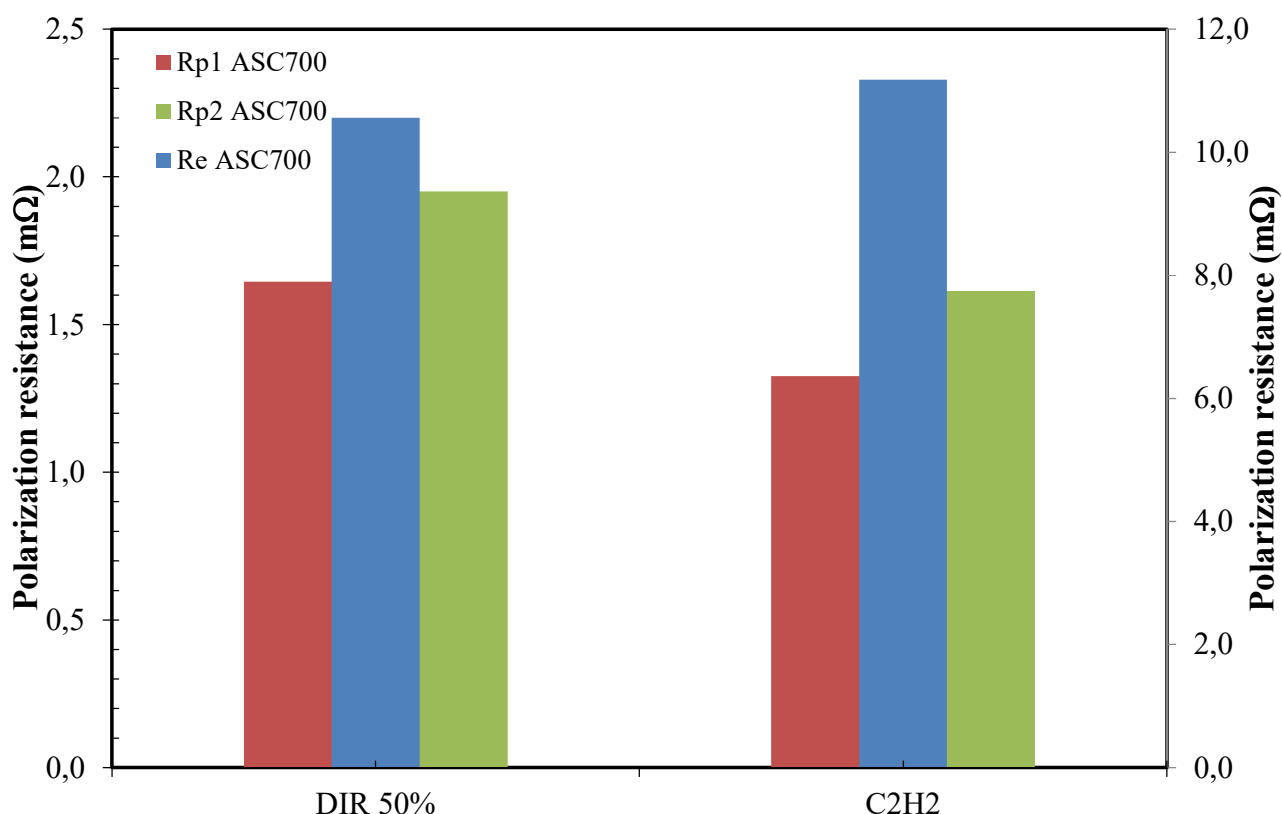


Figure 20 – Re and Rp values for variations of the the C<sub>2</sub>H<sub>2</sub> concentration – ASC700.

#### The influence of Multi concentrations on SOFC performance

Since the H<sub>2</sub>S concentration has been considered as the most dangerous compound for SOFCs, its contemporary presence with other trace compounds has been studied.

#### H<sub>2</sub>S + C<sub>2</sub>H<sub>2</sub>

The addition of a hydrogen sulfide content of 1.34 ppm(v) to a gas mixture influences the SOFC performance. An increase in the total ASR value has been registered, see figure 21. The H<sub>2</sub>S concentration mainly affects the mass transport phenomena and the electrochemical processes, thus reducing the TPB areas, as reported in figure 22.

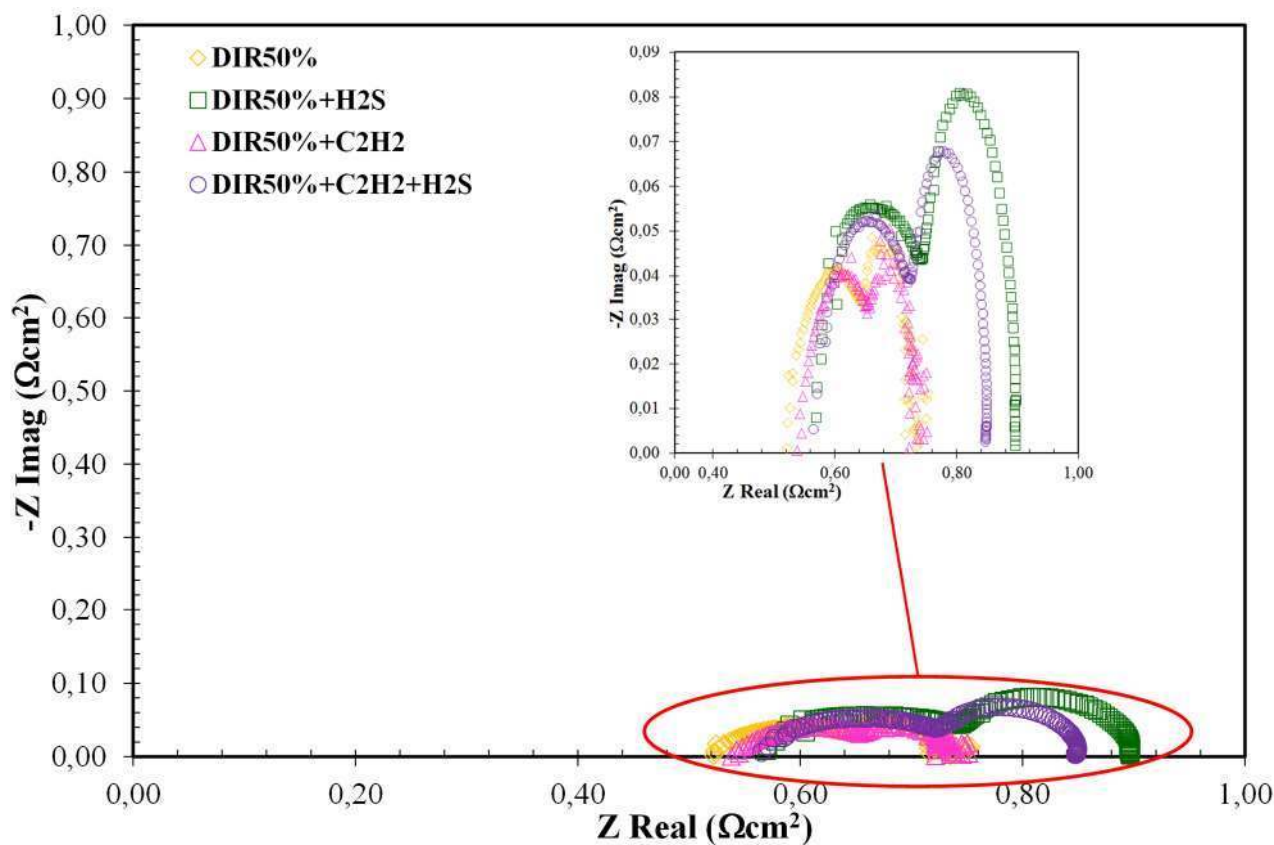


Figure 21 – Nyquist diagram for variations of the C<sub>2</sub>H<sub>2</sub> and C<sub>2</sub>H<sub>2</sub>+H<sub>2</sub>S concentrations – ASC700.

If a C<sub>2</sub>H<sub>2</sub> concentration of 371.2 ppm(v) is added to the H<sub>2</sub>S concentration, the total losses decrease, see figure 20. C<sub>2</sub>H<sub>2</sub> affects the reduction of the polarization losses and in particular the mass transport resistance, see figures 22 and 23.



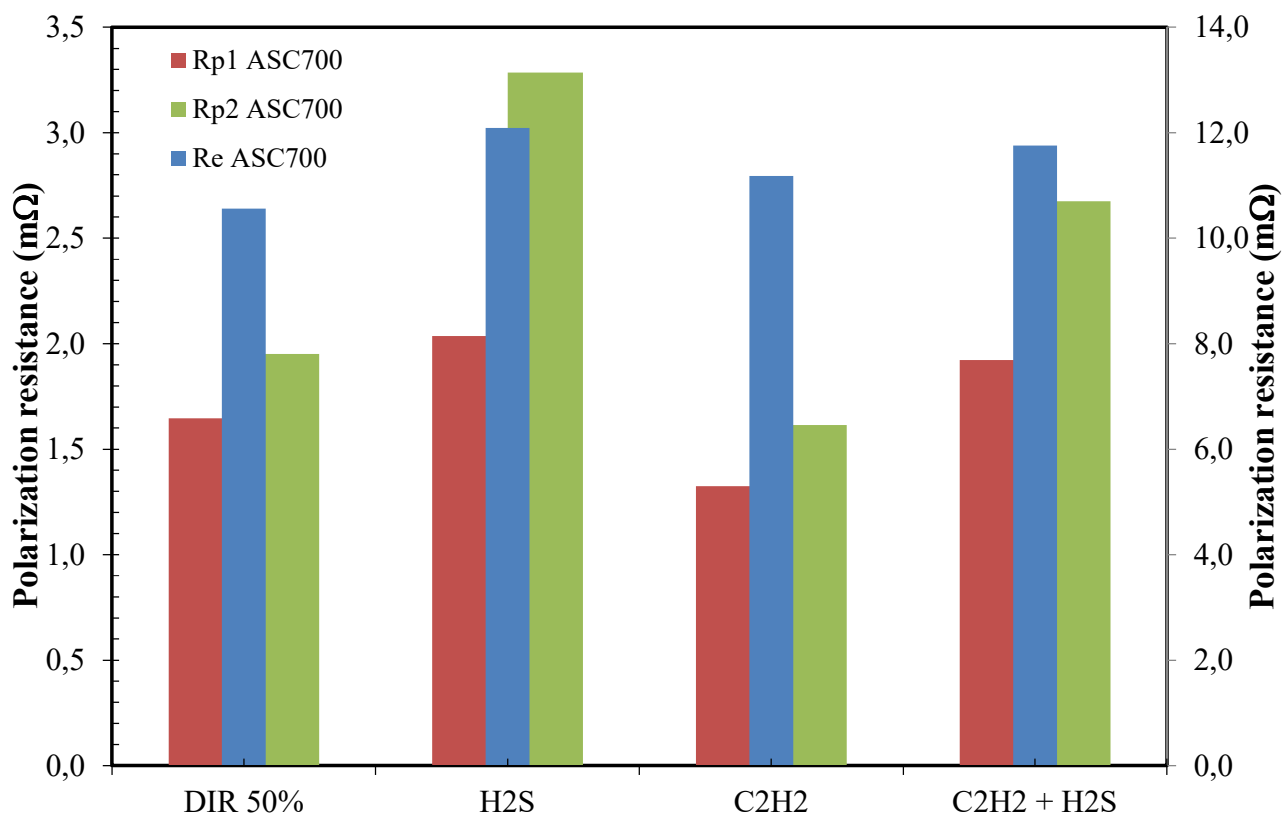
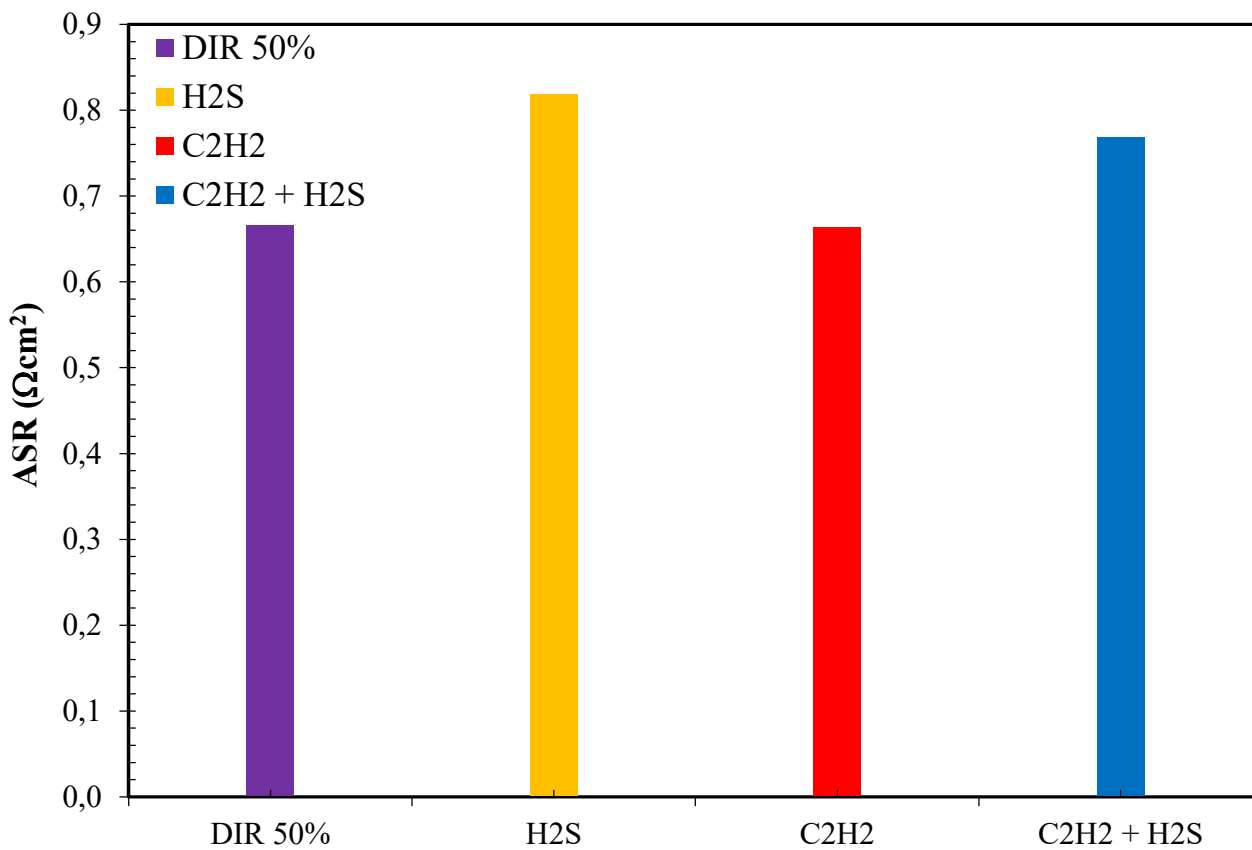


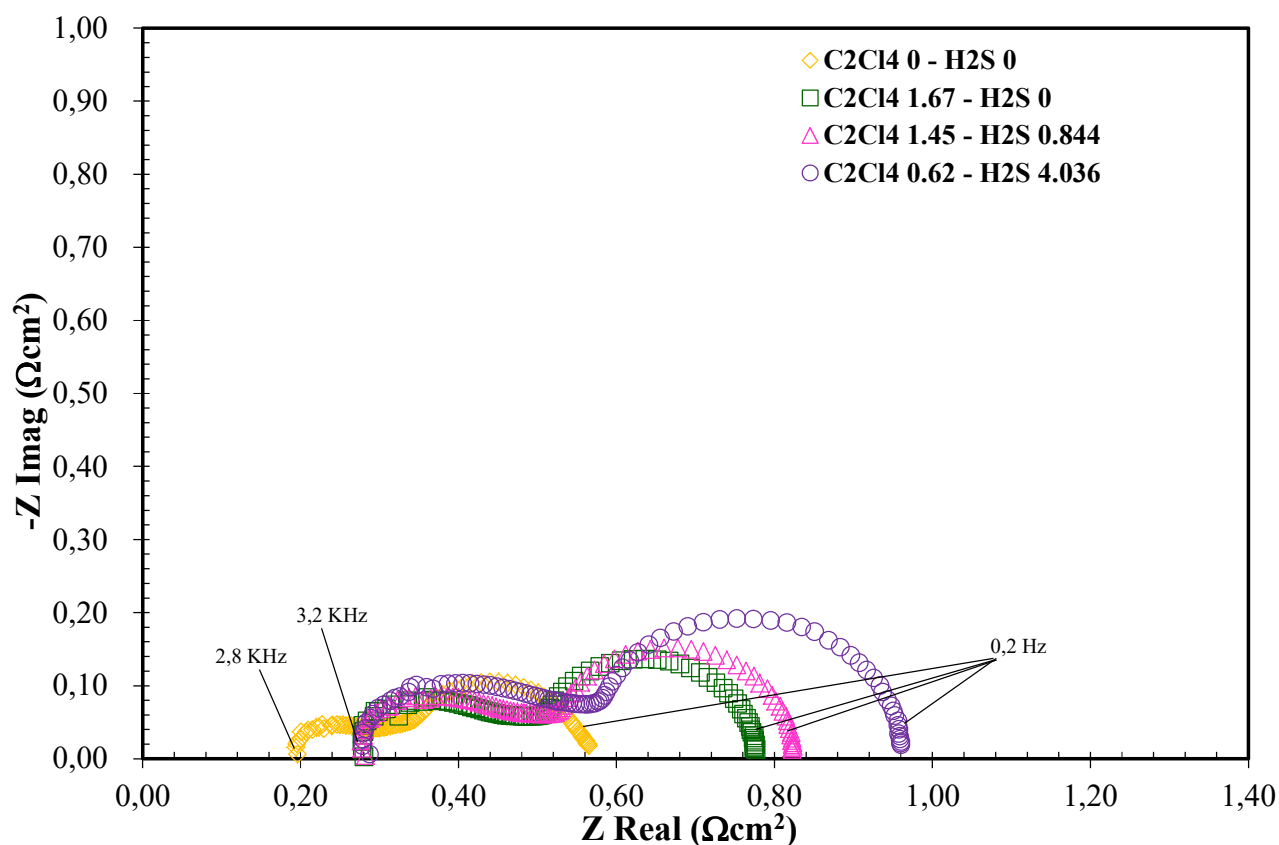
Figure 22 – Re and Rp values for variations of the C<sub>2</sub>H<sub>2</sub> and C<sub>2</sub>H<sub>2</sub>+H<sub>2</sub>S concentration – ASC700.



428 **Figure 23 – Area specific resistance diagram for variations of the  $C_2H_2$  and  $C_2H_2+H_2S$  concentrations – ASC700.**  
 429 The ASR values are influenced positively by the  $C_2H_2$  concentration, and a reduction in the double  
 430 compound case is registered for  $H_2S$ .

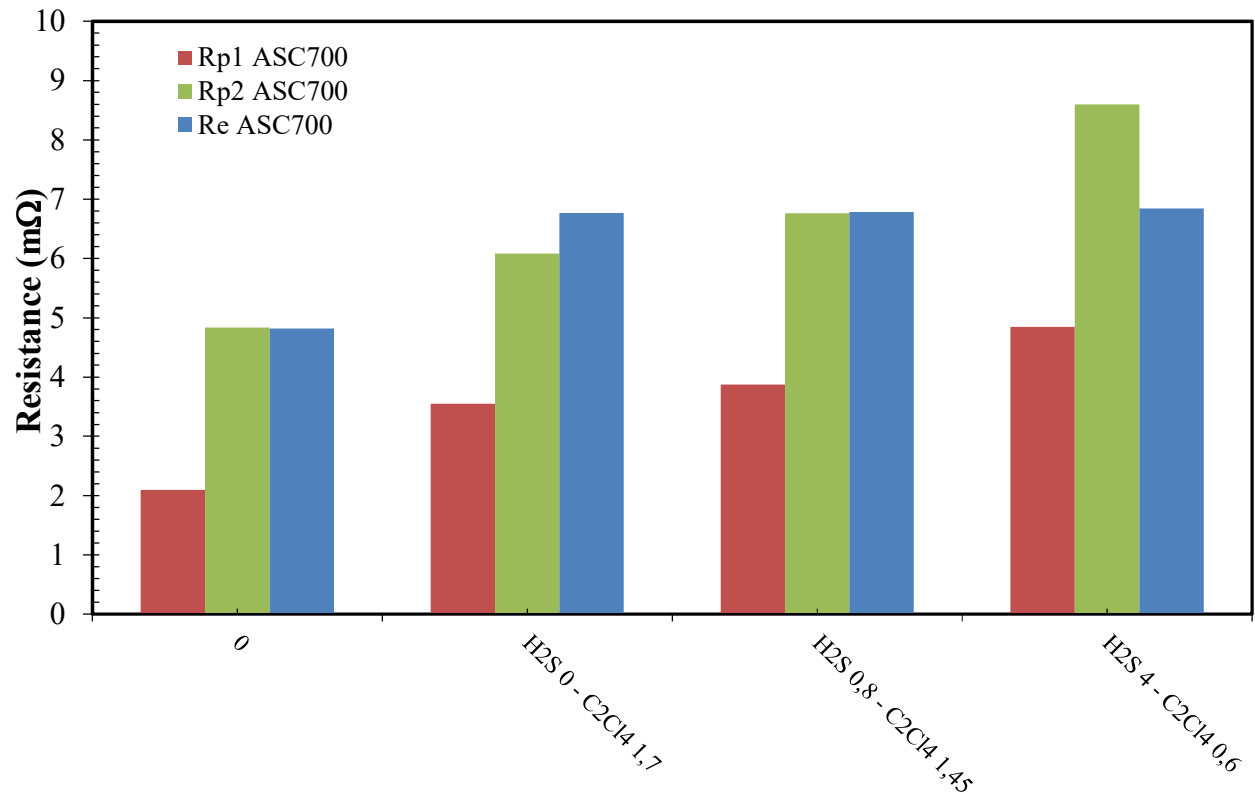
#### 431 $H_2S + C_2Cl_4$

432 As previously mentioned,  $H_2S$  is the most detrimental compound, and the addition of chlorine has  
 433 therefore been studied. Tetrachloroethylene (TCE) is a chloro compound that can be detected in a  
 434 biogenous fuel, especially from waste water sludges. The possible implications of the inclusion of  
 435 this compound on SOFC performance have been studied and the results are presented in this  
 436 section. Concentrations ranging from 0.62 to 1.67 ppm(v) of TCE and 4 to 0 ppm(v) of  $H_2S$  have  
 437 been considered.



438  
 439 **Figure 24 – Nyquist diagram for variations of the  $C_2Cl_4+H_2S$  concentration – ASC700.**

440 If the spectra obtained from the clean condition ( $C_2Cl_4$ -0 ppm(v) +  $H_2S$ -0 ppm(v)) are compared  
441 with those of the other gas mixture, it can be seen that the ohmic part rises by the same quantity in  
442 all three mixtures. This result is related to the different electrochemical molar fuel contents. As  
443 reported in figure 25, the ohmic contribution remains constant in the double contaminant case. The  
444 polarization losses increase the most for the highest  $H_2S$  concentration case. This shows how the  
445 sulfur compound is a heavier contaminant than chlorine.  $C_2Cl_4$  acts mainly on the high frequency  
446 polarization term, that is, on the electrochemical processes caused by the adsorption/desorption  
447 behavior of chlorine. The term related to the transport phenomena is instead influenced more by the  
448 sulfur compound.

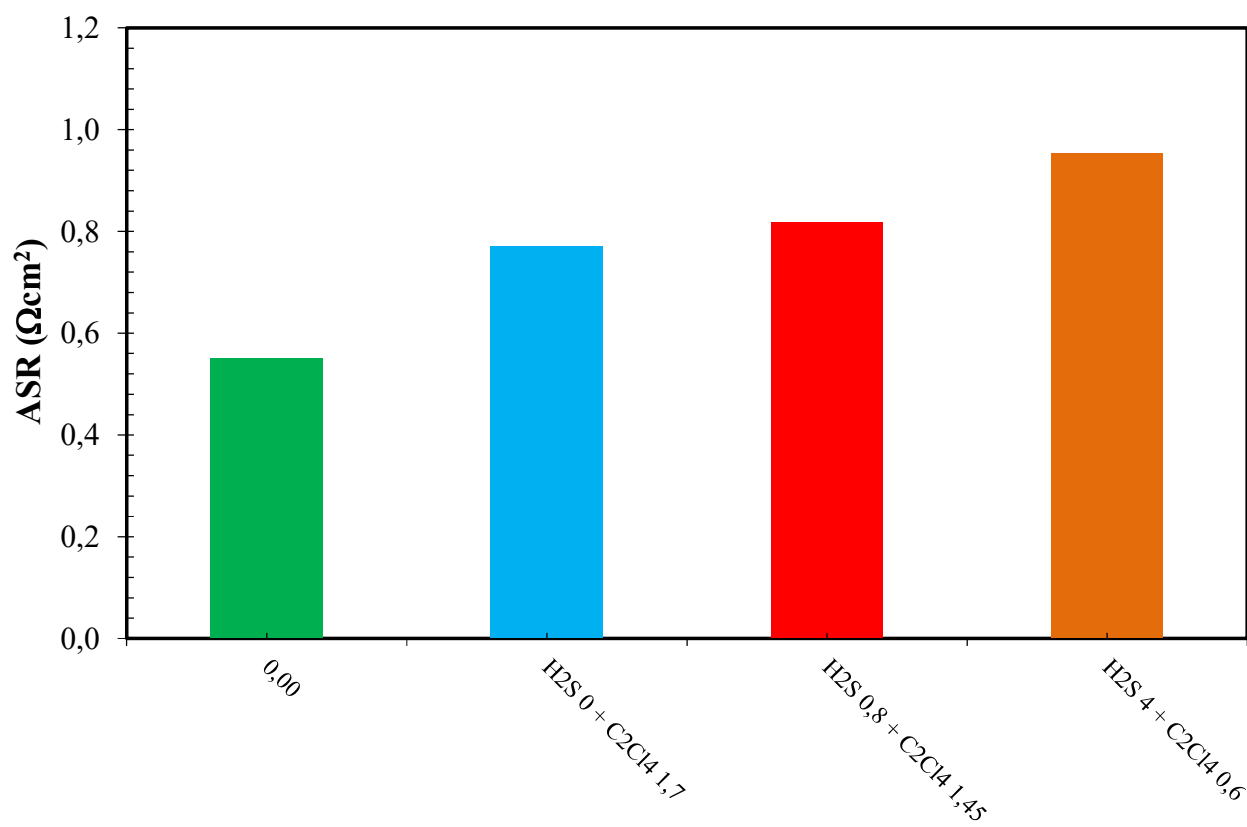


449

450 **Figure 25 – Re and Rp values for variations of the  $C_2Cl_4+H_2S$  concentration – ASC700.**

451 The worst case scenario for the SOFC performance is related to the sulfur compound content, as  
452 reported in figure 25, where the highest ASR value is achieved. If the  $H_2S$  4 ppm(v) +  $C_2Cl_4$  0.6

453 ppm(v) case is compared with the H<sub>2</sub>S 4 ppm(v) case, it can be seen that chlorine does not cause a  
 454 deterioration of the cell performance.



455

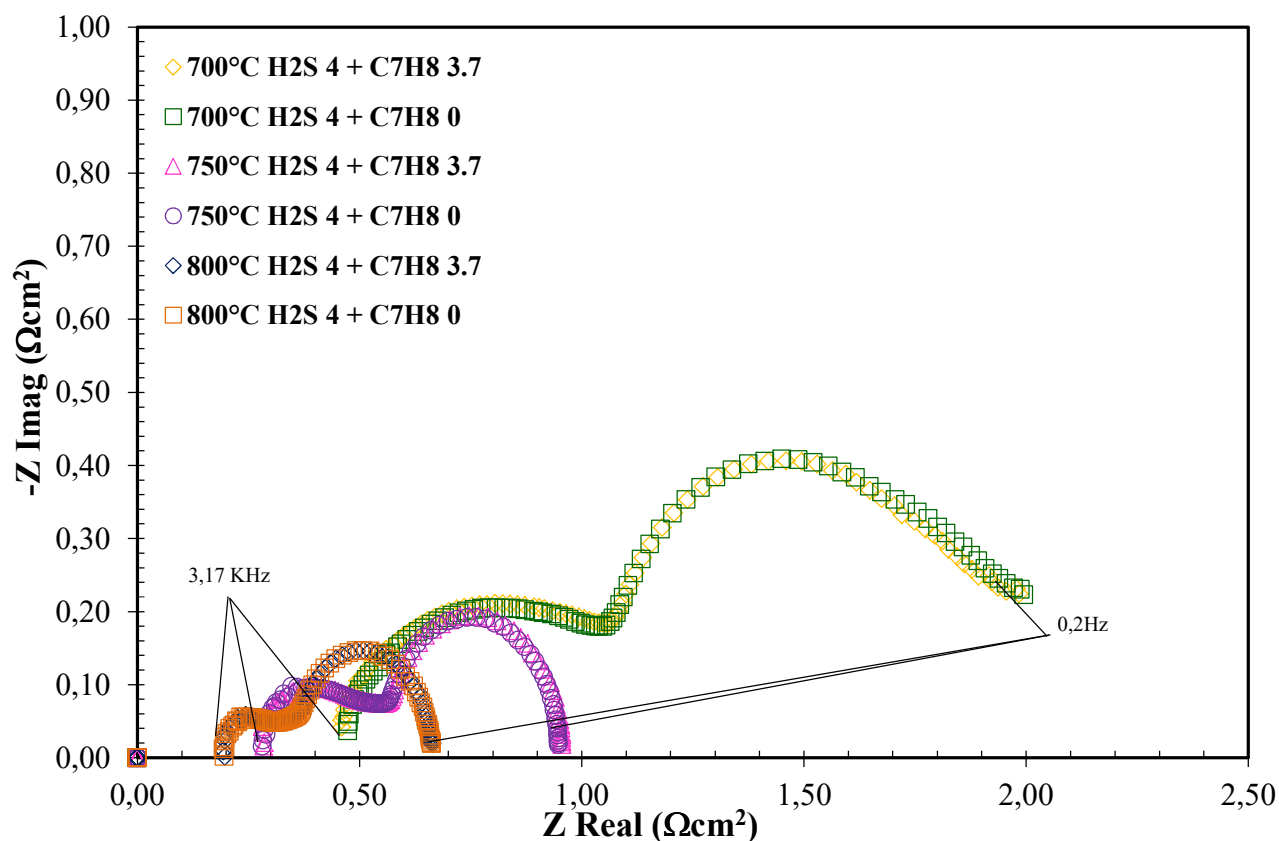
456 **Figure 26 – Area specific resistance diagram for variations of the C<sub>2</sub>Cl<sub>4</sub>+H<sub>2</sub>S concentration – ASC700.**

457 The power loss increases directly as H<sub>2</sub>S concentration increases until it reaches 12.86% of the  
 458 nominal power value at zero time. This means that if the exposure time to the pollutants is  
 459 increased, the electrical power loss will also rise, thereby increasing the resistance value, especially  
 460 as far as the Rp2 term is concerned. The contemporary presence of C<sub>2</sub>Cl<sub>4</sub> and H<sub>2</sub>S causes a two-fold  
 461 power loss compared to the single pollutant case.

462 H<sub>2</sub>S + C<sub>7</sub>H<sub>8</sub>

463 Figure 27 depicts the Nyquist diagram for the case of the contemporary presence of H<sub>2</sub>S and C<sub>7</sub>H<sub>8</sub>.  
 464 The concentration of H<sub>2</sub>S was fixed at 4 ppm(v), while C<sub>7</sub>H<sub>8</sub> was fixed at 3.7 ppm(v). The test was  
 465 conducted by adding or not adding the toluene concentration at three different temperatures. It has

466 been observed that the toluene concentration affects the SOFC performance to a lesser extent than  
 467 the temperature. Figures 27, 28 and 29 show that when the operating temperature is decreased, an  
 468 increase in the cell resistance is registered. This is caused by a decrease in the electronic  
 469 conductivity of the electrodes and in the ionic conductivity of the cell layer. This is especially true  
 470 for the electrolyte layer, but also for the composite electrodes.



472 **Figure 27 – Nyquist diagram for variations of the H<sub>2</sub>S + C<sub>7</sub>H<sub>8</sub> concentration – ASC700.**

473 Figure 28 shows the three term losses considered singularly;  $R_{\text{high}}$  is the only contribution that  
 474 seems to be affected by the addition of toluene to the gas mixture in which H<sub>2</sub>S is already present.  
 475 This percentage increases as the operating temperature decreases. Moreover, the electrochemical  
 476 reaction kinetics is slowed down, and this leads to an increase in the activation polarization  
 477 resistance. Finally, the diffusion capability of the chemical species is reduced both on the bulk flow  
 478 in the channels and on the porous electrodes.

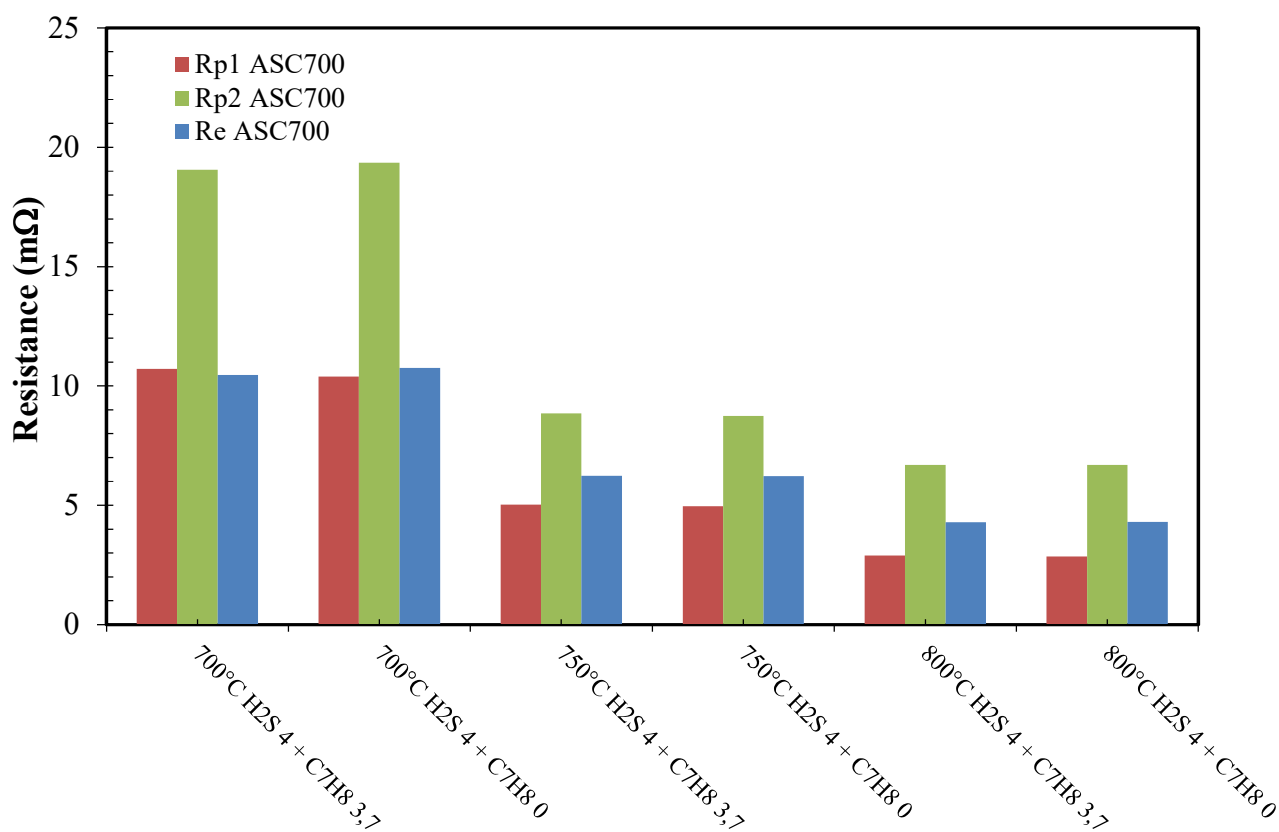


**Figure 28 – Re and Rp values for variations of the H<sub>2</sub>S + C<sub>7</sub>H<sub>8</sub> concentration – ASC700.**

The ASR value is affected more by the temperature variation than by the contemporary presence of toluene and hydrogen sulfide. Even in this case, the sulfur concentration weighs more than the toluene concentration at the same operating temperature. The toluene concentration needs to be increased before significant effects on the SOFC performance can be observed, but this condition is not realistic of a real clean up gas condition used to feed a SOFC system.

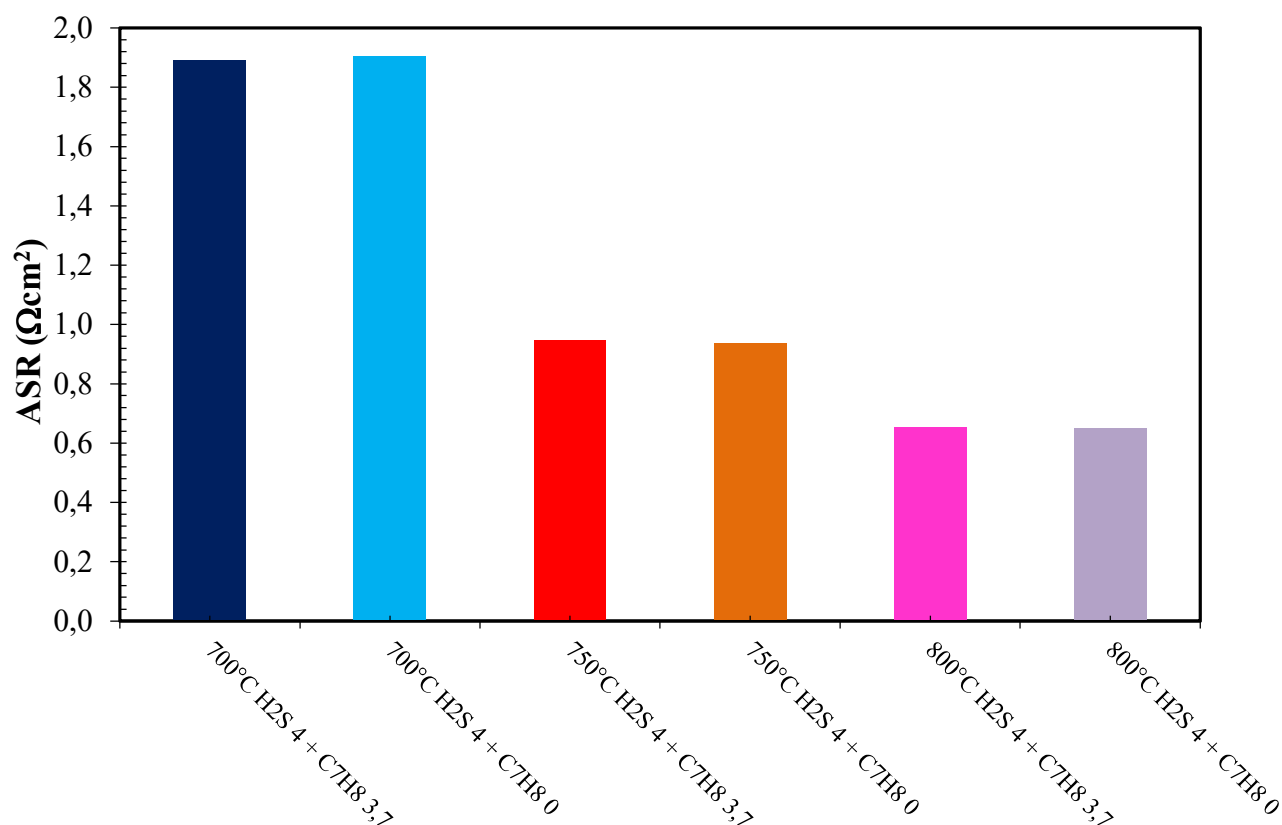


Figure 29 – Area specific resistance diagram for variations of the H<sub>2</sub>S + C<sub>7</sub>H<sub>8</sub> concentration – ASC700.

## Conclusions

This paper has investigated the performance of an anode supported solid oxide fuel cell considering a wide range of trace compounds. These compounds are found in biogenous fuels, such as biogas from OFMSW or from sewage sludge: H<sub>2</sub>S, HCl, D<sub>4</sub>, C<sub>10</sub>H<sub>8</sub>, C<sub>7</sub>H<sub>8</sub>, C<sub>2</sub>H<sub>2</sub>, C<sub>2</sub>Cl<sub>4</sub>. Various concentrations of Hydrogen sulfide have been studied in three tests. The first two tests considered high and low concentration ranges, thus simulating an early breakthrough slip from the clean-up section under operation with digester biogas. The third test considered the literature threshold limit for SOFCs ( $\approx 1$  ppm(v)). The effect of Chlorine has been tested for variable concentrations of HCl, ranging from 1 to 1000 ppm(v). The effect of Siloxanes on SOFC performance has been studied considering concentrations ranging from 111 ppb(v) to 1.9 ppm(v), in order to simulate a clean-up section slip. In the same way, C<sub>10</sub>H<sub>8</sub> and C<sub>7</sub>H<sub>8</sub> have been tested on SOFC performance and in a

499 double compound condition test ( $C_2H_2+H_2S$ ,  $C_2Cl_4+H_2S$  and  $C_7H_8+H_2S$ ). All these tests have been  
500 conducted to simulate possible biogas conditions that could arise from biological matter.

501 Electrochemical impedance spectroscopy has been used to study an SOFC cell in order to identify  
502 the main contribution to the cell losses from trace compound contaminations. This was done with an  
503 electrical equivalent circuit constituted by an ohmic resistance,  $R_e$ , and two parallel combinations  
504 of a resistance and a constant phase element, CPE. The polarization resistance,  $R_p$ , related to the  
505 concentration and activation polarizations, has been obtained from the sum of the low and high  
506 frequency resistances. The different sources of performance limitation have been obtained from fuel  
507 cell impedance considering the action of different trace compounds.

508 In particular it has been found that:

- 509     ▪ The ohmic contribution is almost independent of the fuel composition and it is only affected  
510       minimally by the  $H_2S$  concentration. However, this contribution is influenced by the  
511       modification of the nickel grain caused by cell operation with an  $H_2S$  concentration, as also  
512       reported by Ivey et al., (2010) [51]. The electrochemical fuel content of hydrocarbons can  
513       influence this term: lower values are achieved in an  $H_2$  condition, compared to the same  
514       electrochemical molar value in a  $CH_4 + CO$  condition.
- 515     ▪ The  $H_2S$  concentration mainly affects the polarization losses, especially the mass transport  
516       resistance through the electrodes caused by the sulfur blocking sites. The three-phase boundary  
517       decreases as a consequence of the sulfur action on nickel active sites.
- 518     ▪ Ultra low concentrations of sulfur, around 100 – 200 ppb(v), do not cause any changes in the  
519       loss terms.
- 520     ▪ The influence of  $HCl$  on SOFC performance is mainly due to the increase in  $R_{high}$ , related to the  
521       electrochemical processes that occur at the electrodes. Below 40 ppm(v),  $HCl$  concentrations  
522       only have a slight influence on the SOFC performance.



- 523     ▪ D4, a model compound for siloxanes, already acts on SOFC performance at ppb(v) levels. The  
524     term that is influenced most is  $R_{\text{high}}$ , thus highlighting the action of siloxanes on SOFC  
525     performance. In fact, these compounds, together with the formation of silica oxide in the anode  
526     cermet, reduce the porosity and the flow of the fuel toward the active sites, and thus limit the  
527     energy generation of a SOFC.
- 528     ▪ Naphthalene and toluene have been considered as model compounds for tars. No performance  
529     losses have been observed in an  $\text{H}_2$  mixture. When a syngas mixture was considered, it was  
530     observed that even 9.3 ppm(v) of  $\text{C}_{10}\text{H}_8$  can reduce SOFC performance. The polarization losses  
531     are those that are influenced the most, and the largest increase has been recorded for the low  
532     frequency term  $R_{p2}$ , related to mass transport resistance. The same behavior has been observed  
533     for the toluene case.
- 534     ▪ The tested concentrations of ethylene have been shown to positively influence SOFC  
535     performance and, at the same time, to limit the action of  $\text{H}_2\text{S}$  in a case in which two  
536     contaminants were considered together.
- 537     ▪  $\text{H}_2\text{S}$ , introduced with other contaminants ( $\text{C}_2\text{Cl}_4$ ), has led to an increased instantaneous  
538     deterioration, and the more types of contaminants included, the larger the initial deterioration.
- 539     ▪  $\text{H}_2\text{S}$ , introduced with another contaminant ( $\text{C}_7\text{H}_8$ ), has shown how the operating temperature has  
540     more influence than 3.7 ppm(v) of toluene.

541     The worst case scenario is represented by the presence of higher  $\text{H}_2\text{S}$  concentrations than 1 ppm(v)  
542     and by the presence of D4 already at the ppb(v) level. The contemporary presence of these  
543     compounds has led to an increase in the detrimental effects on SOFC performance, and even to fatal  
544     cell degradation.

545

546

547    **Acknowledgments**

548    This work has been partly funded by the European Union under the SOFCOM project  
549    ([www.sofcom.eu](http://www.sofcom.eu), contract number 278798). In addition, this research has been conducted as a part  
550    of the BioWaste for SOFCs (BWS) project carried out together with Fondazione Edmund Mach and  
551    SOLIDpower SpA. The project has been funded with the contribution of Fondazione Caritro (TN).

552

553

554

555

556

557

558

559

560

561

562

563

564

565

566

567  
568  
569  
570  
571  
572  
573  
574  
575  
576  
577  
578  
579  
580  
581  
582  
583  
584  
585  
586  
587  
588  
589  
590  
591  
592  
593  
594  
595  
596  
597  
598  
599  
600  
601  
602  
603  
604  
605  
606  
607  
608  
609

**References**

[1] D. Papurello, A. Lanzini, L. Tognana, S. Silvestri, M. Santarelli, Waste to energy: Exploitation of biogas from organic waste in a 500 W solid oxide fuel cell (SOFC) stack, *Energy*. 85 (2015) 145–158. doi:10.1016/j.energy.2015.03.093.

[2] A.J. Appleby, Fuel cell technology: Status and future prospects, *Energy*. 21 (1996) 521–653. doi:10.1016/0360-5442(96)00030-8.

[3] D.D. Papadimas, S. Ahmed, R. Kumar, Fuel quality issues with biogas energy - An economic analysis for a stationary fuel cell system, *Energy*. 44 (2012) 257–277. doi:10.1016/j.energy.2012.06.031.

[4] S.W. (Volume E. Narottam P. Bansal (Editor), Mihails Kusnezoff (Editor), Soshu Kirihaara (Volume Editor), *Advances in Solid Oxide Fuel Cells IV: Ceramic Engineering and Science Proceedings*, 2013.

[5] K. Sasaki, K. Haga, T. Yoshizumi, D. Minematsu, E. Yuki, R. Liu, et al., Chemical durability of Solid Oxide Fuel Cells: Influence of impurities on long-term performance, *J. Power Sources*. 196 (2011) 9130–9140. doi:10.1016/j.jpowsour.2010.09.122.

[6] D. Papurello, A. Lanzini, P. Leone, M. Santarelli, S. Silvestri, Biogas from the organic fraction of municipal solid waste: Dealing with contaminants for a solid oxide fuel cell energy generator, *Waste Manag.* (2014).

[7] E. Bocci, A. Di Carlo, S.J. McPhail, K. Gallucci, P.U. Foscolo, M. Moneti, et al., Biomass to fuel cells state of the art: A review of the most innovative technology solutions, *Int. J. Hydrogen Energy*. 39 (2014) 21876–21895. doi:10.1016/j.ijhydene.2014.09.022.

[8] D. Thimsen, *Gas Fueled Power Generation*, 3 (2006).

[9] D. Papurello, C. Soukoulis, E. Schuhfried, L. Cappellin, F. Gasperi, S. Silvestri, et al., Monitoring of volatile compound emissions during dry anaerobic digestion of the Organic Fraction of Municipal Solid Waste by Proton Transfer Reaction Time-of-Flight Mass Spectrometry, in: *Bioresour. Technol.*, 2012: pp. 254–265.

[10] D. Papurello, E. Schuhfried, A. Lanzini, A. Romano, L. Cappellin, T.D. Märk, et al., Influence of co-vapors on biogas filtration for fuel cells monitored with PTR-MS (Proton Transfer Reaction-Mass Spectrometry), *Fuel Process. Technol.* 118 (2014) 133–140.

[11] D. Papurello, L. Tognana, A. Lanzini, F. Smeacetto, M. Santarelli, I. Belcari, et al., Proton transfer reaction mass spectrometry technique for the monitoring of volatile sulfur compounds in a fuel cell quality clean-up system, *Fuel Process. Technol.* 130 (2015) 136–146. doi:10.1016/j.fuproc.2014.09.041.

610

- [12] L. Sigot, G. Ducom, B. Benadda, C. Labouré, Comparison of adsorbents for H<sub>2</sub>S and D<sub>4</sub> removal for biogas conversion in a solid oxide fuel cell, *Environ. Technol.* 3330 (2015) 1–10. doi:10.1080/09593330.2015.1063707.
- [13] A. Weber, S. Dierickx, A. Kromp, E. Ivers-Tiffée, Sulfur poisoning of anode-supported SOFCs under reformat operation, *Fuel Cells*. 13 (2013) 487–493. doi:10.1002/fuce.201200180.
- [14] A. Hauch, A. Hagen, J. Hjelm, T. Ramos, Sulfur Poisoning of SOFC Anodes: Effect of Overpotential on Long-Term Degradation, *J. Electrochem. Soc.* 161 (2014) F734–F743. doi:10.1149/2.080406jes.
- [15] D. Papurello, A. Lanzini, S. Fiorilli, F. Smeacetto, R. Singh, M. Santarelli, Sulfur poisoning in Ni-anode solid oxide fuel cells (SOFCs): Deactivation in single cells and a stack, *Chem. Eng. J.* 283 (2016) 1224–1233. doi:10.1016/j.cej.2015.08.091.
- [16] A.L. da Silva, N.C. Heck, Thermodynamics of sulfur poisoning in solid oxide fuel cells revisited: The effect of H<sub>2</sub>S concentration, temperature, current density and fuel utilization, *J. Power Sources*. 296 (2015) 92–101. doi:10.1016/j.jpowsour.2015.07.046.
- [17] M. Błesznowski, J. Jewulski, A. Zieleniak, Determination of H<sub>2</sub>S and HCl concentration limits in the fuel for anode supported SOFC operation, *Cent. Eur. J. Chem.* 11 (2013) 960–967. doi:10.2478/s11532-013-0228-1.
- [18] E. Lorente, M. Millan, N.P. Brandon, Use of gasification syngas in SOFC: Impact of real tar on anode materials, *Int. J. Hydrogen Energy*. 37 (2012) 7271–7278. doi:10.1016/j.ijhydene.2011.11.047.
- [19] K. Haga, S. Adachi, Y. Shiratori, K. Itoh, K. Sasaki, Poisoning of SOFC anodes by various fuel impurities, *Solid State Ionics*. 179 (2008) 1427–1431. doi:10.1016/j.ssi.2008.02.062.
- [20] H. Madi, A. Lanzini, S. Diethelm, D. Papurello, J. Van herle, M. Lualdi, et al., Solid oxide fuel cell anode degradation by the effect of siloxanes, *J. Power Sources*. 279 (2015) 460–471. doi:10.1016/j.jpowsour.2015.01.053.
- [21] M.J. Jørgensen, S. Primdahl, M. Mogensen, Characterisation of composite SOFC cathodes using electrochemical impedance spectroscopy, *Electrochim. Acta*. 44 (1999) 4195–4201. doi:10.1016/S0013-4686(99)00134-6.
- [22] N. Wagner, K. a. Friedrich, Application of electrochemical impedance spectroscopy for fuel cell characterization: PEFC and oxygen reduction reaction in alkaline solution, *Fuel Cells*. 9 (2009) 237–246. doi:10.1002/fuce.200800071.

653

- 654 [23] H. Schichlein, H. Schichlein, E. Ivers-tiffe, E. Ivers-tiffe, Deconvolution of electrochemical  
655 impedance spectra for the identification of electrode reaction mechanisms in solid oxide fuel  
656 cells, *J. Appl. Electrochem.* 32 (2002) 875–882. doi:10.1023/A:1020599525160.  
657
- 658 [24] P. V. Aravind, J.P. Ouweltjes, J. Schoonman, Diffusion Impedance on Nickel/Gadolinia-  
659 Doped Ceria Anodes for Solid Oxide Fuel Cells, *J. Electrochem. Soc.* 156 (2009) B1417.  
660 doi:10.1149/1.3231490.  
661
- 662 [25] Q.A. Huang, R. Hui, B. Wang, J. Zhang, A review of AC impedance modeling and  
663 validation in SOFC diagnosis, *Electrochim. Acta.* 52 (2007) 8144–8164.  
664 doi:10.1016/j.electacta.2007.05.071.  
665
- 666 [26] E. Brightman, D.G. Ivey, D.J.L. Brett, N.P. Brandon, The effect of current density on H<sub>2</sub>S-  
667 poisoning of nickel-based solid oxide fuel cell anodes, *J. Power Sources.* 196 (2011) 7182–  
668 7187. doi:10.1016/j.jpowsour.2010.09.089.  
669
- 670 [27] P. Leone, T. Matencio, M.E. Garciä, Z.R. Domigues, A. Lanzini, M. Santarelli, Limiting  
671 Factors for a Planar Solid Oxide Fuel Cell Under Different Flow and Temperature  
672 Conditions, *Fuel Cells.* (2013) n/a–n/a. doi:10.1002/fuce.201200154.  
673
- 674 [28] S.H. Jensen, A. Hauch, P.V. Hendriksen, M. Mogensen, N. Bonanos, T. Jacobsen, A Method  
675 to Separate Process Contributions in Impedance Spectra by Variation of Test Conditions, *J.*  
676 *Electrochem. Soc.* 154 (2007) B1325. doi:10.1149/1.2790791.  
677
- 678 [29] A. Leonide, V. Sonn, A. Weber, E. Ivers-Tiffée, Evaluation and Modeling of the Cell  
679 Resistance in Anode-Supported Solid Oxide Fuel Cells, *J. Electrochem. Soc.* 155 (2008)  
680 B36. doi:10.1149/1.2801372.  
681
- 682 [30] W.G. Bessler, S. Gewies, Gas Concentration Impedance of Solid Oxide Fuel Cell Anodes, *J.*  
683 *Electrochem. Soc.* 154 (2007) B548. doi:10.1149/1.2720639.  
684
- 685 [31] M. Lang, C. Auer, A. Eismann, P. Szabo, N. Wagner, Investigation of solid oxide fuel cell  
686 short stacks for mobile applications by electrochemical impedance spectroscopy,  
687 *Electrochim. Acta.* 53 (2008) 7509–7513. doi:10.1016/j.electacta.2008.04.047.  
688
- 689 [32] L.R.F. Allen J. Bard, *Electrochemical methods: Fundamentals and Applications*, New York,  
690 2000. doi:10.1146/annurev.matsci.30.1.117.  
691
- 692 [33] S. S, *High-Temperature Solid Oxide Fuel Cells: Fundamentals, Design and Applications*,  
693 Elsevier science, Amsterdam The Netherlands, 2003.  
694

- [34] F.T. and E.I.-T. Cornelia Endler, André Leonide, André Weber, Cells, Long-Term Study of MIEC Cathodes for Intermediate Temperature Solid Oxide Fuel Cells, ECS Trans. 25 (2009) 2381–2390. doi:10.1149/1.3205791.
- [35] L.P. Hendriksen PV, Koch S, Mogensen M, Liu YL, Solid Oxide Fuel Cells VIII, (Eds. S. C. Singhal, M. Dokiya), in: Electrochem. Soc. Proc. Ser., Pennington, NJ, USA, 2003.
- [36] Z. Cheng, S. Zha, M. Liu, Influence of cell voltage and current on sulfur poisoning behavior of solid oxide fuel cells, J. Power Sources. 172 (2007) 688–693. doi:10.1016/j.jpowsour.2007.07.052.
- [37] Y. Zhang, Z. Lu, Z. Yang, T. Woo, Short communication the mechanism of sulfur poisoning on the nickel/yttrium-stabilized zirconia anode of solid oxide fuel cells: The role of the oxygen vacancy, J. Power Sources. 237 (2013) 128–131. doi:10.1016/j.jpowsour.2013.03.030.
- [38] Z. Cheng, J.-H. Wang, Y. Choi, L. Yang, M.C. Lin, M. Liu, From Ni-YSZ to sulfur-tolerant anode materials for SOFCs: electrochemical behavior, in situ characterization, modeling, and future perspectives, Energy Environ. Sci. 4 (2011) 4380. doi:10.1039/c1ee01758f.
- [39] A. Hagen, J.F.B. Rasmussen, K. Thydén, Durability of solid oxide fuel cells using sulfur containing fuels, J. Power Sources. 196 (2011) 7271–7276. doi:10.1016/j.jpowsour.2011.02.053.
- [40] J.F.B. Rasmussen, A. Hagen, The Effect of H<sub>2</sub>S on the Performance of SOFCs using Methane Containing Fuel, (2010) 1135–1142. doi:10.1002/fuce.201000012.
- [41] D. Papurello, R. Borchellini, P. Bareschino, V. Chiodo, S. Freni, A. Lanzini, et al., Performance of a Solid Oxide Fuel Cell short-stack with biogas feeding, Appl. Energy. 125 (2014) 254–263.
- [42] F.N. Cayan, M. Zhi, S.R. Pakalapati, I. Celik, N. Wu, R. Gemmen, Effects of coal syngas impurities on anodes of solid oxide fuel cells, J. Power Sources. 185 (2008) 595–602. doi:10.1016/j.jpowsour.2008.06.058.
- [43] P. V. Aravind, J.P. Ouweltjes, N. Woudstra, G. Rietveld, Impact of Biomass-Derived Contaminants on SOFCs with Ni/Gadolinia-Doped Ceria Anodes, Electrochem. Solid-State Lett. 11 (2008) B24. doi:10.1149/1.2820452.
- [44] Veyo, EVALUATION OF FUEL IMPURITY EFFECTS ON SOLID OXIDE FUEL CELL PERFORMANCE Final Technical Report, 1998.
- [45] M. Arnold, T. Kajolinnä, Development of on-line measurement techniques for siloxanes and

- 738 other trace compounds in biogas, *Waste Manag.* 30 (2010) 1011–1017.  
 739 doi:10.1016/j.wasman.2009.11.030.  
 740
- 741 [46] M. Arnold, Reduction and monitoring of biogas trace compounds, 2009.  
 742
- 743 [47] T. Namioka, T. Naruse, R. Yamane, Behavior and mechanisms of Ni/ScSZ cermet anode  
 744 deterioration by trace tar in wood gas in a solid oxide fuel cell, *Int. J. Hydrogen Energy*. 36  
 745 (2011) 5581–5588. doi:10.1016/j.ijhydene.2011.01.165.  
 746
- 747 [48] T. Namioka, Y. Nagai, K. Yoshikawa, T. Min, A tolerance criterion for tar concentration in a  
 748 model wood gas for a nickel/scandia-stabilized zirconia cermet anode in a solid oxide fuel  
 749 cell, *Int. J. Hydrogen Energy*. 37 (2012) 17245–17252. doi:10.1016/j.ijhydene.2012.09.005.  
 750
- 751 [49] R. Coll, J. Salvadó, X. Farriol, D. Montané, Steam reforming model compounds of biomass  
 752 gasification tars: Conversion at different operating conditions and tendency towards coke  
 753 formation, *Fuel Process. Technol.* 74 (2001) 19–31. doi:10.1016/S0378-3820(01)00214-4.  
 754
- 755 [50] W.Z. Zhu, S.C. Deevi, A review on the status of anode materials for solid oxide fuel cells,  
 756 *Mater. Sci. Eng. A*. 362 (2003) 228–239. doi:10.1016/S0921-5093(03)00620-8.  
 757
- 758 [51] D.G. Ivey, E. Brightman, N. Brandon, Structural modifications to nickel cermet anodes in  
 759 fuel cell environments, *J. Power Sources*. 195 (2010) 6301–6311.  
 760 doi:10.1016/j.jpowsour.2010.04.059.  
 761

1    **Table captions**

2    Table 1 – Test conditions.

3

4

5

6

7

8

9

10

11

12

13

14

15

16

17

18

19



20 **Table 1**

Pollutant test	Conc. Range (ppm(v))	Cell adopted	H <sub>2</sub> (ml min <sup>-1</sup> )	CO (ml min <sup>-1</sup> )	CO <sub>2</sub> (ml min <sup>-1</sup> )	CH <sub>4</sub> (ml min <sup>-1</sup> )	N <sub>2</sub> (ml min <sup>-1</sup> )	H <sub>2</sub> O (ml min <sup>-1</sup> )	H <sub>2</sub> O (g h <sup>-1</sup> )	T (°C)	FU	Fuel condition
H <sub>2</sub> S high conc.	0,84-6,4	ASC700	151,5	136,4	68,2	15,2	386,4	60,2	2,9	750	30,0	syngas
H <sub>2</sub> S high conc.	0,8-6,7	ASC4	250	0	41,7	62,5	0	124,5	6	750	20,9	DIR 50% biogas
H <sub>2</sub> S low conc.	0,078-0,174	ASC4	250	0	41,7	62,5	0	124,5	6	750	20,9	DIR 50% biogas
HCl	1-1000	ASC700	348	133,7	62,1	5		136,5	6,58	750	29,9	biogas reformate
D4	0,11-1,92	TOFC	348	133,7	62,1	5		136,5	6,58	750	20,8	biogas reformate
C <sub>7</sub> H <sub>8</sub>	3,8-24,2	ASC700	151,5	136,4	68,2	15,2	386,4	269,8	13	750	30,0	syngas
C <sub>10</sub> H <sub>8</sub>	0-9,3	ASC700	151,5	136,4	68,2	15,2	386,4	269,8	13	750	30,0	syngas
C <sub>2</sub> H <sub>2</sub>	371,2	ASC700	250	0	42	63	0	0,0	0	750	20,8	POx 50% biogas
H <sub>2</sub> S	1,34	ASC700	250	0	42	63	0	0,0	0	750	20,8	POx 50% biogas
H <sub>2</sub> S +C <sub>2</sub> Cl <sub>4</sub>	0-4/1,7-0	ASC700	151,5	136,4	68,2	15,2	386,4	269,8	13	750	30,0	syngas
H <sub>2</sub> S +C <sub>2</sub> H <sub>2</sub>	1,34/371,2	ASC700	250	0	42	63	0	0,0	0	750	20,8	POx 50% biogas
H <sub>2</sub> S + C <sub>7</sub> H <sub>8</sub>	4/3,7	ASC700	151,5	136,4	68,2	15,2	386,4	269,8	13	750	30,0	syngas

1    **Figure captions**

- 2    Figure 1 – Equivalent fuel cell circuit:  $R_e$ ,  $R_{high}$  and  $CPE_{high}$  are associated with the high frequency  
3    semi-circle,  $R_{low}$  and  $CPE_{low}$  with the low frequency semi-circle.
- 4    Figure 2 – Nyquist diagram for variations of the  $H_2S$  concentration – ASC700.
- 5    Figure 3 – Nyquist diagram for variations of the  $H_2S$  concentration – ASC4.
- 6    Figure 4 –  $R_e$  and  $R_p$  values for variations of the  $H_2S$  concentration – ASC700.
- 7    Figure 5 –  $R_e$  and  $R_p$  values for variations of the  $H_2S$  concentration – ASC4.
- 8    Figure 6 – Nyquist diagram for the  $H_2S$  threshold concentration value – ASC700.
- 9    Figure 7 – Nyquist diagram for the  $H_2S$  threshold concentration value – time variation – ASC700.
- 10    Figure 8 – Nyquist diagram for variations of the  $H_2S$  “low concentration level” – ASC4.
- 11    Figure 9 –  $R_e$  and  $R_p$  values for variations of the  $H_2S$  “low concentration level” – ASC4.
- 12    Figure 10 – Nyquist diagram for variations of the  $HCl$  concentration – ASC700.
- 13    Figure 11 –  $R_e$  and  $R_p$  values for variations of the  $HCl$  concentration – ASC700.
- 14    Figure 12 – Nyquist diagram for variations of the  $D4$  concentration – TOFC.
- 15    Figure 13 –  $R_e$  and  $R_p$  values for variations of the  $D4$  concentration – TOFC.
- 16    Figure 14 – Nyquist diagram for variations of the  $C_{10}H_8$  concentration FU 30% – ASC700.
- 17    Figure 15 –  $R_e$  and  $R_p$  values for variations of the  $C_{10}H_8$  concentration – ASC700.
- 18    Figure 16 – Nyquist diagram for variations of the  $C_7H_8$  concentration – ASC700.
- 19    Figure 17 –  $R_e$  and  $R_p$  values for variations of the  $C_7H_8$  concentration – TOFC.
- 20    Figure 18 – Area specific resistance diagram for variations of the  $C_7H_8$  concentration – ASC700.
- 21    Figure 19 – Nyquist diagram for variations of the  $C_2H_2$  concentration – ASC700.
- 22    Figure 20 –  $R_e$  and  $R_p$  values for variations of the the  $C_2H_2$  concentration – ASC700.
- 23    Figure 21 – Nyquist diagram for variations of the  $C_2H_2$  and  $C_2H_2+H_2S$  concentrations – ASC700.

24 Figure 22 – Re and Rp values for variations of the  $C_2H_2$  and  $C_2H_2+H_2S$  concentration – ASC700.

25 Figure 23 – Area specific resistance diagram for variations of the  $C_2H_2$  and  $C_2H_2+H_2S$

26 concentrations – ASC700.

27 Figure 24 – Nyquist diagram for variations of the  $C_2Cl_4+H_2S$  concentration – ASC700.

28 Figure 25 – Re and Rp values for variations of the  $C_2Cl_4+H_2S$  concentration – ASC700.

29 Figure 26 – Area specific resistance diagram for variations of the  $C_2Cl_4+H_2S$  concentration –

30 ASC700.

31 Figure 27 – Nyquist diagram for variations of the  $H_2S + C_7H_8$  concentration – ASC700.

32 Figure 28 – Re and Rp values for variations of the  $H_2S + C_7H_8$  concentration – ASC700.

33 Figure 29 – Area specific resistance diagram for variations of the  $H_2S + C_7H_8$  concentration –

34 ASC700.

35

36

37

38

39

40

41

42

43

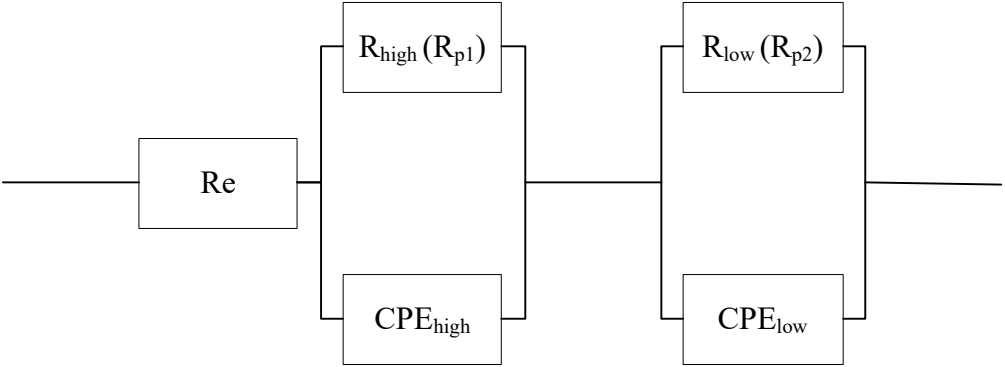
44

45

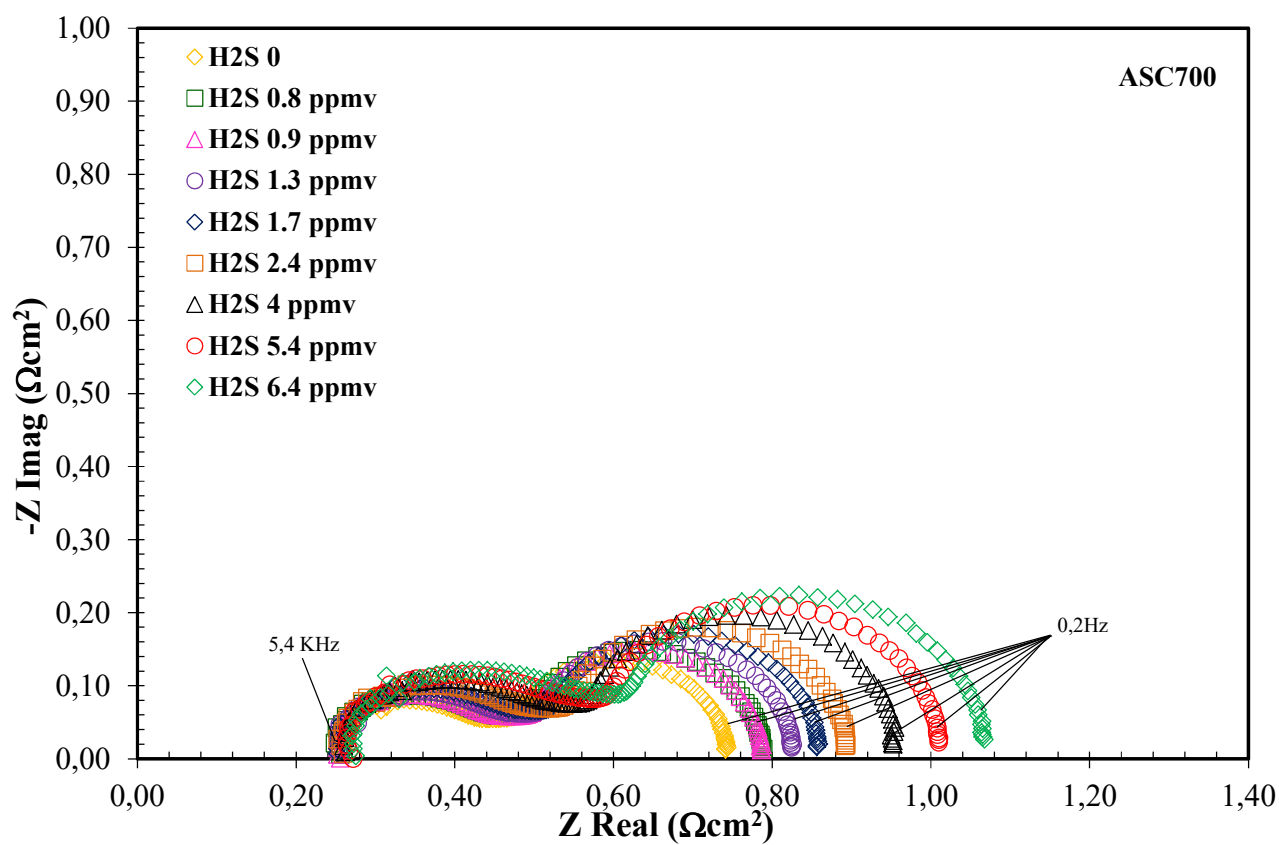
46

47

48 **Figure 1**



67 **Figure 2**



68

69

70

71

72

73

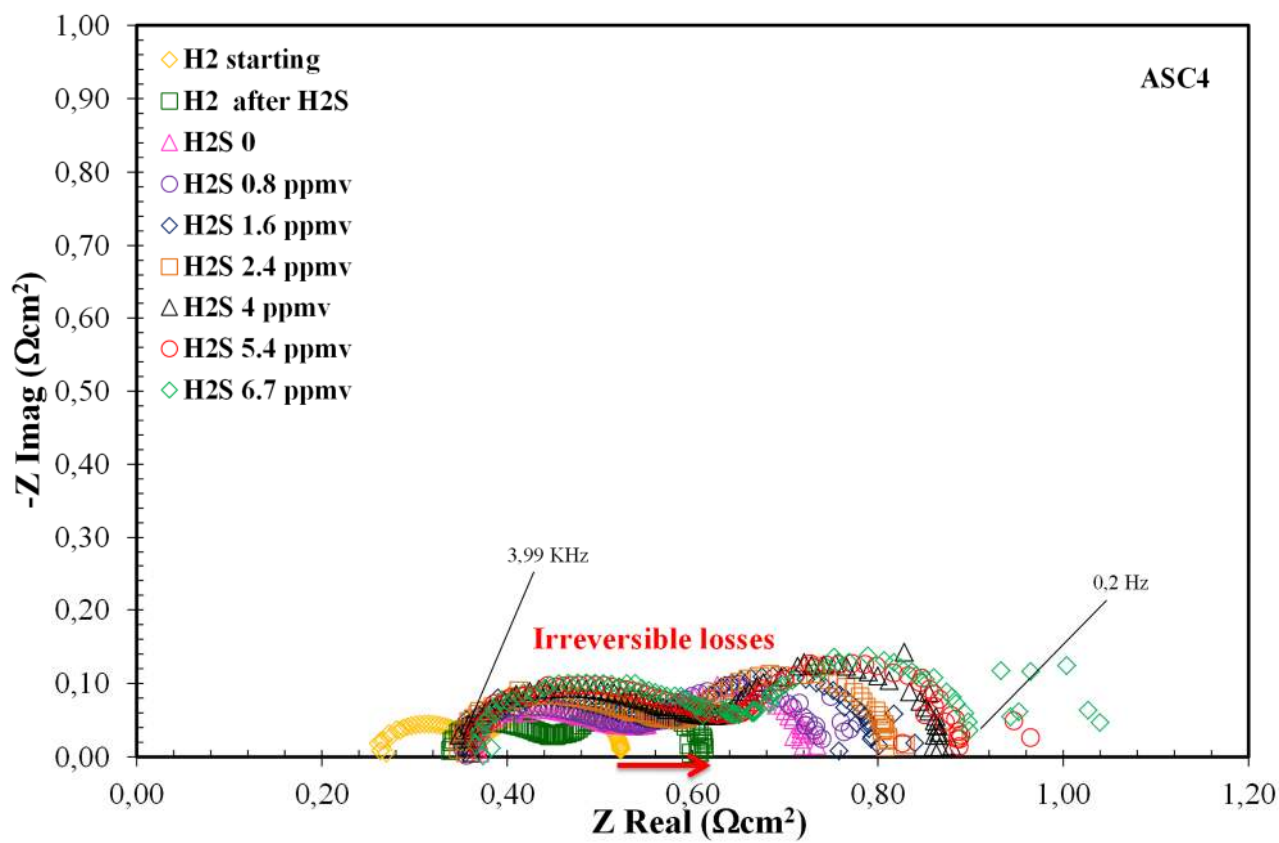
74

75

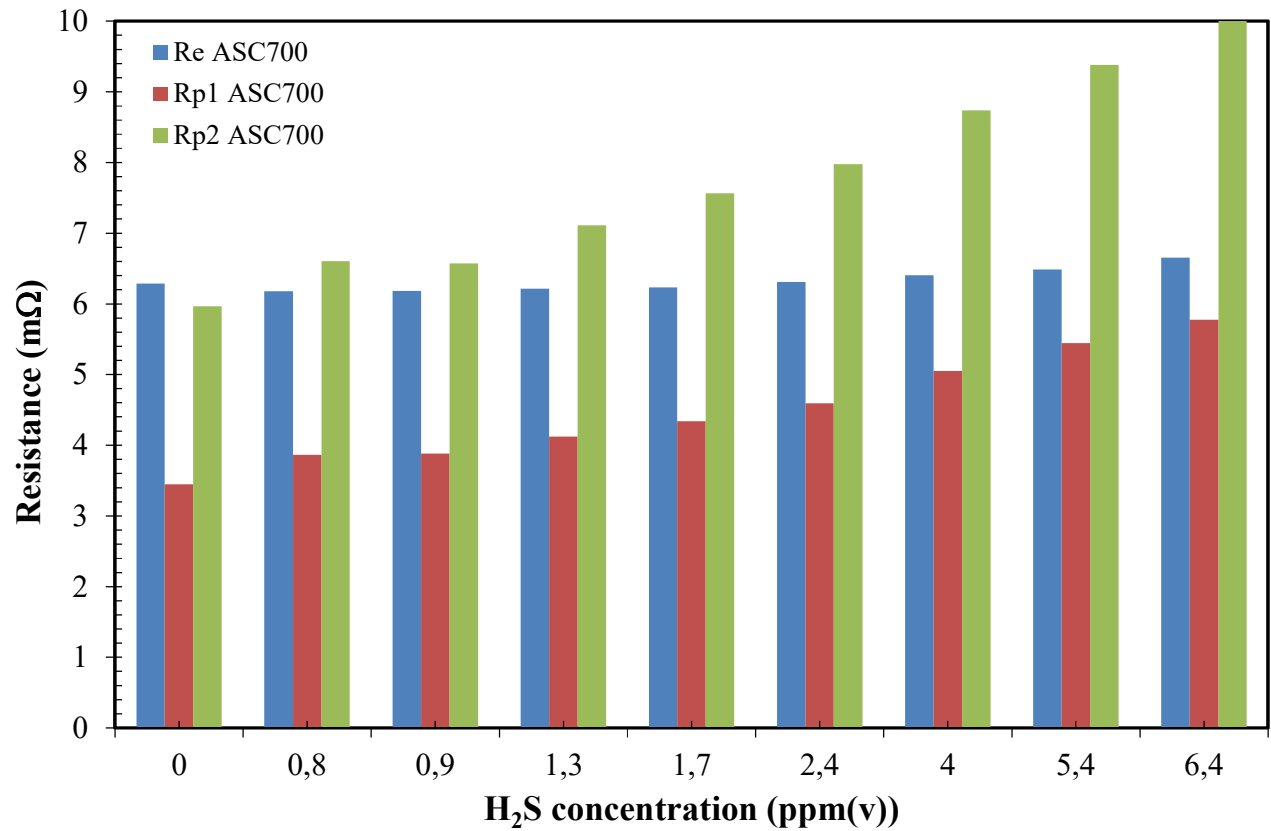
76

77

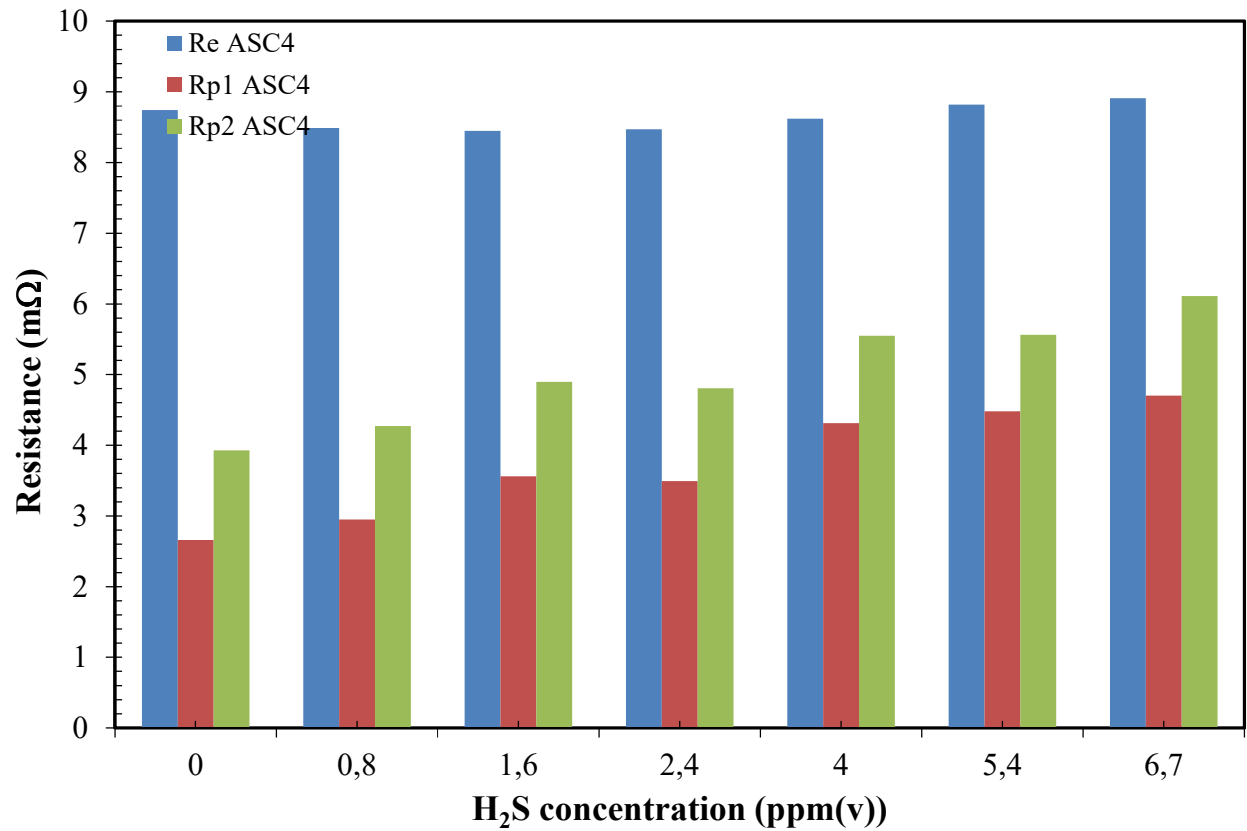
78 **Figure 3**



89 **Figure 4**



100 **Figure 5**



101

102

103

104

105

106

107

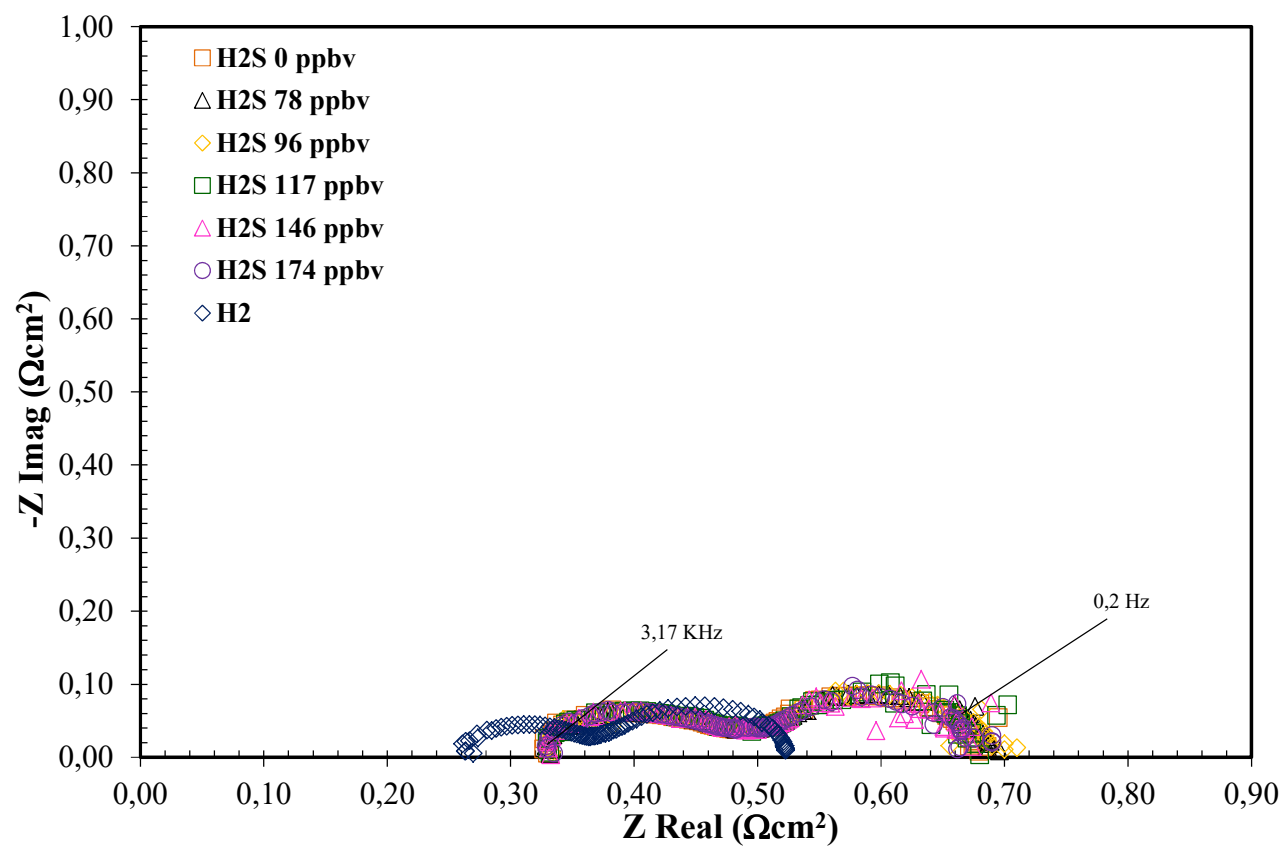
108

109

110



111 **Figure 6**



112

113

114

115

116

117

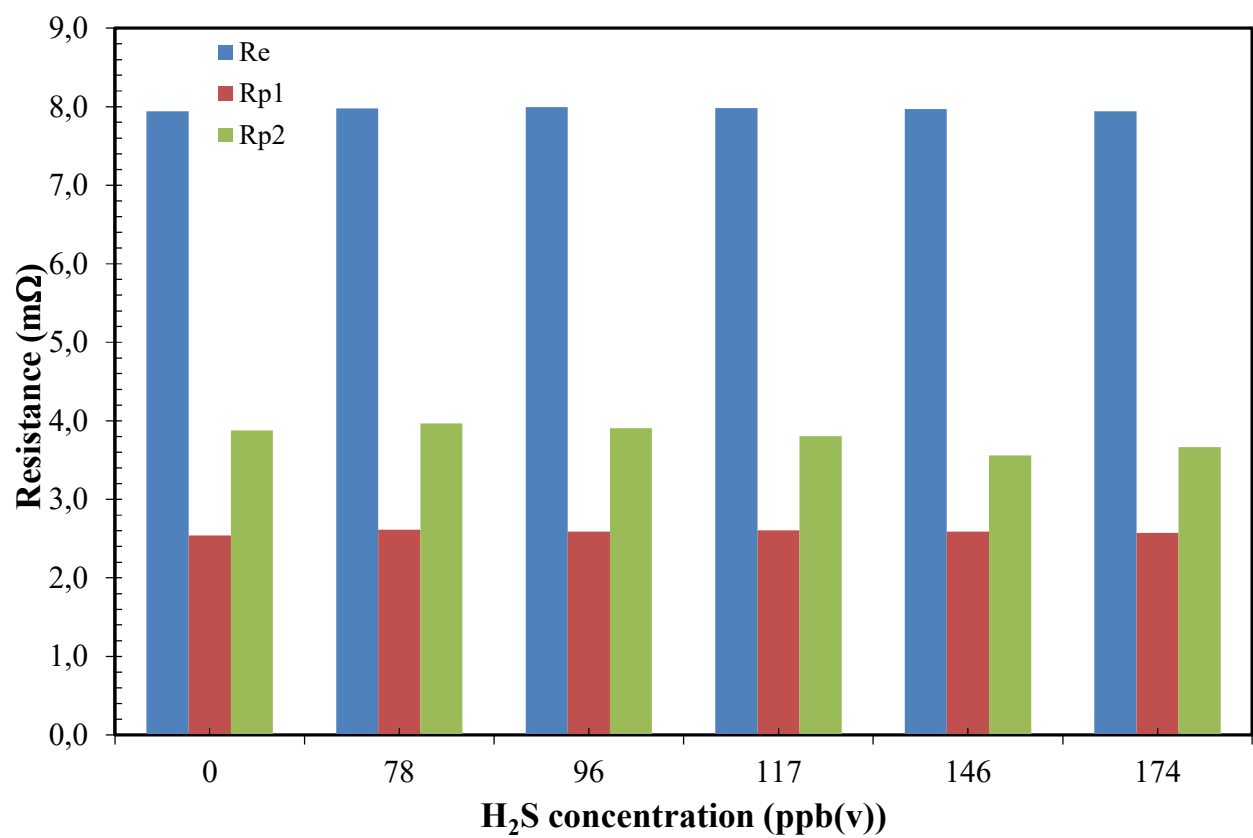
118

119

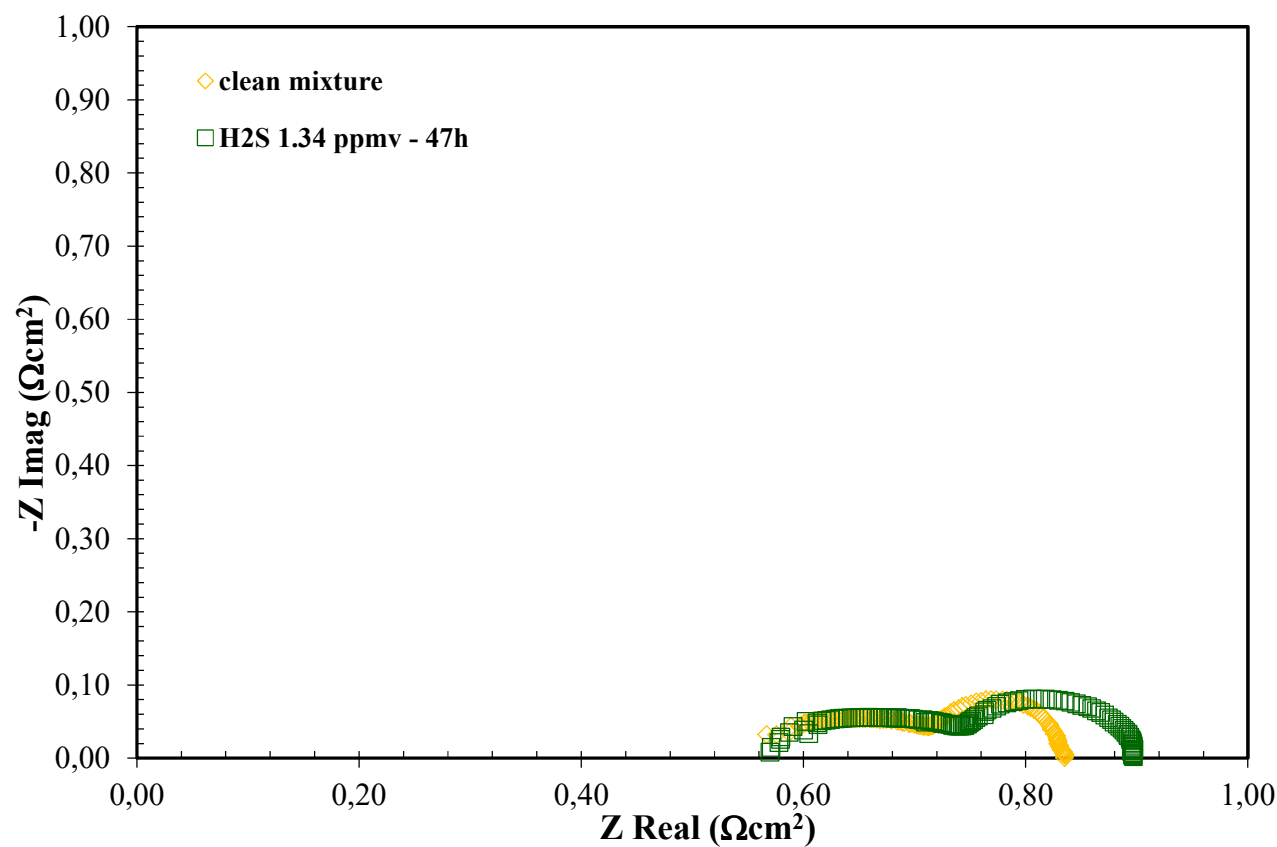
120

121

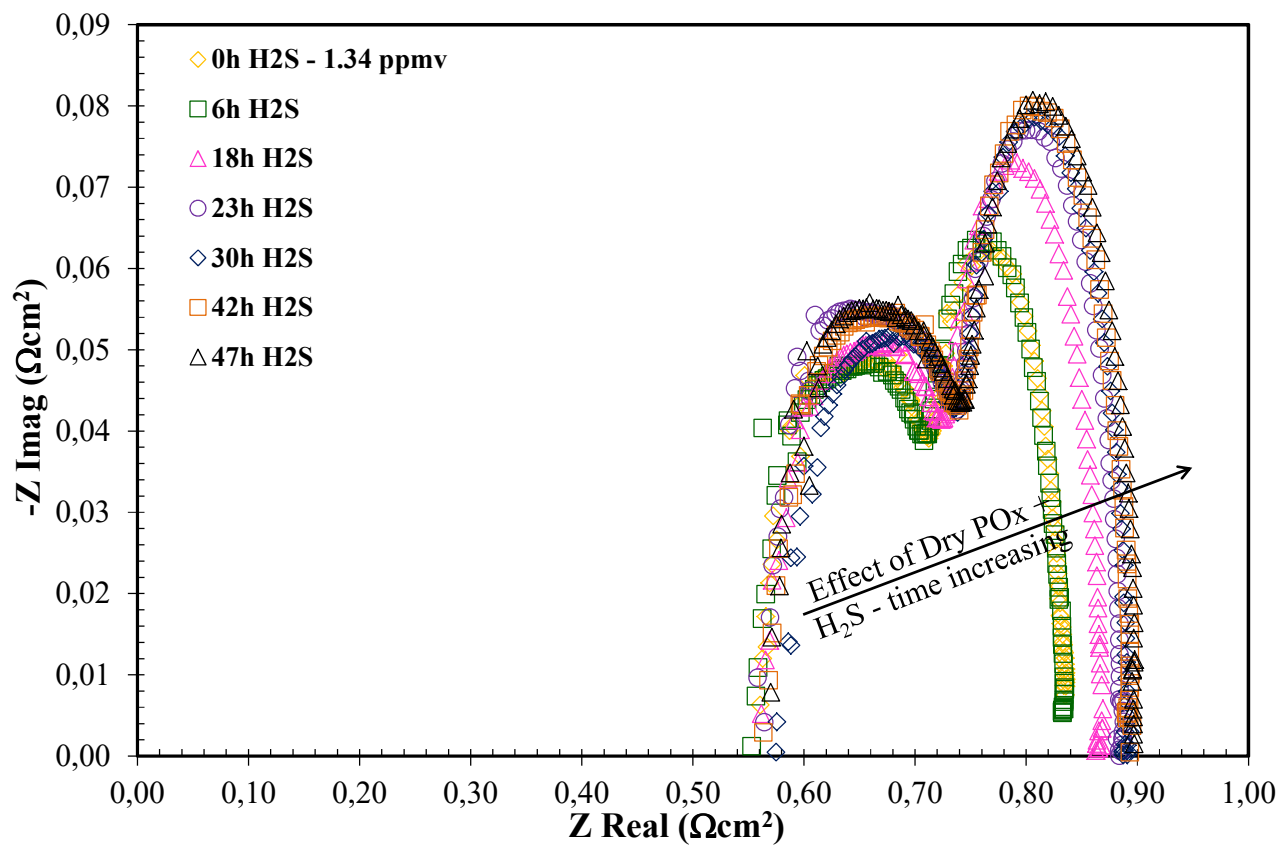
122 **Figure 7**



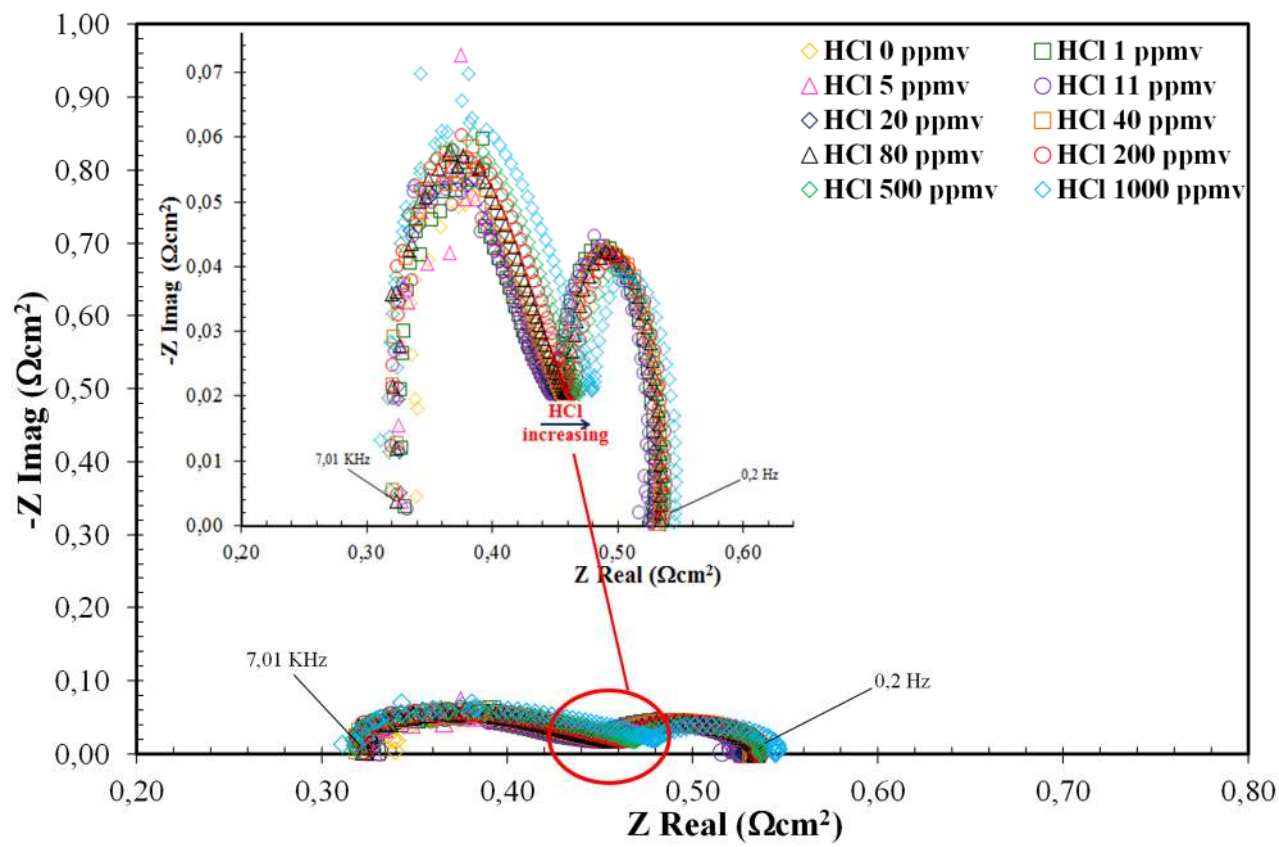
133 **Figure 8**



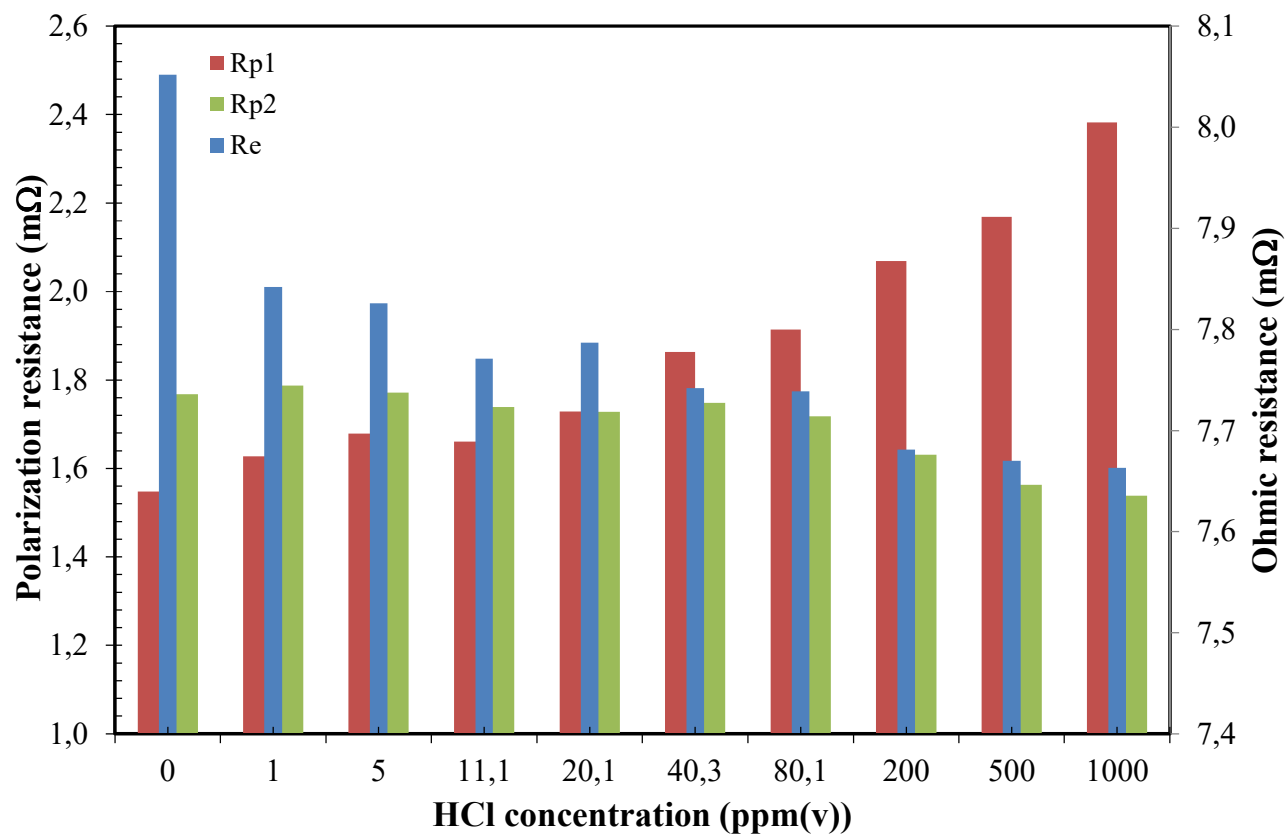
144 **Figure 9**



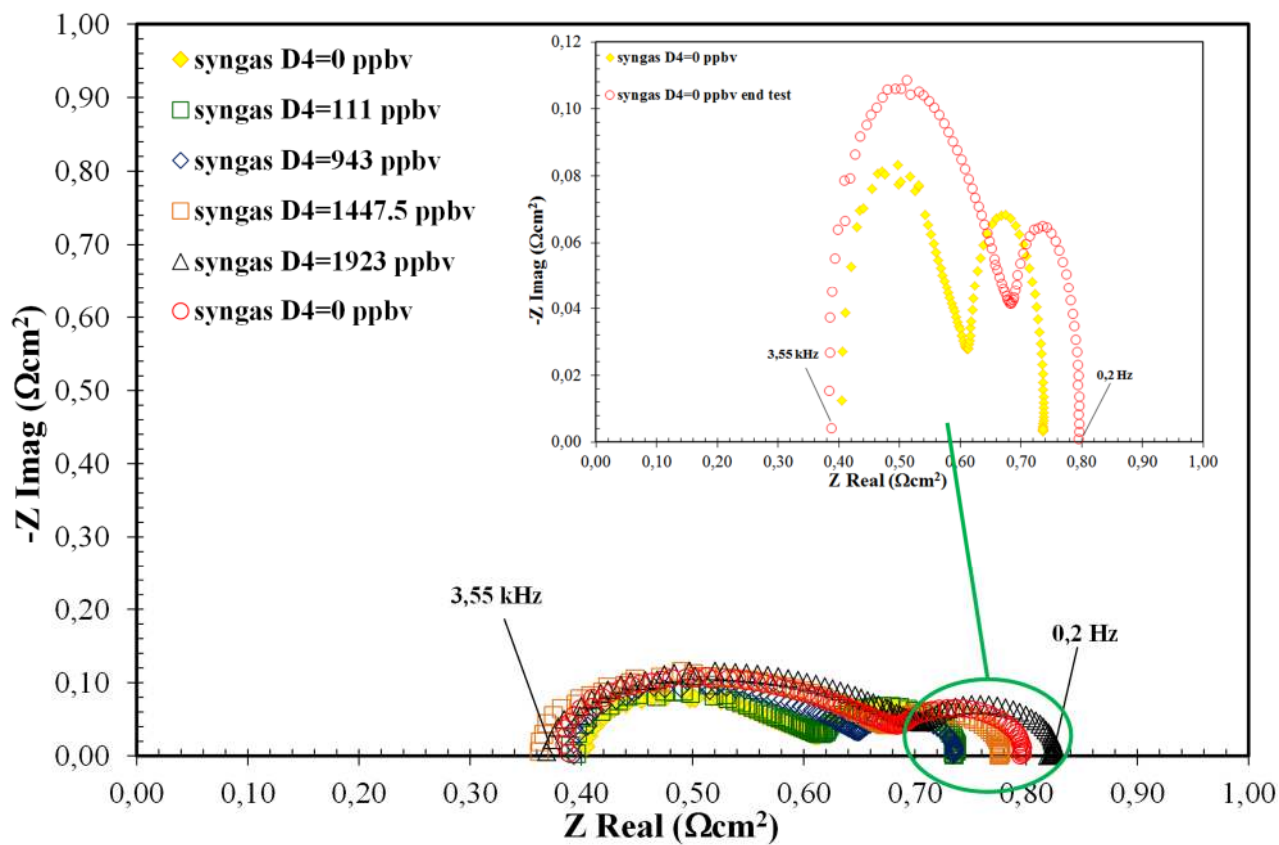
155 **Figure 10**



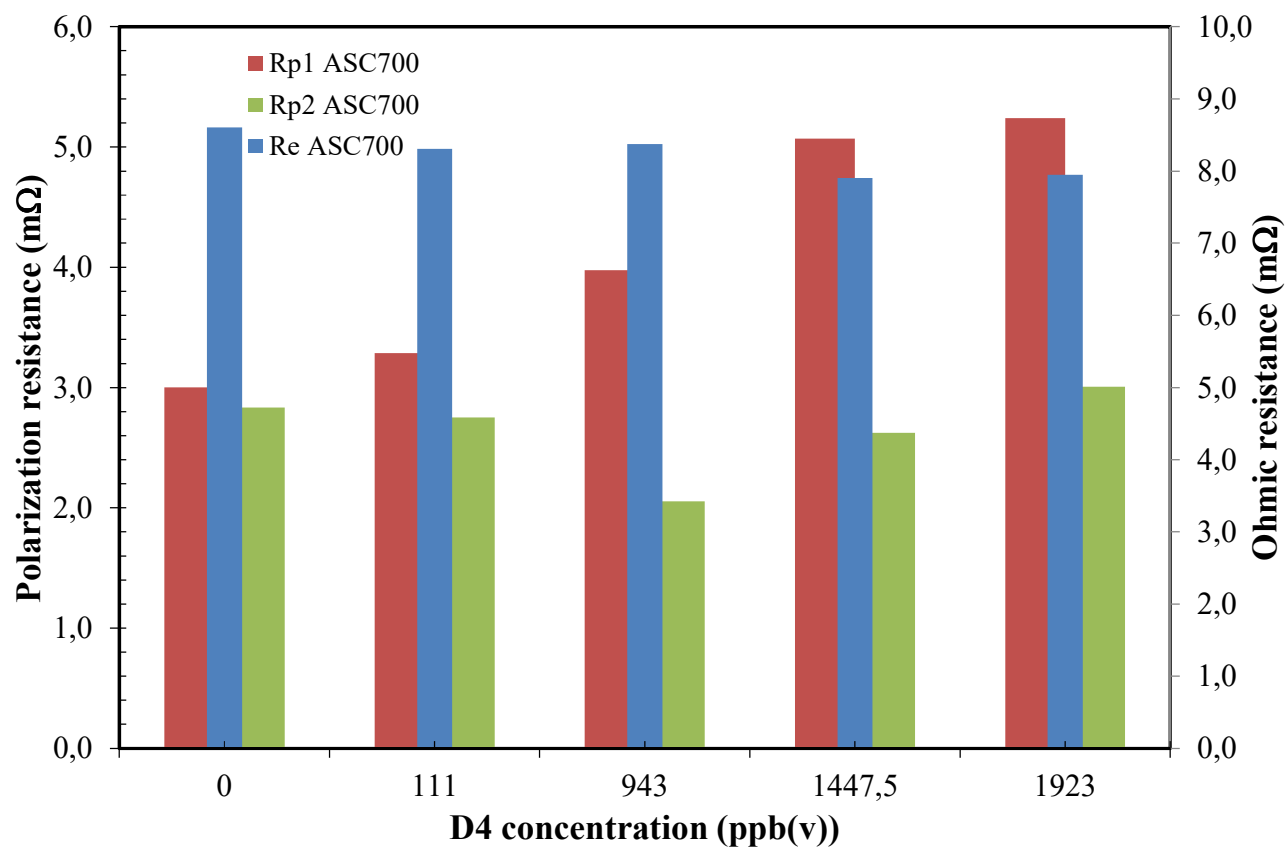
166 **Figure 11**



177 **Figure 12**

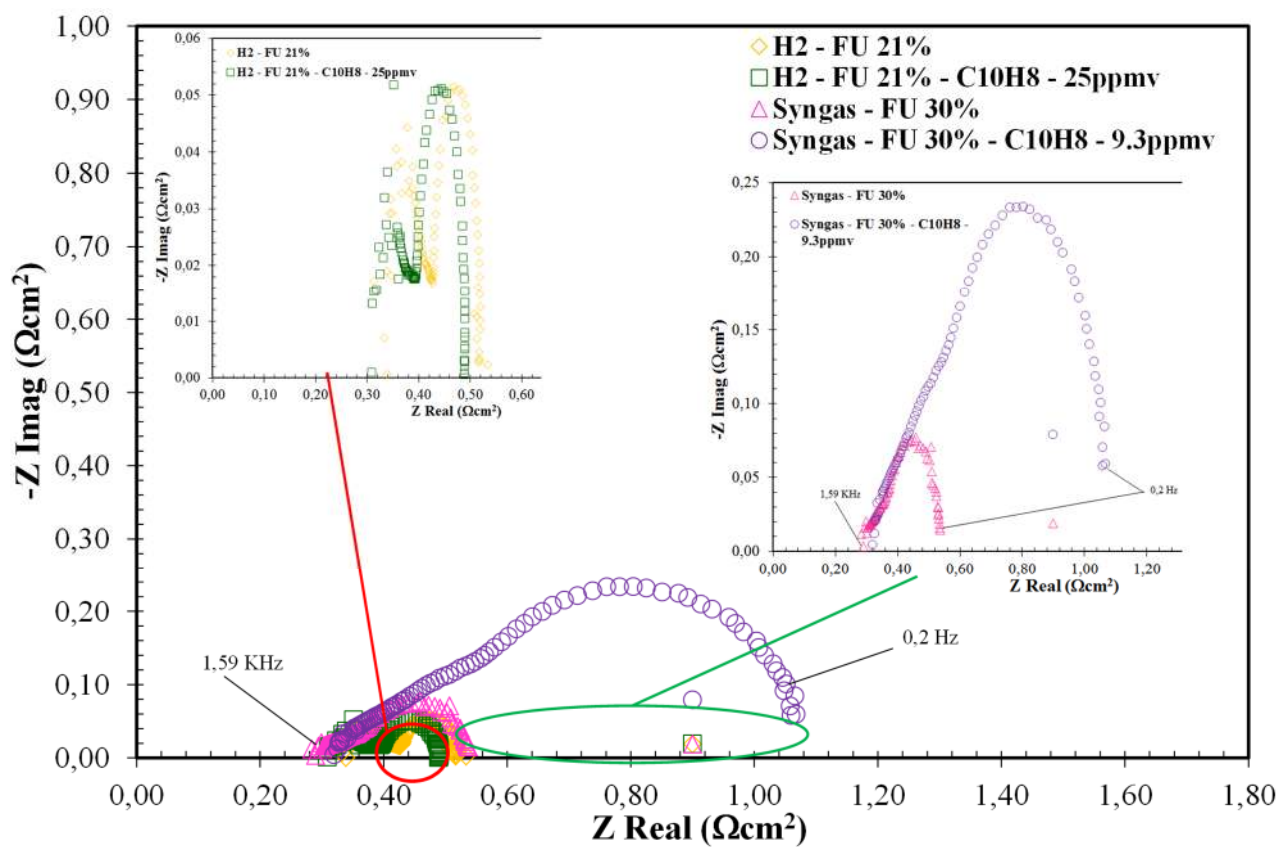


188 **Figure 13**

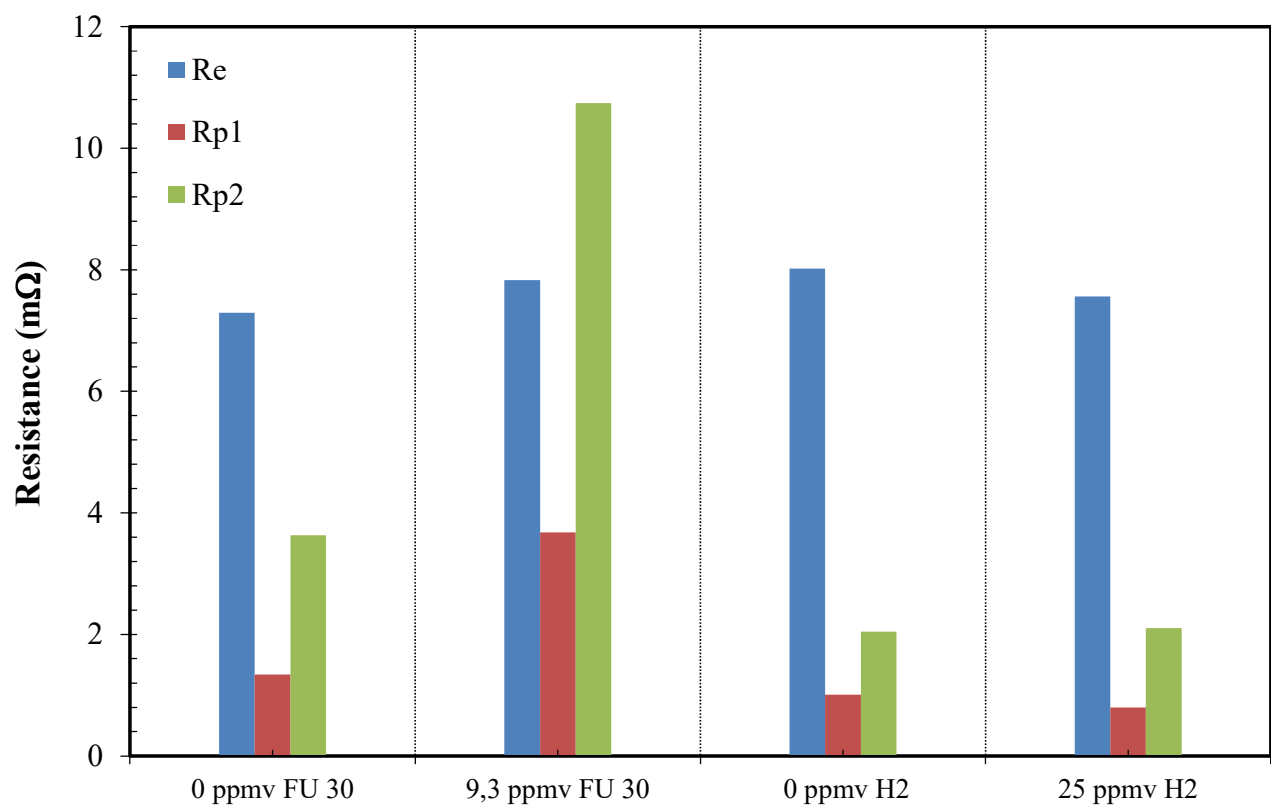




199 **Figure 14**



210 **Figure 15**



211

212

213

214

215

216

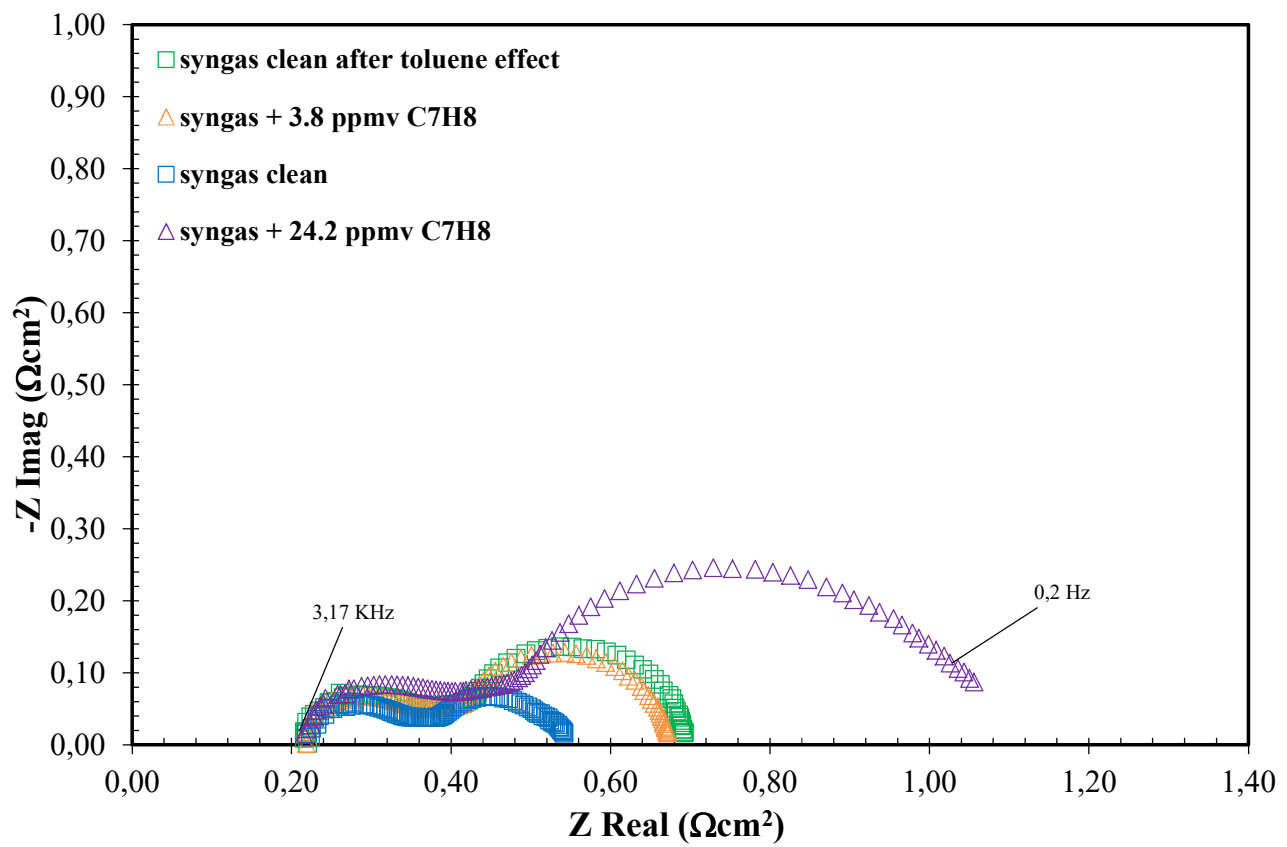
217

218

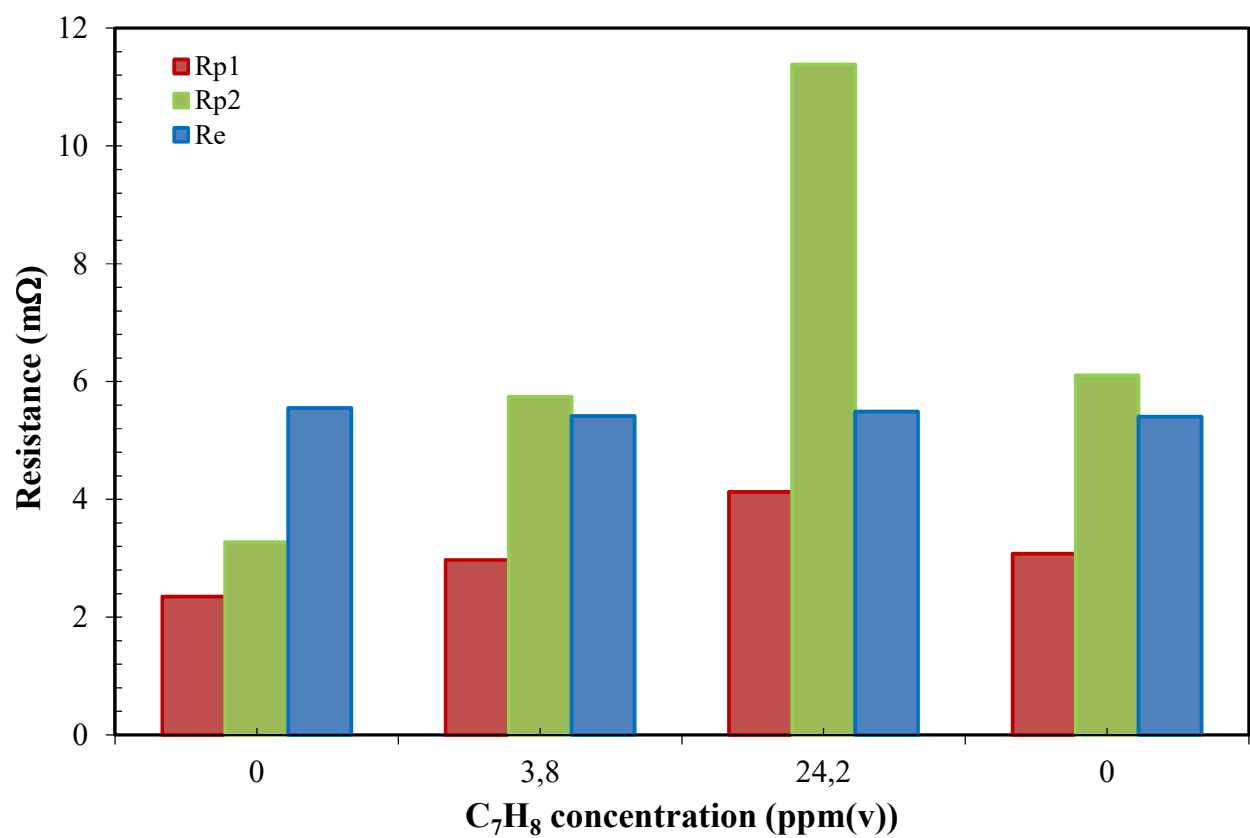
219

220

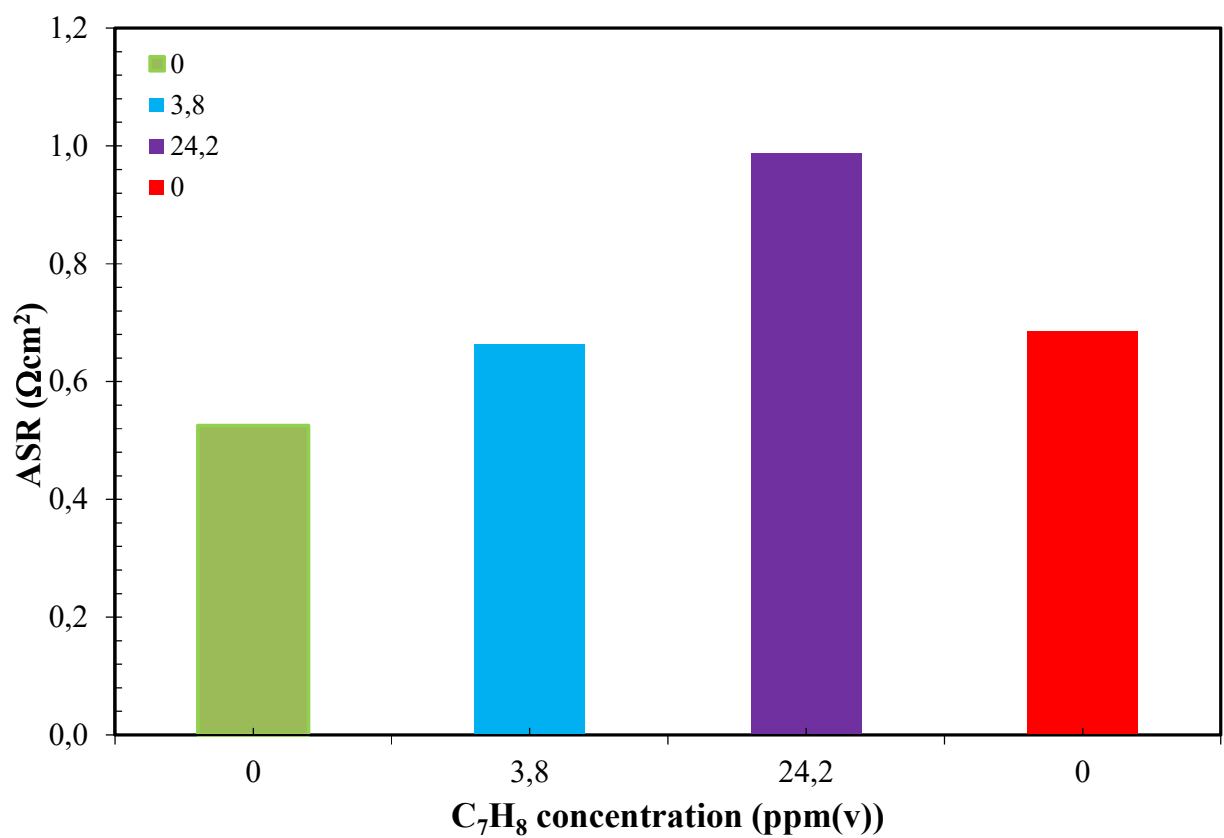
221 **Figure 16**



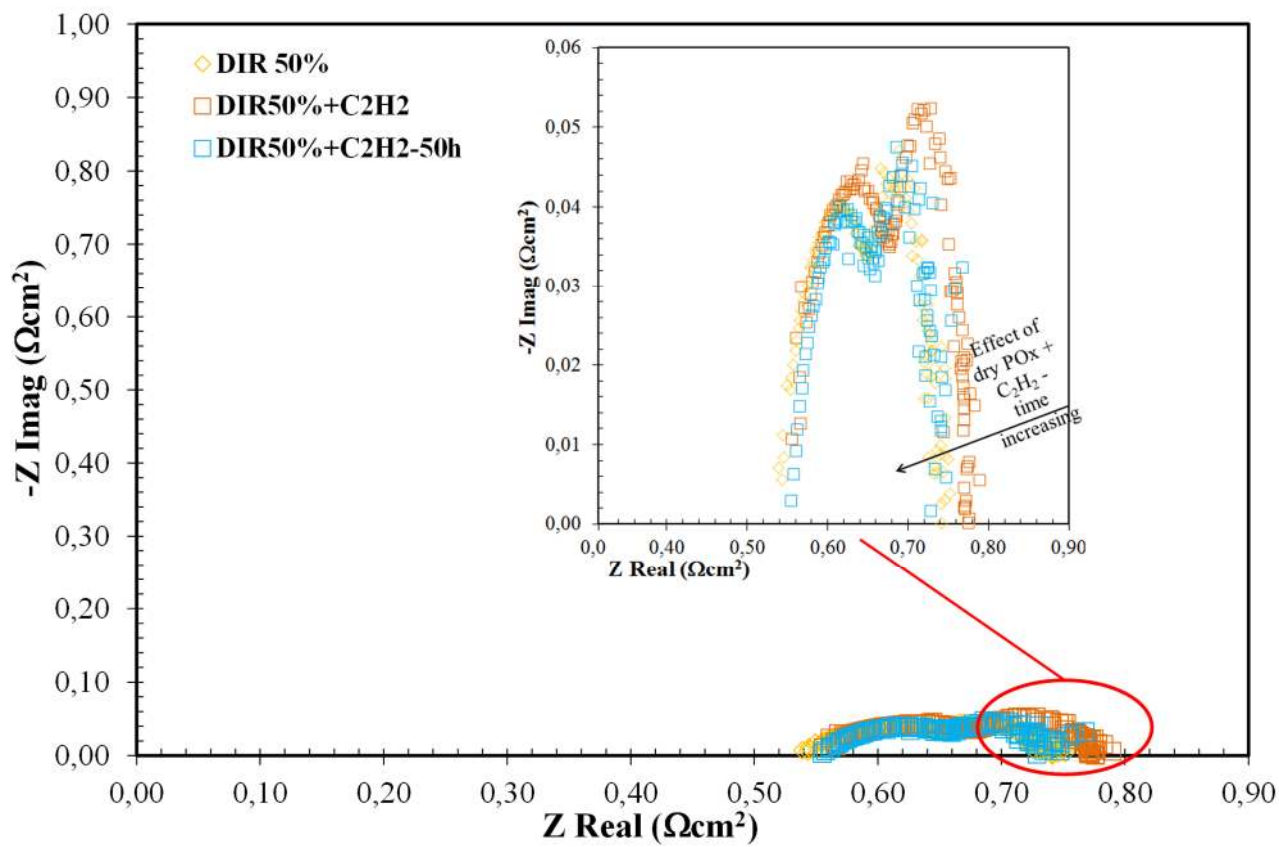
232 **Figure 17**



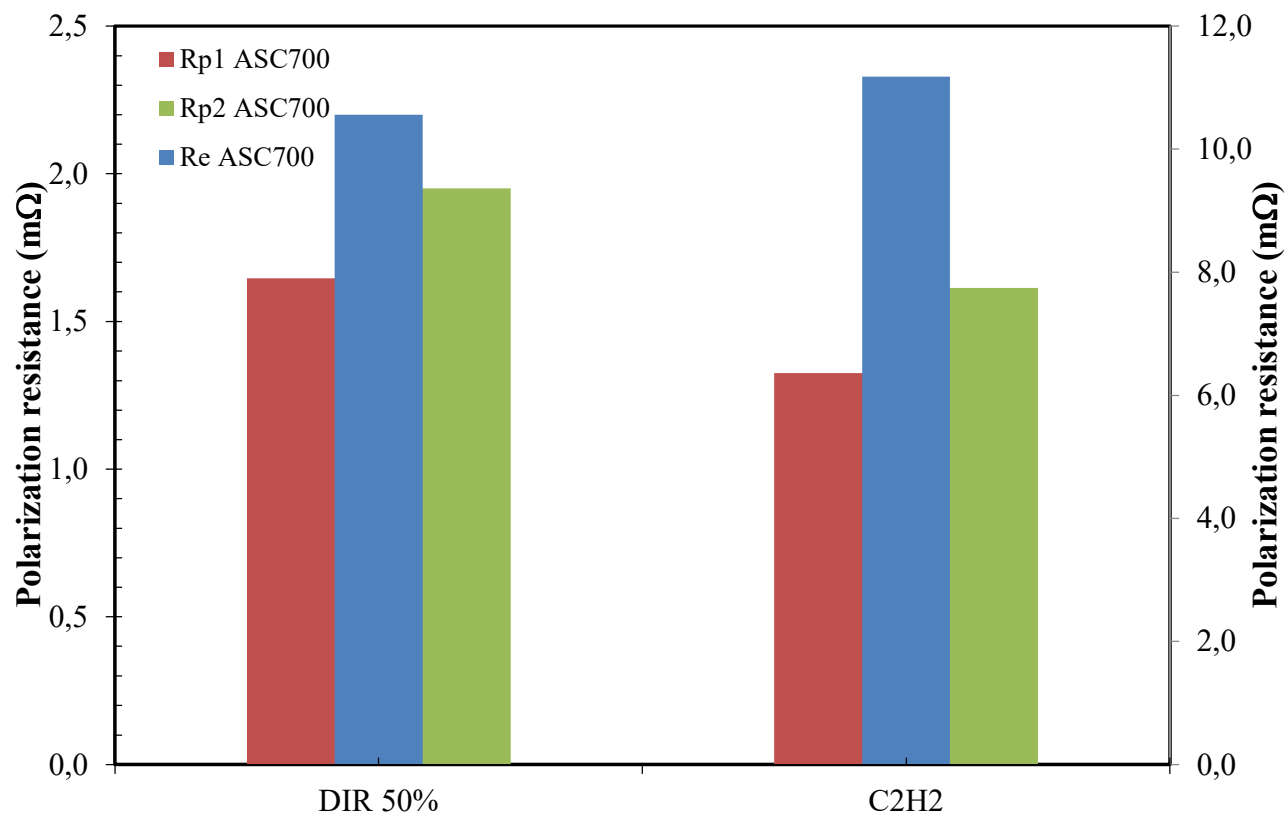
243 **Figure 18**



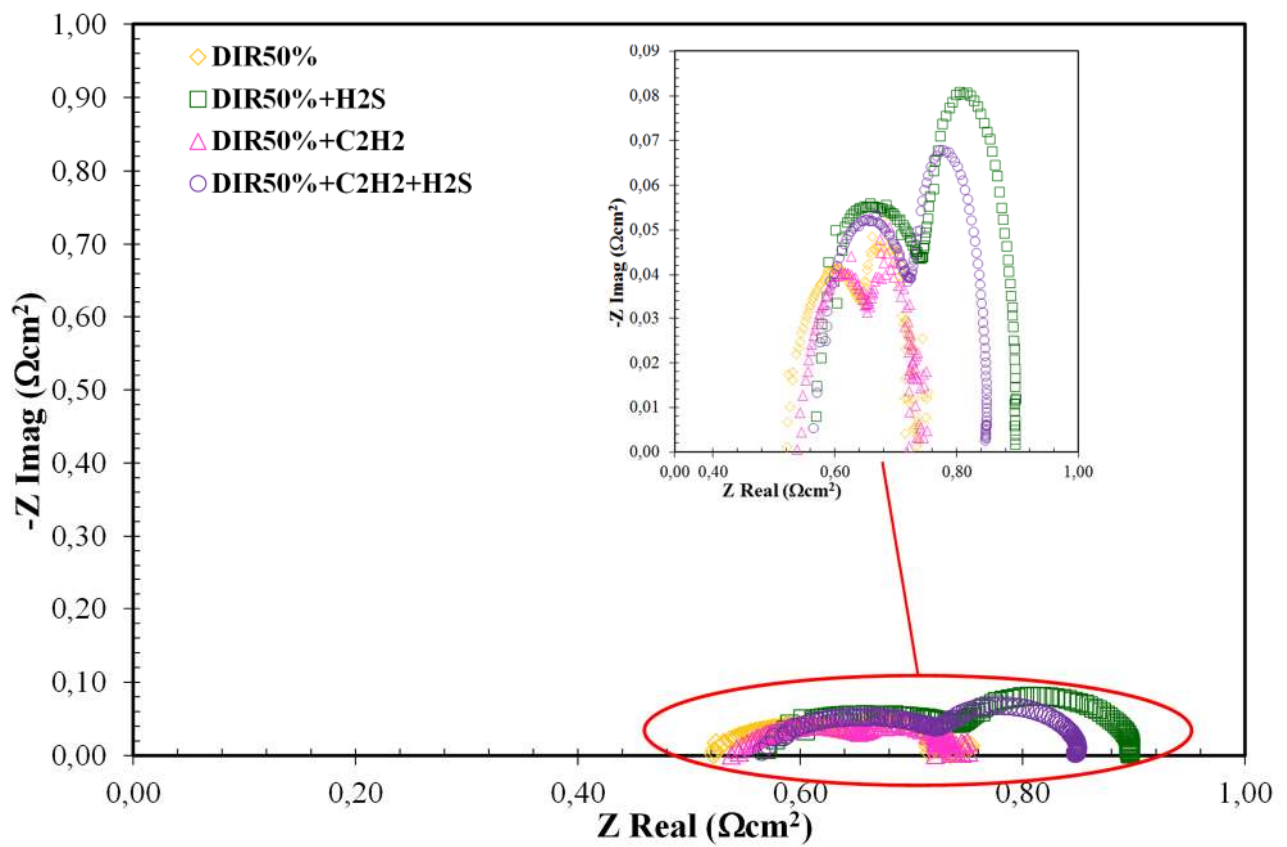
254 **Figure 19**



265 **Figure 20**

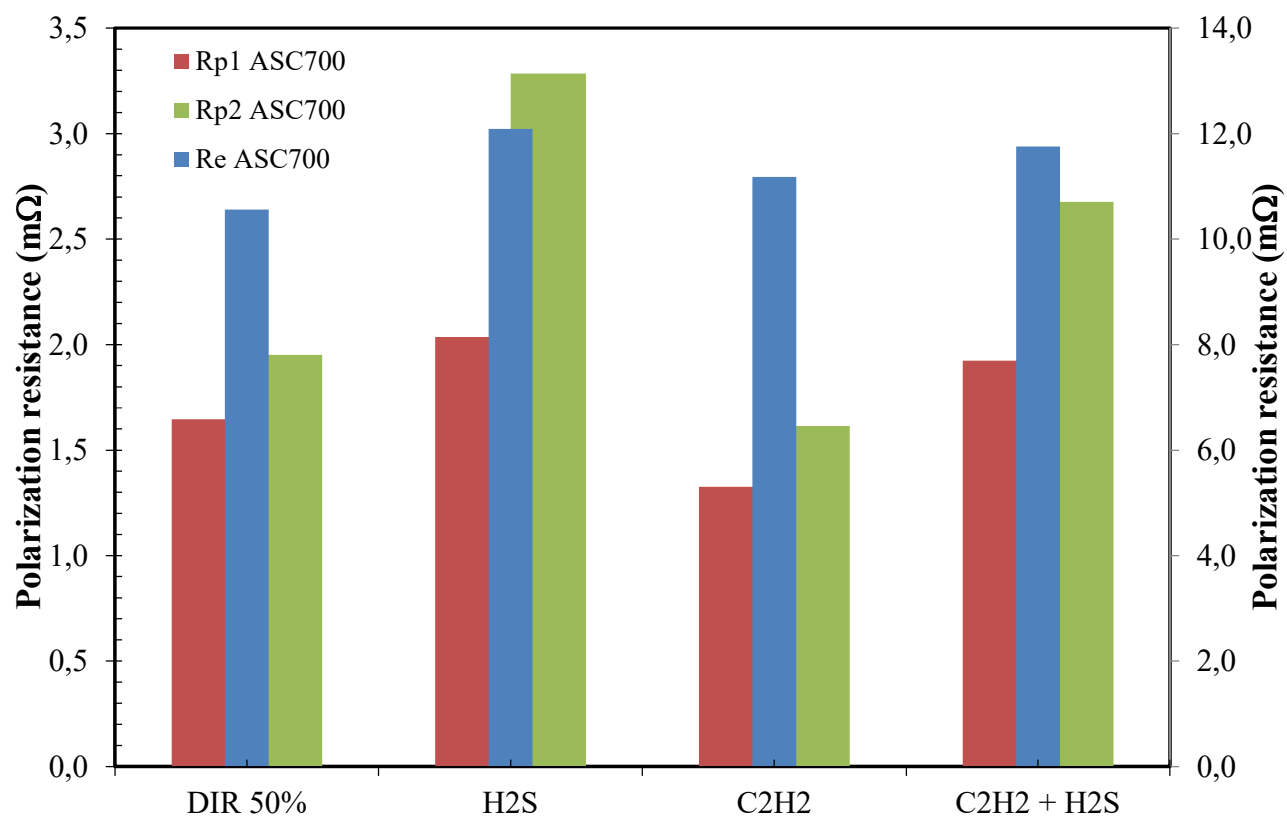


276 **Figure 21**

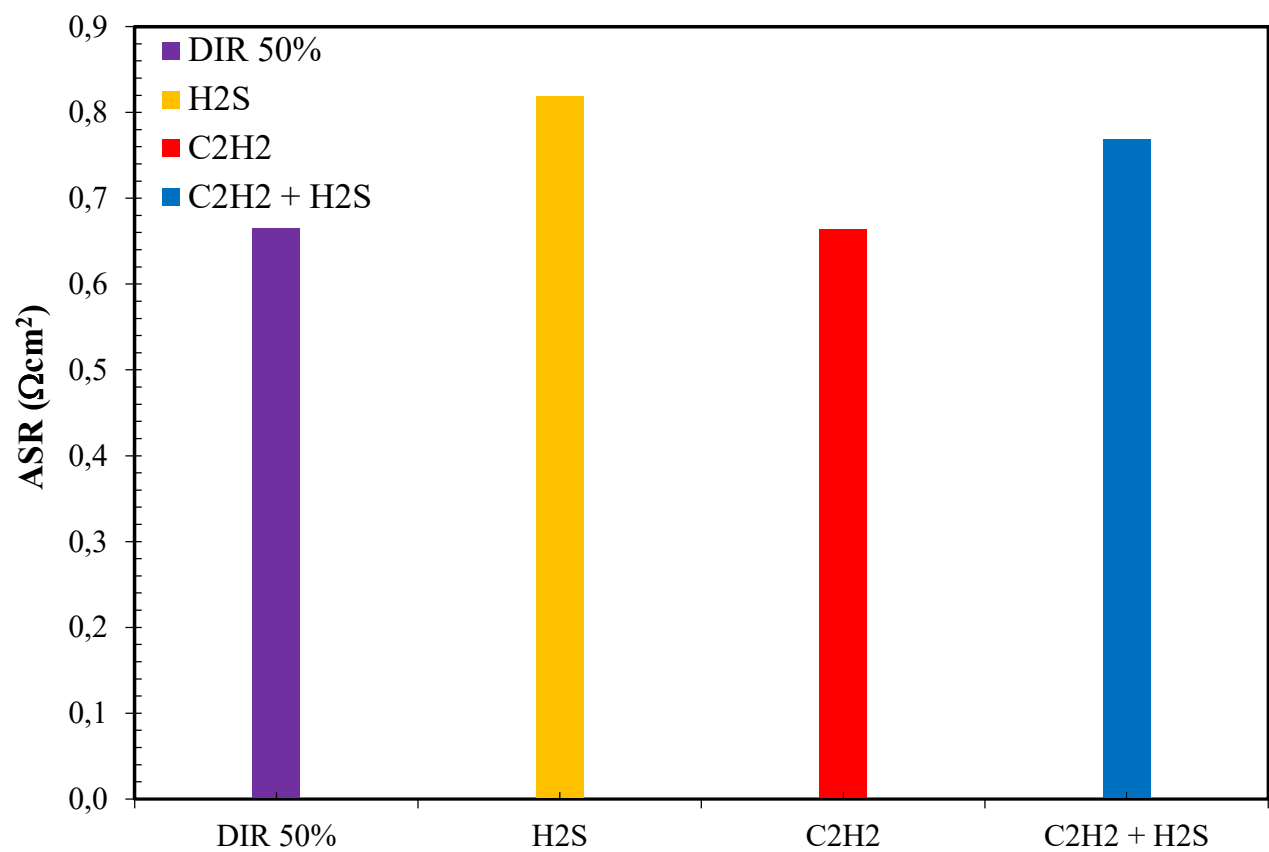




287 **Figure 22**



298 **Figure 23**



299

300

301

302

303

304

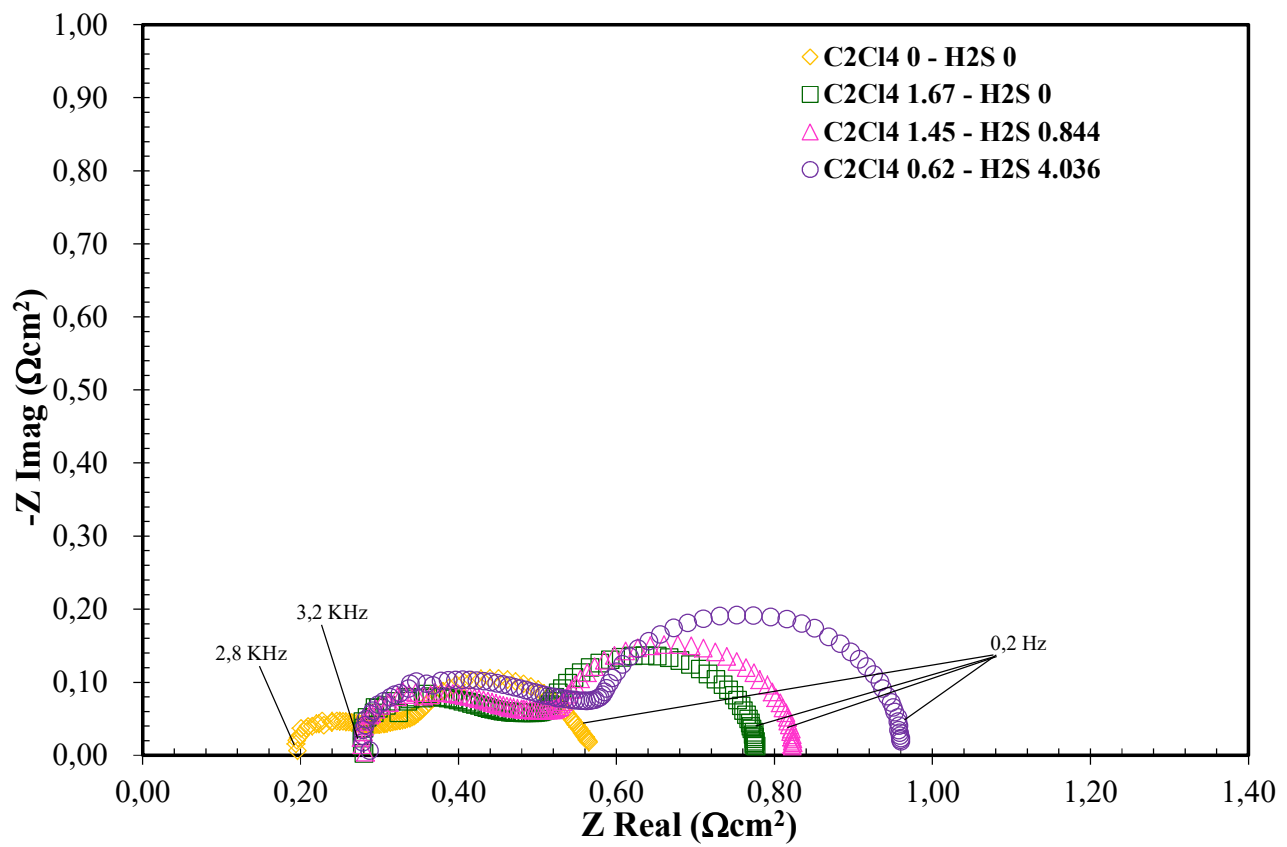
305

306

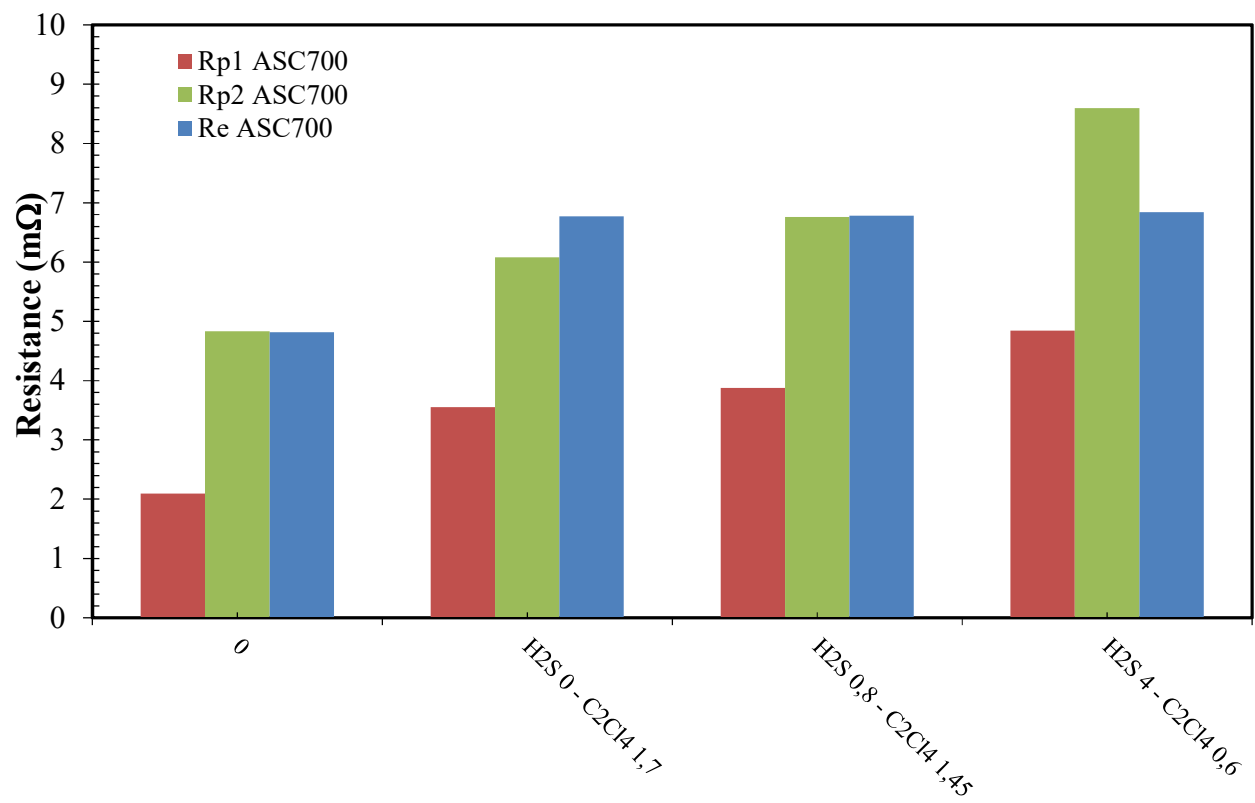
307

308

309 **Figure 24**



320 **Figure 25**



321

322

323

324

325

326

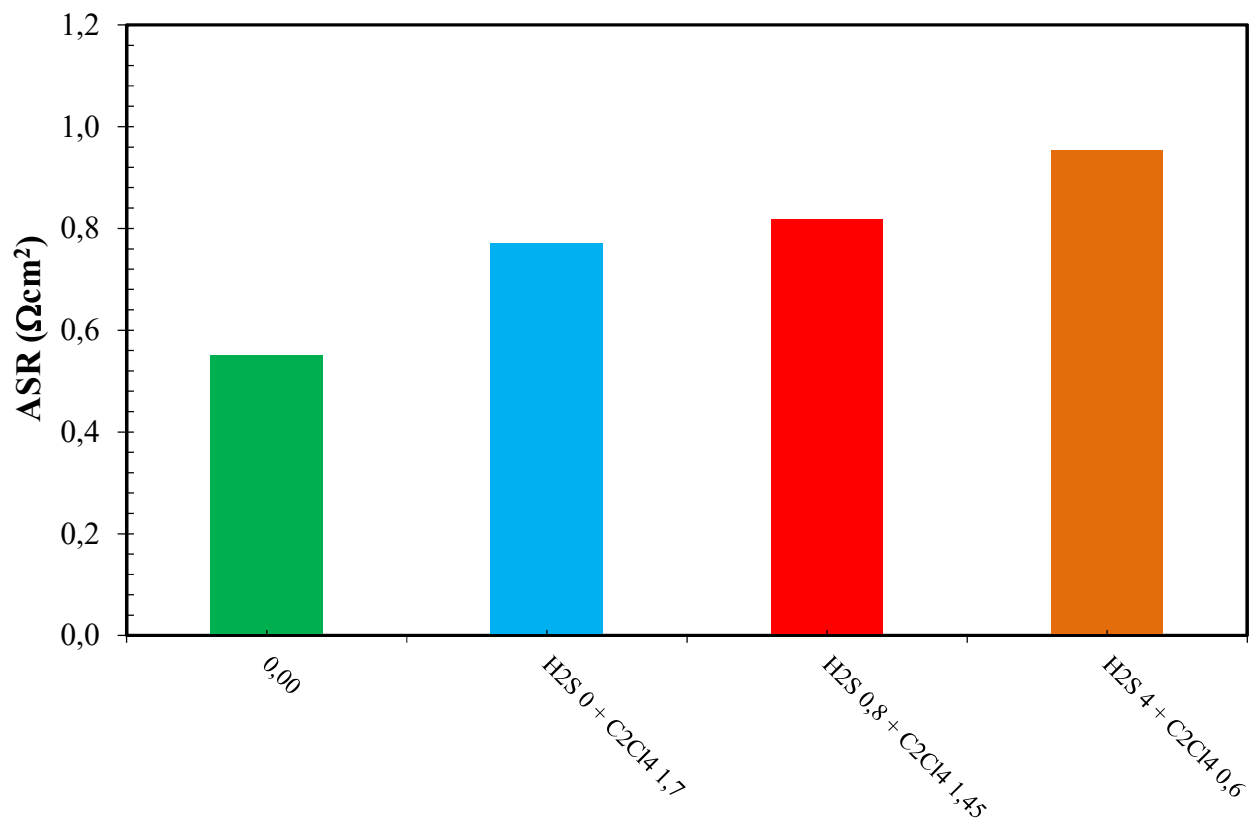
327

328

329

330

331 **Figure 26**



332

333

334

335

336

337

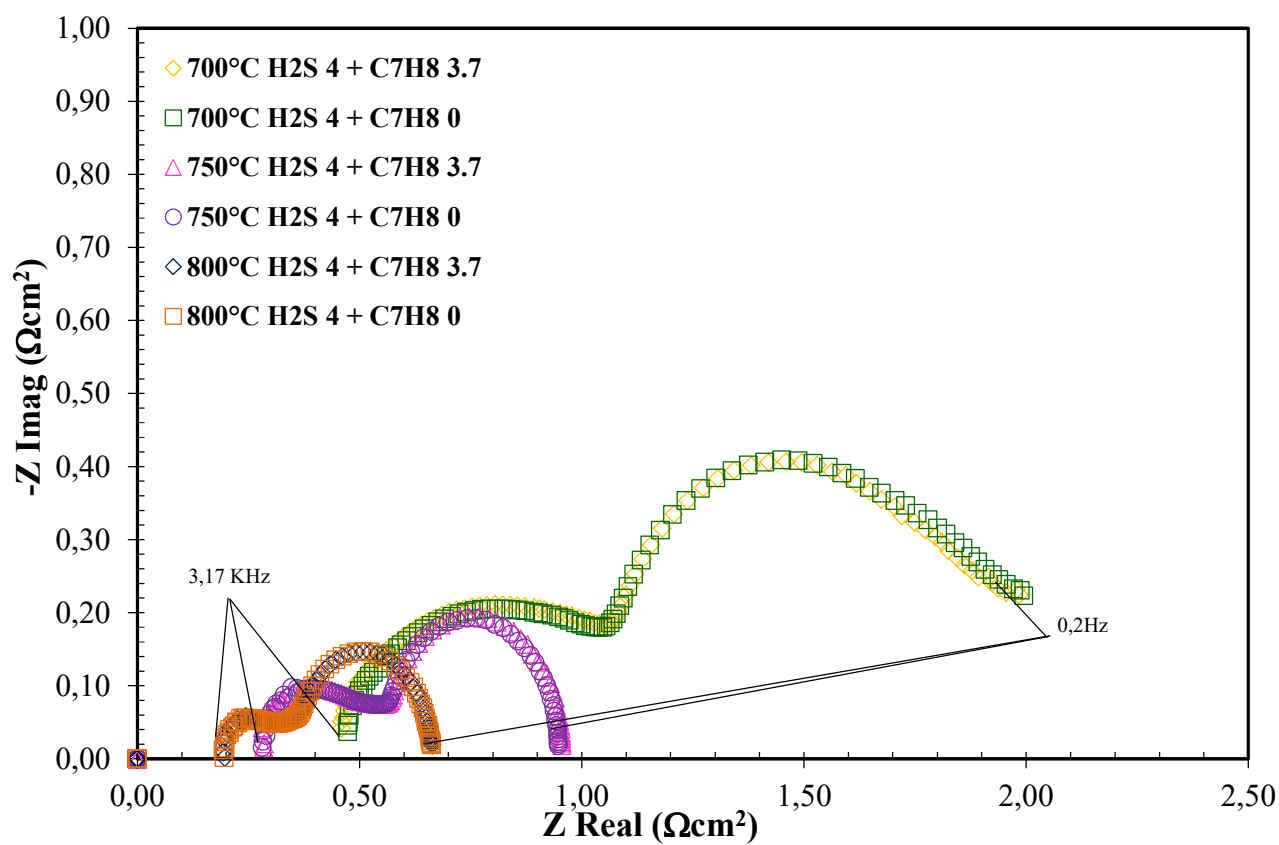
338

339

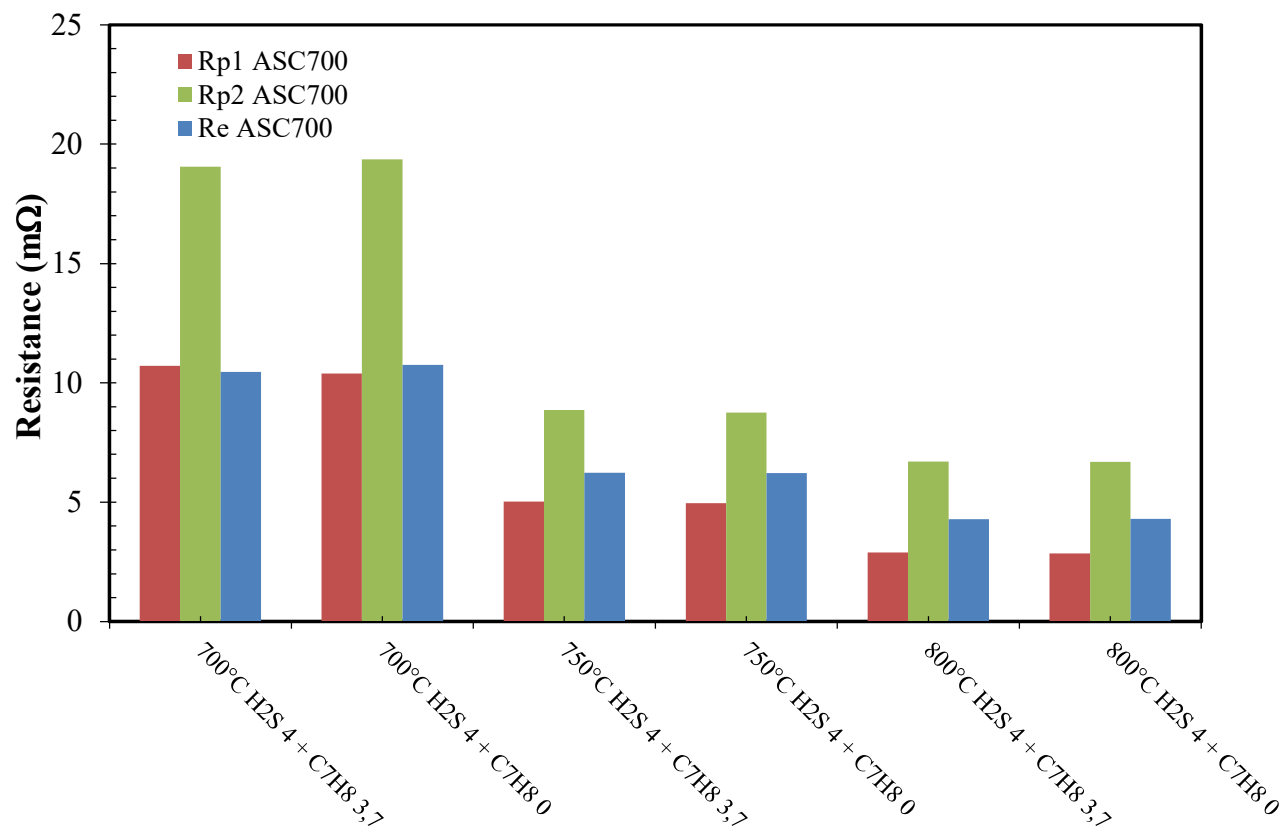
340

341

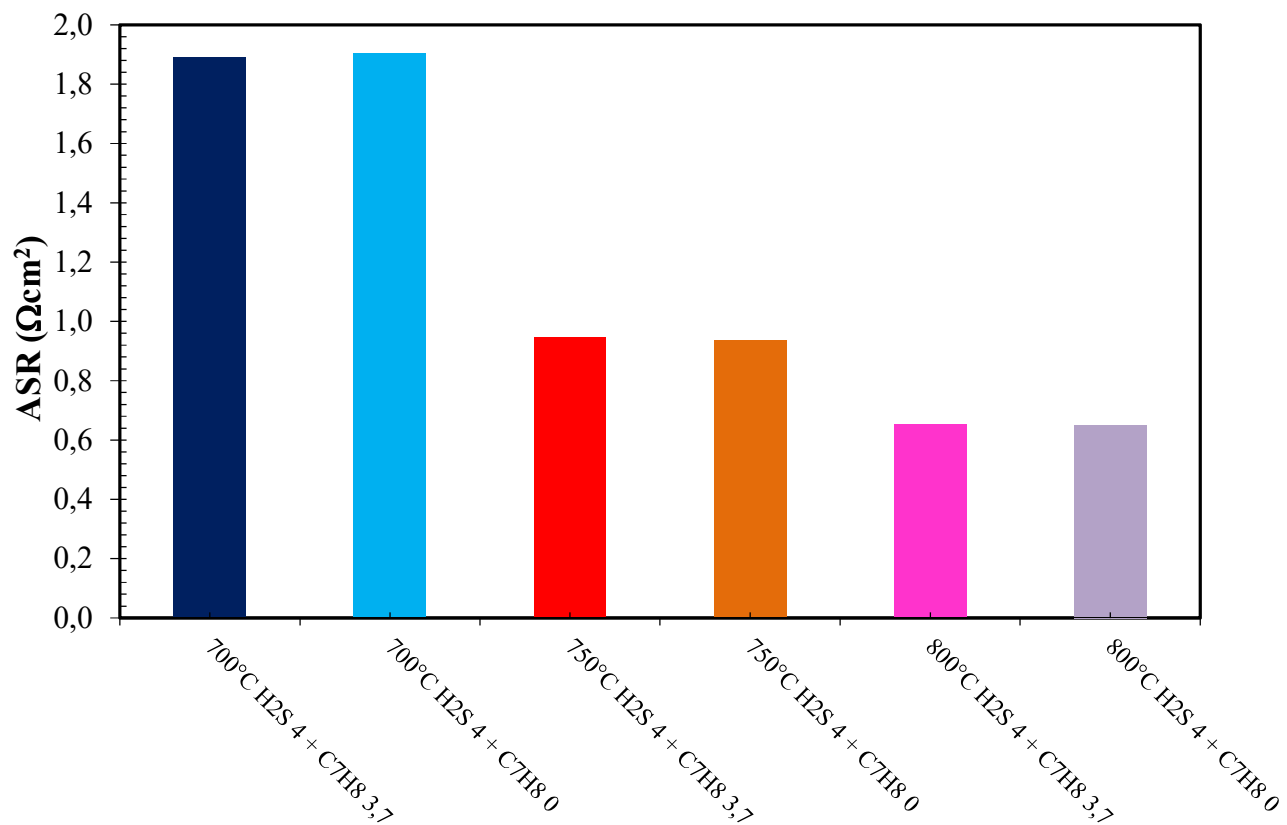
342 **Figure 27**



353 **Figure 28**



364 **Figure 29**



365

366

367

368

369

370

371

372

373

374



375

376

377

378